DYNAMIC MODELLING AND SIMULATION OF A WIND TURBINE

A THESIS SUBMITTED TO
THE GRADUATE SCHOOL OF NATURAL AND APPLIED SCIENCES
OF
MIDDLE EAST TECHNICAL UNIVERSITY

BY

AYŞE HAZAL ALTUĞ

IN PARTIAL FULFILLMENT OF THE REQUIREMENTS
FOR
THE DEGREE OF MASTER OF SCIENCE
IN
AEROSPACE ENGINEERING

SEPTEMBER 2015

Approval of the thesis:

DYNAMIC MODELLING AND SIMULATION OF A WIND TURBINE

submitted by **AYŞE HAZAL ALTUĞ** in partial fulfillment of the requirements for the degree of **Master of Science in Aerospace Engineering Department, Middle East Technical University** by,

Prof. Dr. Gülbin Dural Ünver _____
Dean, Graduate School of **Natural and Applied Sciences**

Prof. Dr. Ozan Tekinalp _____
Head of Department, **Aerospace Engineering**

Assoc. Prof. Dr. İlkay Yavrucuk _____
Supervisor, **Aerospace Engineering Department, METU**

Examining Committee Members:

Prof. Dr. Ozan Tekinalp
Aerospace Engineering Department, METU _____

Assoc. Prof. Dr. İlkay Yavrucuk
Aerospace Engineering Department, METU _____

Assoc. Prof. Dr. Oğuz Uzol
Aerospace Engineering Department, METU _____

Assist. Prof. Dr. Ali Türker Kutay
Aerospace Engineering Department, METU _____

Assist. Prof. Dr. Monier Elfarra
Flight Training Department,UTAA _____

Date: _____

I hereby declare that all information in this document has been obtained and presented in accordance with academic rules and ethical conduct. I also declare that, as required by these rules and conduct, I have fully cited and referenced all material and results that are not original to this work.

Name, Last Name: AYŞE HAZAL ALTUĞ

Signature :

ABSTRACT

DYNAMIC MODELLING AND SIMULATION OF A WIND TURBINE

Altuğ, Ayşe Hazal
M.S., Department of Aerospace Engineering
Supervisor : Assoc. Prof. Dr. İlkay Yavrucuk

September 2015, 103 pages

In this thesis, a dynamic model for a horizontal axis wind turbine is developed for an upwind configuration using the MATLAB/Simulink environment. Blade Element Momentum Theory is used to model the rotor. It is assumed that the rotor blades are rigid and wind speed is uniform. Aerodynamic and gravitational forces are calculated as distributed loads. Verification of the model is done by using the LMS Samtech, Samcef for Wind Turbines software. Aerodynamic properties of the blades, sectional loads and moments acting on the blades sections and performance outputs are compared for verification. Generator torque controller is designed to maximize power conversion at below rated regime. For above rated regime, a pitch controller is designed to keep generator speed at rated value.

Keywords: Wind Turbine, Dynamic Model, Simulation, Generator Torque Controller, Pitch Controller

ÖZ

RÜZGAR TÜRBİNİ DİNAMİK MODELLEMESİ VE SİMÜLASYONU

Altuğ, Ayşe Hazal
Yüksek Lisans, Havacılık ve Uzay Mühendisliği Bölümü
Tez Yöneticisi : Doç. Dr. İlkay Yavrucuk

Eylül 2015 , 103 sayfa

Bu tezde dikey eksenli, rüzgarı karşıdan alacak yapıda bir rüzgar türbini dinamik modeli tasarımı MATLAB/Simulink ortamında geliştirilmiştir. Rotoru tasarlarken Pal Elemanı Teorisi kullanılmıştır. Paller rijit, gelen akış düzgün kabul edilmiştir. Aerodinamik ve yerçekimsel yükler dağılımlı kuvvetler şeklinde modellenmiştir. LMS Samtech, Samcef for Wind Turbines yazılımı kullanılarak model doğrulanmıştır. Palin aerodinamik özellikleri, pale etki eden bölgesel yük ve momentler, ve performans çıktıları doğrulama amaçlı karşılaştırılmıştır. Nominalin altındaki bölgelerde, güç çıktısını azami seviyeye ulaştırmak için üreteç torku kontrolcüsü tasarlanmıştır. Nominalin üstündeki bölgelerde ise bir hatve açısı kontolcüsü tasarlanarak üreteç hızı nominal değerinde tutulmuştur.

Anahtar Kelimeler: Rüzgar Türbini, Dinamik Model, Simülasyon, Üreteç Torku Kontrolcüsü, Hatve Açısı Kontrolcüsü

to those who are always there for me...

ACKNOWLEDGMENTS

İlk olarak, tez danışmanım Assoc. Prof. Dr. İlkay Yavrucuk'a bu süreç boyunca bana verdiği katkılardan dolayı teşekkür ederim. Sizin yeni çalışma alanlarına olan heyecanınız beni bu tez konusuna yöneltti. Sizin yardımlarınız sayesinde öğretici olduğu kadar eğlenceli de bir tez dönemi geçirdim.
Tez süresince yaşadığım problemlere farklı bakış açıları sunduğu, tecrübelerini bana aktardığı için Assoc. Prof. Dr. Oğuz Uzol'a ve Samcefle ilgili tüm sorularımı yılmadan cevapladığı için Prof. Dr. Altan Kayran'a çok teşekkür ederim.
Gönenç Gürsoy ve Feyyaz Güner, tezimin ilk adımlarını atarken ve sonrasında karşılaştığım tüm problemlerde bana her zaman yardımcı oldunuz, teşekkür ederim.
Sevgili oda arkadaşım Bulut Akmenek, bu sürecin en sancılı zamanlarının şahidi sensin. Sorduğum bütün soruları anlamaya, benimle oturup çözümler bulmaya çalıştığın için teşekkür ederim.
Çalışma arkadaşları olarak şanslı insanlardan biriyim. Pınar Eneren, Özgür Harputlu, Arda Akay, Kenan Cengiz, Özcan Yırtıcı, Sinem Özçakmak, Oğuz Onay, Emre Can Suiçmez ve Emre Yılmaz, sayenizde bölüme görev olduğunu düşünerek değil severek, isteyerek geldim. Tez sürecimde maddi, manevi hiç bir desteği esirgemediniz benden varolun.
Sadece yüksek lisansta değil, lisans hayatım boyunca da yanımda olan, okumayı eğlenceli bir hale getiren canım arkadaşım Nihan iyi ki varsın. Bitaneciğim Çise, tezimi benden daha çok okumuş olabilirsin. Hiç şikayet etmeden defalarca gramer kontrolü yaptın benim için. Yerin doldurulamaz.
Beni ben yapan canım ailem, alkışları en çok siz hak ediyorsunuz. Canım babam, ilk idolüm, her zaman arkamdaydın, her zaman limitlerimi zorlamamı sağladın. Canım annem, benim için her zaman bir güvenlik ağı oldun, bir telefonun yetti tüm bulutları dağıtmaya. Ve canım kardeşim, moralimin bozuk olduğunu sesimden anlayan atlayıp geleyim mi diyen danam, sen olmasan hayatın renkleri benim için eksik kalırdı. Evimizin en küçük üyesi, Biber, varlığın neşe kaynağımız.
Son olarak sevgilim Özgür, kendi yoğunluğuna rağmen yardımıma koşmakta asla tereddüt etmedin. Bütün kriz anlarında yanımdaydın, her zaman beni sakinleştirip çözümleri bulmamı sağladın. Bu tezin bugünkü halini almasında senin de benim kadar katkın vardır. Oturup benimle defalarca kod ve gramer kontrolü yaptın. Desteklerin için, bana ayırdığın zaman için çok teşekkür ederim. Hep yanımda ol.

TABLE OF CONTENTS

LIST OF TABLES

TABLES

LIST OF FIGURES

FIGURES

LIST OF ABBREVIATIONS

VAWT	Vertical Axis Wind Turbine
HAWT	Horizontal Axis Wind Turbine
S4WT	Samcef for Wind Turbines
$\dot{m}$	Mass flow rate
ρ	Density
U	Velocity of freestream
A	Rotor area
T	Thrust force
p	Pressure
a	Axial induction factor
a'	Tangential induction factor
Q	Torque moment
r	Distance measured from blade root to tip
P	Power
R	Rotor radius
R_{hub}	Hub radius
Ω	Rotational speed
C_l	Lift coefficient
C_d	Drag coefficient
α	Angle of attack
θ_{twist}	Twist angle
β	Pitch angle
ϕ	Inflow angle
L	Lift force
D	Drag force
c	Chord length
V_{rel}	Relative wind velocity
F_T	Tangential force

F_N	Normal force
B	Blade number
σ	Solidity
F_{tip}	Tip loss factor
F_{hub}	Hub loss factor
F	Total loss factor
C_T	Thrust coefficient
C_p	Power coefficient
$(0XYZ)_{HUB}$	Hub frame
$(0XYZ)_{TILT}$	Tilt frame
$(0XYZ)_{ROTOR}$	Rotor frame
$(0XYZ)_{BLADE}$	Blade frame
$(0XYZ)_{BS}$	Blade Section frame
β_{TILT},β_T	Tilt angle
ψ	Azimuth angle
$\beta_{PRECONE}$,β_P	Precone angle
$T(\beta_T)$,$T(\psi)$	Transformation matricies
$T(\beta_P)$,$T(\phi)$	Transformation matricies
U_r,U_t,U_p	Velocity components
$\vec{r}$	Displacement vector
$\vec{a}$	Acceleration
$\dot{\Omega}$	Rotational acceleration
u, v, w	Wind velocity components
N	Number of blades
λ	Tip speed ratio
N_{gear}	Gear box ratio
k	Generator torque controller gain
I	Rotational inertia
PID	Proportional Integral Derivative Controller
PI	Proportional Integral Controller
K_p	Proportional gain
K_i	Integral gain
K_d	Derivative gain
TF_c	Closed-loop transfer function

ξ	Damping ratio
ω	Natural frequency

CHAPTER 1

INTRODUCTION

The motivation of this thesis is to create a dynamic model of a horizontal axis wind turbine whose working principles are simple enough to understand and adequate to expand to more complex models.
In this introductory chapter, firstly, motivation behind the wind energy choice as a sustainable energy resource is explained in Section 1.1 and 1.2. Then the background information about wind energy and wind turbines is given in Section 1.3 and 1.4. Major control objectives and methods applied to wind turbines are explained in Section 1.5. In Section 1.6 previous studies on wind turbine dynamic models and controllers are summarized. Finally, the objective and the scope of the thesis are explained in Sections 1.7 and 1.8, separately.

1.1 Importance of Sustainable Energy

Nowadays, electricity is mostly generated using fossil fuels and nuclear plants. The increasing level of energy consumption with increasing world population required to find alternatives to fossil fuels, which are finite resources. In fact fossil fuels are consumed almost one million times faster than the rate they were formed [34]. Besides, there are environmental concerns regarding the carbon dioxide emissions caused by the combustion of the fossil fuels is another concern. They seem to cause global warming and climate change, as countless million tones of greenhouse carbon dioxide and large quantities of other pollutants are poured into the atmosphere [42]. It is predicted that the results on the environment will be irreversible and there will be

environmental refugees, with widespread suffering, economic disruption and consequent social and politic instability[34]. Realizing the need for electricity, investment on sustainable resources such as wind, water, sun, biomass and geothermal energy has increased.

1.2 Advantages of Wind Energy

Worldwide energy consumption rate is very high but it is dwarfed considering the energy that falls from the Sun to Earth, which could meet energy consumption of the world if the solar energy of one hour could be harvested [35]. Yet all energy coming from the sun cannot be transformed to solar power, because the power density of direct solar radiation is low. To have significant electrical output, large areas should be covered with power conversion devices [34].

The sun is also the source of the wind energy. The amount of the solar radiation absorbed at the equator is higher than at the poles, which causes temperature variation. This variation gives rise to pressure difference, the source of the wind. Approximate 2 % of the solar energy received at earth is transformed into wind energy, which is still 100 times more than the total worldwide power consumption [41]. Wind power is obtained by transforming kinetic energy of the wind into the mechanical energy, which is then converted to electrical energy.

The energy that can be produced by a wind turbine is a function of the wind strength but also the wind turbine design. The design limits the operational envelope. The turbine has to shut down at higher wind speeds. This situation caused a misapprehension that the wind turbines operate only for a limited time hence they are less effective. In appropriate location selection for construction will increase the operation time[47]. Another concern about wind energy is the costs for construction, installation and decommission. However, the cost repays itself during the first few months of the operation. Furthermore unlike fossil fuels, wind energy costs are constant over the life of the operation [34].

1.3 History of Wind Energy

Wind power has been a part of human civilization. Wind power once used to sail ships is later used for grinding or pumping water. Traditional windmills first came into use in the late twelfth century [34]. They are evolved from watermills. Windmills are more advantageous compared to water mills since they can only be located next to rivers or fast flowing streams.

To prevent the sails from breaking at high wind speeds windmills were controlled. This is achieved by reducing the amount of canvas spread over the lattice framework of the sails by the miller for each sail. To stop the mill, millers were turning them out of the wind firstly by manpower then by mechanical brakes as windmills become heavier and larger [34].

Windmills were an essential part of the rural economy until the progression of fossil-fuelled engines and then rural electrification [11]. Fossil fuels were considered cheaper and easier way to generate electricity. The oil shortages of the 1970s changed this perception and showed the importance of the sustainable energy, since fossil fuels are finite resources and they also cause political dependency. In the 1980s and 1990s decreasing oil prices threatened the wind power improvement as wind power seem to be an uneconomical way to produce electricity. New tax policies came into place to incite investment on the renewable energy resources since scientific studies showed that economical concerns are just the tip of the iceberg. If the usage of the fossil fuels continues to increase it is predicted that there will be an irreversible outcome on global climate [15].

By 2001, the wind energy capacity around the world is increased 37 %, and 70 % of all wind energy is produced in Europe, mainly due to laws encouraging wind power investments. The US forced the pace and increased their capacity by 45 % in 2007[38]. Nowadays, 3 % of the world wide electricity usage has been obtained from wind power [13] and installed wind capacity across the world has been increasing year by year as seen in Figure 1.1. Using wind energy for electricity production ,beside being an inexhaustible and clean energy source, will make the electricity prices less vulnerable to oil spikes and supplier countries arrangements.

According to WWEA, in the year 2014 brought a new record in the wind power installations and the market volume for a new wind capacity was 40 % bigger than in 2013

[4]. EWEA claims that the ratio between European Union's electricity consumption and installed wind capacity will be raised from 7 % to 15 % by 2020 [3].

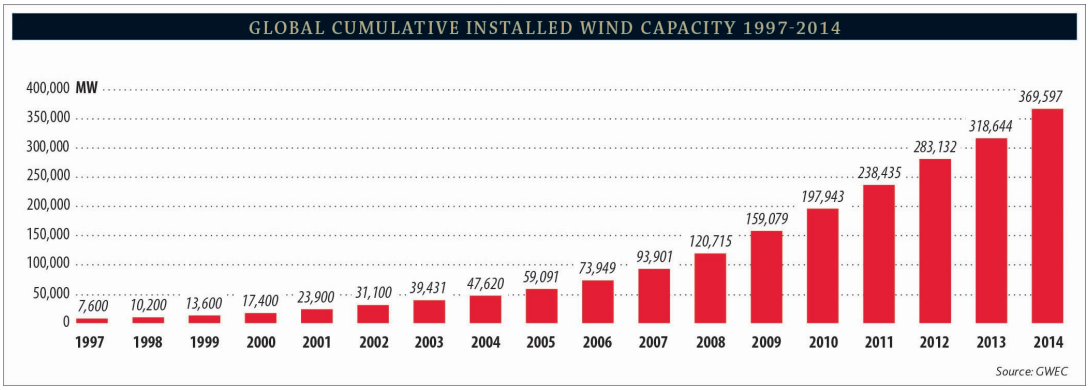

Figure 1.1: Global Cumulative Installed Wind Capacity 1997-2014[13]

1.4 Wind Turbines

Wind turbine can basically be defined as a revolving machine that transforms rotational kinetic energy in the wind into electrical energy. They include a rotor with airfoil shaped blades that rotates using aerodynamic forces occurring when blades interact with incoming air stream.

Wind turbines are classified mainly into two categories as horizontal axis wind turbines (HAWT) and vertical axis wind turbines (VAWT) depending on their rotor axis placement. A typical VAWT type Darrieus and a typical three-bladed HAWT are shown in Figure1.2.

An advantage of a vertical axis wind turbine is that its generator and transmission devices are located at the ground. Secondly, they can capture the wind coming from any direction without yawing. However, being close to the ground decreases the efficiency of turbines as wind power capacity increases with increasing height [46].

Horizontal axis wind turbines have a rotor located at the top of a long tower. Therefore they can capture the wind with higher power density and less turbulence at high altitude. Beside, the rotor the tower also carries a nacelle including a gearbox, to adjust rotor shaft rotational speed to a proper rotational speed for generator, and a generator that transforms rotational kinetic energy into the electrical energy. Unlike the vertical axis wind turbines, horizontal axis wind turbines need a yawing mech-

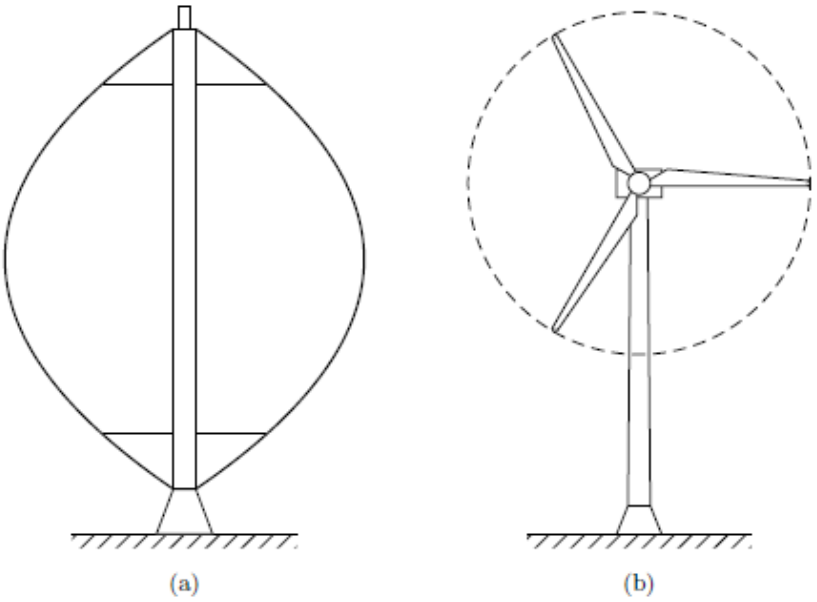

Figure 1.2: (a) Vertical Axis Wind Turbine (b) Horizontal Axis Wind Turbine[7]

anism to capture the wind. Because of their their efficiency almost all commercial wind turbines are two or three-bladed horizontal axis wind turbines.

The generation capacity is defined by taking physical and economical limitations into consideration. The representation of this power capacity varying with wind speed is shown in Figure 1.3 and called ideal power curve.

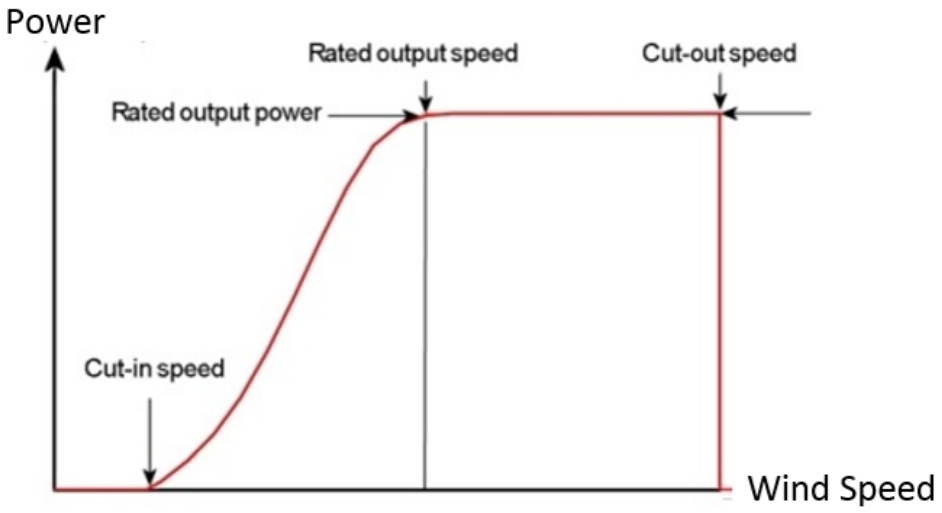

Figure 1.3: Ideal Power Curve[13]

The turbine does not operate on the wind speeds below the cut-in speed since the power density is too low to bear the cost of the operation. After the cut-in wind speed, turbine starts to produce energy. The available power, which can be defined as maximum power that can be extracted from the wind passing through the rotor using a particular rotor design, is proportional to the cubic wind speed. Rated speed is the wind speed where rated power is reached. After rated speed, the power is limited with the rated power of the turbine despite increasing available power. The rated power of a turbine is derived by finding a balance between the available energy and operating costs [7]. The purpose of this limitation is to avoid facing higher electrical and mechanical loads than the design loads. The cut-out wind speed is the high speed end of the wind turbine's operation range. Beyond this speed the turbine is stopped to prevent structural damages.

The power output of a wind turbine is directly related to the rotor speed and the rotor torque. Based on operational rotor speed there are two types of wind turbine; fixed-speed and variable-speed.

Fixed-speed turbines have a constant rotor speed regardless of the wind speed. They are the earlier wind turbines. Their simplicity may be seen as an advantage. However, they can only reach their maximum aerodynamic efficiency for one wind speed. Power output variation with wind speeds can be seen from Figure 1.4 for different fixed rotational speeds. If low operational rotational speed is chosen, maximum power is reached at low wind speeds, and as a result it is low, too. The other way around, high operational rotational speed would be chosen so high power values could be reached at high wind speeds. For this instance, wind speeds lower than the rated will be inefficacious because of high drag losses. To maximize energy capture, wind turbines are designed to operate with variable rotational speed, which can be achieved by changing the blade pitch angle or torque of the generator. Their advantages made them mainstream products [2]. Variable-speed wind turbines increase their energy capture for the wind speeds lower than the rated. They adjust their rotational speed to achieve optimum tip speed ratio for the incoming wind speed so they reach maximum aerodynamic efficiency. As a result an ideal power curve like in Figure 1.3 could be achieved for the variable-speed wind turbines. Moreover, variable-speed wind turbines can reduce the aerodynamic noise level [11].

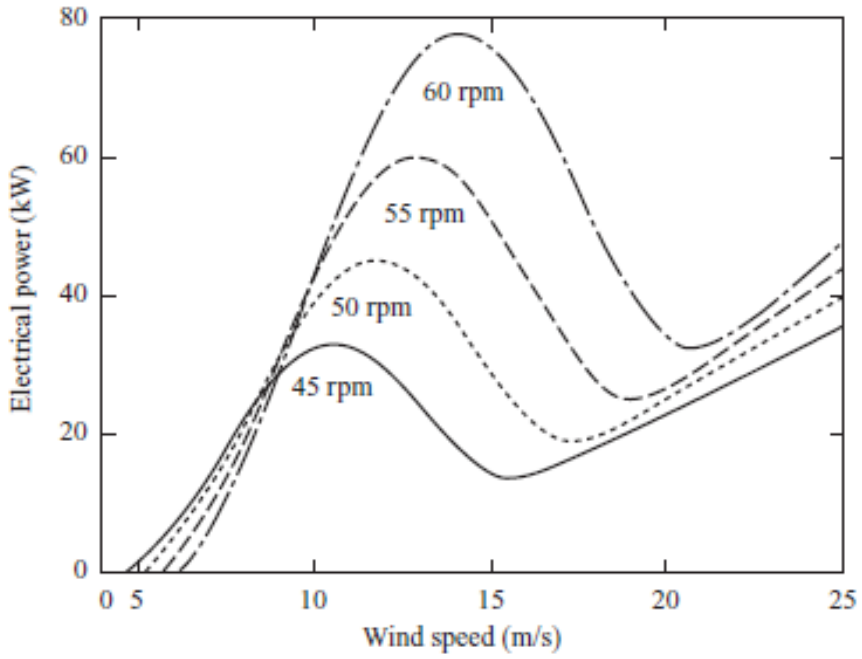

Figure 1.4: Effect of Rotational Speed on Extracted Power [11]

1.5 Control Systems for Wind Turbines

Wind is an uncontrolled energy resource since its speed varies with the time and the power demand is an uncontrolled energy sink [1]. Thus, adjusting the wind turbine for incoming wind plays a crucial role. Hence, control becomes a necessity for wind turbines.

For windmills, this is done by the miller to prevent sails from breaking. Initially, the control objective for the wind turbines was the same as the windmills. The power and the rotational speed were limited to prevent the turbine from unsafe operation under high wind conditions. With enlarging size and power of wind turbines, control specifications also evolved. Improving the efficiency of turbine became a control objective besides keeping the turbine within its safe operating envelope [7].

Nowadays utility scale wind turbines have several layers of controllers [37]. Supervisory control is the outer layer. It determines the start and the stop time of the turbine using the wind speed information. Operational control is the one responsible from the performance of the turbine. The inner layer is consists of the subsystem controllers. They track the generator, yaw drive and the other actuators. In this thesis operational control algorithm is developed.

For fixed-speed turbines neither aerodynamic nor generator torque is controlled. Some of fixed-speed turbines have variable-pitch, whose pitch angle is arranged to limit the power for the wind speeds higher than the rated wind speed.
While the control strategy for the fixed-speed turbines is applied at the above rated region and straight forward, variable-speed turbines should be controlled for the entire operation. The control objective changes during the operation from the below rated region to the above rated region. At the below rated region, aerodynamic efficiency of the turbine is an important concern. Turbine operates at variable rotational speed to capture the maximum energy from the wind. Blade pitch angle is kept constant at the optimum angle at this region. The rotor speed variation is provided by the generator torque controller. Changing the generator torque affects net torque; thus, the rotational acceleration. At the above rated region, power output is limited. The generator torque is kept constant at its optimum value. The pitch angle changes with wind speed to ensure the rotational speed of the rotor does not exceed the rated value. Thereby avoiding dangerously high structural loads is assured.

1.5.1 Generator Torque Controller

The main goal of the generator torque controller is to maximize power conversion at the below rated regime. Maximum aerodynamic power is achieved when the power coefficient, which is a function of pitch and tip speed ratio, is maximum. The pitch angle is constant at its optimum value and the only variable is the tip speed ratio. The generator torque controller adjusts the generator torque to obtain optimum the tip speed ratio. Total torque on the turbine designates the rotational acceleration hence the rotational speed. By increasing/decreasing the torque on the generator of the turbine, the rotor accelerates/decelerates towards to the optimum tip speed ratio with regard to the incoming wind speed.

1.5.2 Pitch Controller

The pitch angle is fixed to its optimum value during the below rated region. After the rated wind speed, the pitch controller is active. Its main goal is to avoid power and

rotational speed exceeding their limits. The pitch controller rotates all blades upon their own axis to change the angle of attack hence the aerodynamic torque. Structural and electrical loads are kept in safe operation regime by reducing aerodynamic torque. With the help of the pitch controller, an ideal power curve like in Figure 1.3 could be provided for a variable-speed wind turbine.

1.6 Literature Review

Dynamic modelling is an essential task to examine aerodynamic and structural properties of the wind turbine or to develop a control algorithm.

In literature, modelling of a wind turbine focuses on aerodynamics of the system and dynamic behaviour of the system [31, 11].

Modelling a wind turbine rotor with rigid blades is an essential part for wind turbine research. However, today wind turbine blades can be as large as 80 meters [14]. Hence, aeroelastic blade models are used [23, 28, 27, 43, 6, 20, 12]. Aeroelastic models cover deformations in three axes which are flapping, lead-lag and feathering [23, 6, 20]. Some studies also include the axial extension [28]. Only a minority of them considers one axis deformation which is an out-of-plane bending, i.e. flapping[43]. Euler-Bernoulli Beam Theory is a commonly used method to model aeroelastic blades [5]. On the other hand, the similarity between helicopter rotors and wind turbine rotors allow to use Hodges and Dowell's method to calculate equations of motions for deformed blade [19].

Aerodynamics of a wind turbine is an important part of wind turbine models to understand the sources of forces and moments on the rotor blades. Blade Element Momentum Theory is the most common method to examine aerodynamics of wind turbines [18, 31, 11, 45, 26]. However, there are some limitations of BEM theory arisen from assumptions made. In most research, these limitations are overcome by modifications applied to the model [40, 33, 26].

Since the variable speed wind turbines are more advantageous than the fixed speed ones the use of them is more common. This circumstance has increased the importance of control systems of wind turbines. The main objective of the controllers is to regulate the wind turbine's power. For the below rated regions, a generator torque

controller with a gain proportional to the square of the generator speed is commonly used and even called as a standard below rated region control [48, 25, 29]. However, in some cases theory and practice do not overlap because of uncertainty. Adaptive generator torque controllers are designed to deal with this uncertainty [21]. Some studies tried to increase the respond speed of the generator speed to changes in wind speeds by using the generator acceleration and/or the aerodynamic torque as a feedback [30]. Moreover, the PI (proportional-integral) controllers with torque estimators are used to avoid a mismeasurement of the generator torque [32].

At the above rated regions, pitch controllers are used. The most common type pitch controllers are the PID (proportional-integral-derivative) ones [16, 25, 29, 1]. In these studies, the model is linearized around one equilibrium point and a linear controller is designed using the data of this point. At points far from the equilibrium point the linear controller with fixed gain might be insufficient. Therefore, some studies propose gain scheduling [48, 7].

Studies spoken until now aims to regulate power output. However, with increasing size of wind turbines, another control objective appears; load mitigation. Aerodynamic loads are the problems at the above rated regions. Hence, individual pitch controllers are become widespread as a solution [24, 44, 9].

1.7 The objectives of the Thesis

The objectives of the thesis could be summarized as follows;

- The development of a dynamic model for rigid horizontal axis wind turbine using BEM Theory.

- The development of a generator torque controller to maximize the power extracted from wind for wind speeds below the rated values.

- The development of a pitch controller to maintain the rated generator speed value for wind speeds above the rated values.

1.8 The Scope of the Thesis

In Chapter 2, aerodynamics of a wind turbine rotor is explained. Both Momentum Theory and Blade Element Theory are introduced to do groundwork for Blade Element Momentum Theory (BEM). Aerodynamic properties of the turbine such as sectional velocities and aerodynamic forces are calculated using BEM Theory. Hub-tip losses and Glauert correction are implemented to BEM Theory as essential modifications. Tilt and precone angle effects are added to the model.

In Chapter 3, the dynamic model of a wind turbine is derived. Coordinate systems used to create the model and transformations between them are presented. Gravitational forces are added to the model besides aerodynamic forces. Moments caused from total forces are calculated to find rotor torque. Power output of the turbine is found using resulting torque.

In Chapter 4, control algorithms used to maximize power production are explained. Firstly, operating regions of a variable speed wind turbines and control objectives at these regions are defined. Generator torque controller is designed to maximize power production at below rated regions. Standard proportional controller is used. For above rated regions, the pitch controller is used to limit generator speed at the rated value. PI controller with gain scheduling is used as pitch controller.

In Chapter 5, verification of the model is done by using the LMS Samtech, Samcef for Wind Turbines software. Simulation of the model is performed by the MATLAB/Simulink for the same wind turbine properties. Axial and tangential induction factors, inflow angle, angle of attack, velocities, forces and moments at blade sections are compared. After verification the NREL 5MW reference wind turbine [22] is used to check if controllers fulfil control objectives.

CHAPTER 2

ROTOR AERODYNAMIC MODEL

In this chapter, the aerodynamic model used in this thesis is explained. Firstly, Momentum Theory is explained as a building block of wind turbine aerodynamics in Section 2.1. Then, Blade Element Theory is introduced in Section 2.2. Finally, Blade Element Momentum Theory is summarized in Section 2.3 with some corrections. Derived aerodynamical forces, axial and tangential induction factors are used in Chapter 3 to create the dynamic model of wind turbine.

2.1 Momentum Theory

Wind turbine produces power by extracting the kinetic energy from wind using airfoil shaped blades. This slows down wind passing through the rotor disc. Momentum theory analysis assumes a control volume whose boundaries are the surface and two cross-sections of a stream tube. Flow passes through only streamwise direction.
Assumptions used for momentum theory are;

- incompressible and steady state flow
- infinite number of blades
- uniform thrust over the rotor area
- no rotation at the wake
- static pressures equal to the ambient pressure at far upstream and far downstream

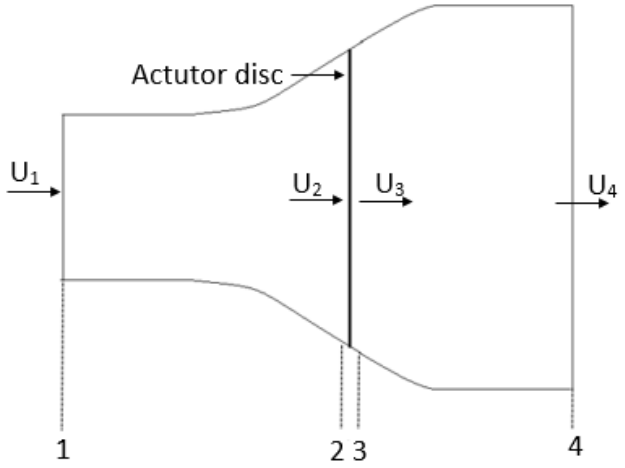

Figure 2.1: Actuator Disc Model of a Wind Turbine

The turbine, which is modelled as an actuator disc, causes a discontinuity of pressure in the stream tube [31]. Flow slows down after passing the rotor but mass flow rate is preserved. Hence, the stream tube expands as seen from Figure 2.1. This is why the upstream end of the stream tube has smaller area than the downstream end of the stream tube. Mass flow rate across the stream tube is calculated as;

$$\dot{m} = \rho A_1 U_1 = \rho A_2 U_2 = \rho A_3 U_3 = \rho A_4 U_4 \tag{2.1}$$

Net force acting on the control volume can be found by applying the conservation of linear momentum. Thrust force, T, on the wind turbine is equal but opposite to this net force.

$$T = U_1(\rho A_1 U_1) - U_4(\rho A_4 U_4) = \dot{m}(U_1 - U_4) \tag{2.2}$$

The thrust can also be expressed by in terms of pressure difference;

$$T = A_2(p_2 - p_3) \tag{2.3}$$

Bernoulli's equation states that total energy in the flow remains constant as long as no work is done on or by the fluid [11]. Bernoulli's equation for the upstream of the disc is as follows;

$$p_1 + \frac{1}{2}\rho {U_1}^2 = p_2 + \frac{1}{2}\rho {U_2}^2 \tag{2.4}$$

Bernoulli's equation for the downstream of the disc is;

$$p_3 + \frac{1}{2}\rho {U_3}^2 = p_4 + \frac{1}{2}\rho {U_4}^2 \tag{2.5}$$

$p_1 = p_4$ and $U_2 = U_3$ from assumptions made earlier. Combining Equations 2.2, 2.3 and Bernoulli equations, thrust can be found as;

$$T = \frac{1}{2}\rho A_2({U_1}^2 - {U_4}^2) \tag{2.6}$$

The axial induction factor, a, is defined as a fractional decrease in wind velocity between the free stream and the rotor plane;

$$a = \frac{U_1 - U_2}{U_1} \tag{2.7}$$

or equivalently;

$$U_2 = U_1(1 - a) \tag{2.8}$$

And from equations 2.1 and 2.6;

$$U_4 = U_1(1 - 2a) \tag{2.9}$$

Axial thrust on the disc is finally written as;

$$T = \frac{1}{2}\rho A U^2[4a(1 - a)] \tag{2.10}$$

where $A = A_2 = A_3$ and $U = U_1$, free stream velocity.

2.1.1 Wake Rotation

Previously a non-rotating wake is assumed. However, air passing through the rotor disc imposes a torque equal and opposite to the torque that rotates the rotor. This reaction torque causes the flow behind the rotor to rotate in opposite direction which is called wake rotation. Wake rotation causes a loss in rotational kinetic energy extraction by the rotor.

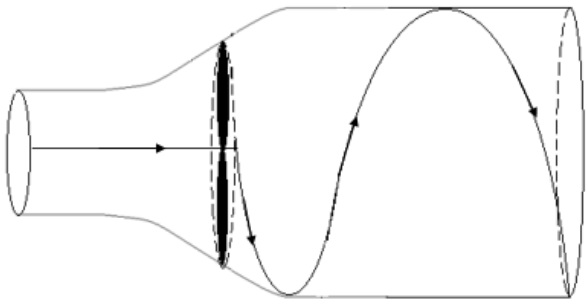

Figure 2.2: Wake Rotation

In order to extent actuator disc model to a model with wake rotation, a control volume moving with the angular velocity of the blades is chosen (see Figure 2.3). Hence, energy equation can be applied in the sections before and after the blades.

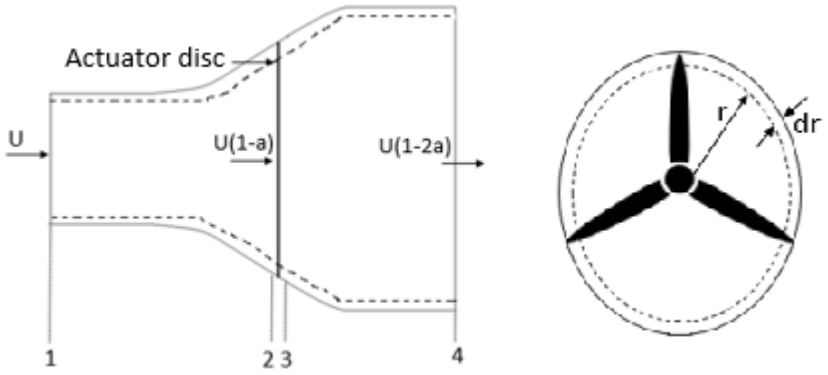

Figure 2.3: Control Volume for Wake Rotation

While flow entering the actuator disc has no rotational motion, there is a rotation behind the disc. The change in tangential velocity is defined as axial induction factor, a'. Wake rotation adds an induced velocity component in the rotor plane, $r\Omega a'$ in addition to axial component, Ua.

The torque on the rotor can be derived by conservation of angular momentum. Torque exerted on the rotor, Q, is equal to change in angular momentum of the wake. Torque on an incremental annular element is found as;

$$dQ = 4a'(1-a)\frac{1}{2}\rho U\Omega r^2 2\pi r dr \tag{2.11}$$

Thrust on an annular element;

$$dT = 4a(1-a)\frac{1}{2}\rho U^2 2\pi r dr \tag{2.12}$$

Power generated at each element;

$$dP = \Omega dQ \tag{2.13}$$

2.2 Blade Element Theory

The rate of change of angular and axial momentum of air passing through the annular element can also be expressed in terms of aerodynamic forces on spanwise blade

elements.
Assumptions used for Blade Element Theory are;

- no interaction between blade elements
- only lift and drag characteristics are used to calculate aerodynamic forces

Blade is divided into N elements. Elements are placed along a radius radius r measured from the root of the blade with length dr. Calculations are done for each section with changing properties such as chord and twist starting from the blade root to the blade tip, where r equals to blade radius, R. Aerodynamic forces can be calculated

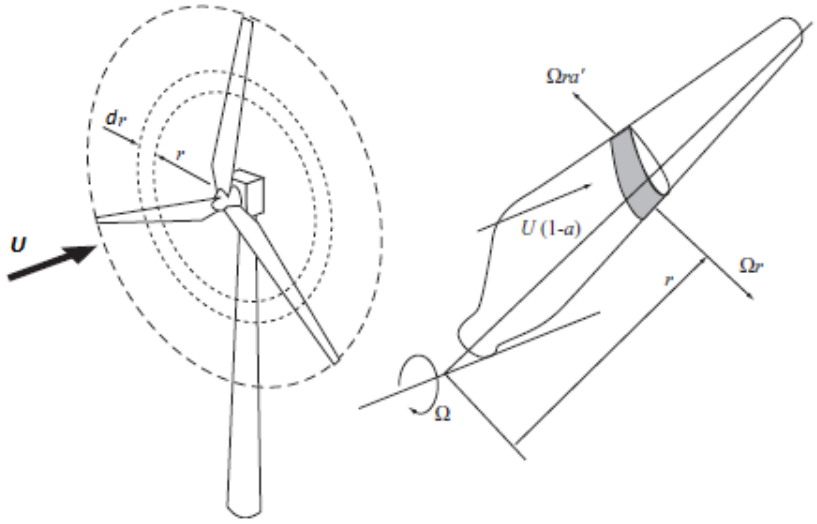

Figure 2.4: Blade Element [11]

for a given a and a' if airfoil characteristic coefficients C_l and C_d are known for varying angle of attack, which is the angle between the relative wind and the chord line. Lift and drag forces are formed perpendicular and parallel, respectively to relative wind as seen from Figure 2.5. Relative wind velocity, V_{rel}, is calculated as a vector sum of axial, $U(1-a)$, and tangential, $\Omega r(1+a')$, components of the wind velocity that blade element faces. The angle of attack, α, is given as;

$$\alpha = \phi - \theta \tag{2.14}$$

where ϕ represents the inflow angle and θ represents the sum of twist, θ_{twist}, and pitch angle, β.

$$\theta = \theta_{twist} + \beta \tag{2.15}$$

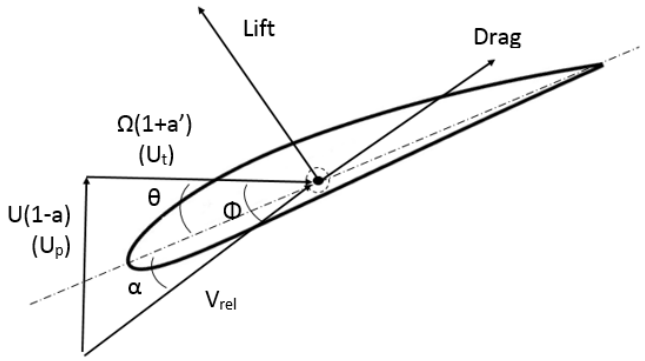

Figure 2.5: Velocities and Forces Acting on a Blade Element

Lift and drag forces on an element can be calculated as;

$$dL = \frac{1}{2}\rho {V_{rel}}^2 C_l(\alpha) c dr \tag{2.16}$$

$$dD = \frac{1}{2}\rho {V_{rel}}^2 C_d(\alpha) c dr \tag{2.17}$$

where,

$$V_{rel} = \sqrt{\left(U(1-a)\right)^2 + \left(\Omega r(1+a')\right)^2} \tag{2.18}$$

or

$$V_{rel} = \frac{U(1-a)}{sin(\phi)} \tag{2.19}$$

Blade element analyses can be done by using tangential and normal force components of aerodynamic forces, which are parallel and normal to the chord line, respectively. The tangential and the normal force components of a blade element are;

$$dF_T = dLsin(\phi) - dDcos(\phi) \tag{2.20}$$

$$dF_N = dLcos(\phi) + dDsin(\phi) \tag{2.21}$$

If the rotor has a number of B blades, total normal force, which is equal to the thrust force, on a section is found as;

$$dF_N = B\frac{1}{2}\rho {V_{rel}}^2 (C_l cos(\phi) + C_d sin(\phi)) c dr \tag{2.22}$$

The tangential force creates a torque on the rotor. The differential torque on the section at r as follows;

$$dQ = BrdF_T = B\frac{1}{2}\rho {V_{rel}}^2 (C_l sin(\phi) - C_d cos(\phi)) c r dr \tag{2.23}$$

2.3 Blade Element Momentum Theory

Blade Element Momentum (BEM) Theory originates from Momentum Theory and Blade Element Theory. BEM theory enables to examine a rotor model with known airfoil and blade shape properties.

By equating dT and dQ equations derived using Momentum Theory to the ones derived from Blade Element Theory axial and tangential induction factors are found as;

$$a = \frac{1}{\left[1 + \frac{4sin^2(\phi)}{\sigma(C_l cos(\phi) + C_d sin(\phi))}\right]} \tag{2.24}$$

$$a' = \frac{1}{\left[-1 + \frac{4sin(\phi)cos(\phi)}{\sigma(C_l sin(\phi) - C_d cos(\phi))}\right]} \tag{2.25}$$

Where σ, solidity, is defined as;

$$\sigma = \frac{Bc}{2\pi r} \tag{2.26}$$

BEM theory is commonly used to model rotors because of its simplicity. However, there are some limitations. It is assumed that flow passes around the airfoil is in equilibrium, which is not the case in reality. Furthermore, no radial flow assumption coming from Blade Element Theory is not valid for real rotors. Moreover, hub and tip vortices affect the induced velocities which are not included in BEM theory. In order to deal with limitations listed above some corrections must be done in BEM theory.

2.3.1 Tip and Hub Losses

At blade tips air flows from lower surface to upper surface because of pressure difference between the suction side and the pressure side of the blade. This creates vortices which affect the wake on induced velocity field and reduce the lift. In order to include tip loss effect, Prandtl's method can be used. A correction factor, F_{tip}, is defined as;

$$F_{tip} = \frac{2}{\pi} cos^{-1}(e^{-f_{tip}}) \tag{2.27}$$

where,

$$f_{tip} = \frac{B}{2}\frac{R-r}{rsin(\phi)} \tag{2.28}$$

In the same manner with tip loss, hub loss correction also should be implemented to BEM theory in order to consider vortices being shed near the hub as;

$$F_{hub} = \frac{2}{\pi} cos^{-1}(e^{-f_{hub}}) \tag{2.29}$$

where,

$$f_{hub} = \frac{B}{2} \frac{r - R_{hub}}{r sin(\phi)} \tag{2.30}$$

Finally, the total loss is calculates as,

$$F = F_{tip} F_{hub} \tag{2.31}$$

This correction factor is used to modify Momentum Theory equations. Force and moment equations that come from Blade Element Theory remain same. Then, thrust and torque on an annular section derived from Momentum Theory are found as;

$$dT = 4\pi r \rho U^2 (1 - a) a F dr \tag{2.32}$$

$$dQ = 4\pi r^3 \rho U \Omega (1 - a) a' F dr \tag{2.33}$$

2.3.2 Glauert Correction

Wind turbines generally operate at windmill state and BEM theory is applicable. However, when the axial induction factor becomes greater than 0.5, turbulent wake state, momentum theory is no longer valid. For an axial induction factor values greater than 0.5, far wake velocity becomes negative according to Momentum Theory and violates the assumptions of BEM theory.

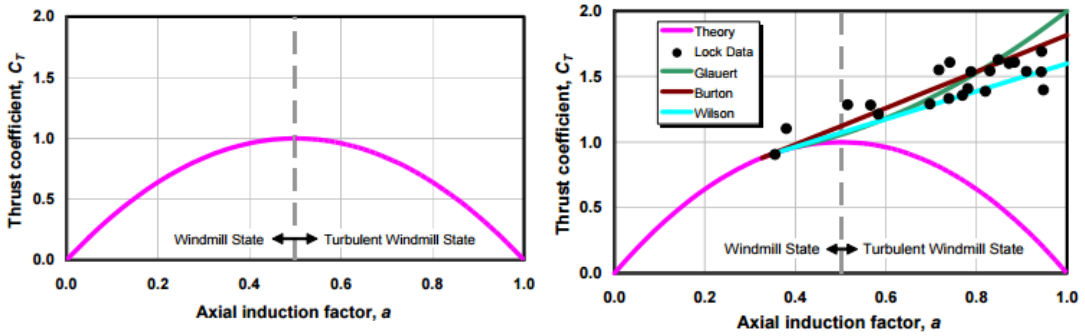

(a) when losses are ignored

(b) when losses are considered

Figure 2.6: Classical C_T vs a Curve[10]

Glauert develops an empirical relation for axial induction factor using experimental measurements of helicopter rotors with high induction factors [33]. The Glauert relation between the axial induction factor and the thrust coefficient when $a > 0.4$ can be found as;

$$a = \frac{1}{F}\left[0.143 + \sqrt{0.0203 - 0.6427(0.889 - C_T)}\right] \tag{2.34}$$

This relationship was derived for the overall thrust coefficient for a rotor but it can also be used for a correction of individual blade elements with BEM theory. Local thrust coefficient is found as;

$$C_T = \frac{dF_N}{\frac{1}{2}\rho U^2 2\pi r dr} \tag{2.35}$$

From dF_N equation derived using Blade Element Theory, C_T is calculated as;

$$C_T = \frac{\sigma(1-a)^2(C_l cos(\phi)) + C_d sin(\phi))}{sin^2(\phi)} \tag{2.36}$$

2.3.3 Effect of Tilt and Precone Angle

In order to include effect of tilt and precone angle, whose definitions are given in Chapter 3, BEM Theory is needed to be corrected. Inplane velocity components ,U_p and U_t, should be recalculated. Then relative velocity, V_{rel}, is calculated as;

$$V_{rel} = \sqrt{\left(U_p\left(1-a\right)\right)^2 + \left(U_t\left(1+a'\right)\right)^2} \tag{2.37}$$

2.3.4 Iterative Solution for Axial Induction Factor and Tangential Induction Factor

The axial and the tangential induction factors are functions of inflow angle. Inflow angle is a function of a and a'. Therefore they can be calculated using iterations. Following steps are used;

1. Guess a value for a and a'.
2. Calculate the inflow angle, ϕ.
3. Calculate the angle of attack, α and C_l, C_d values.
4. Calculate a using below formulas,

if $a > 0.4$

$$a = \frac{1}{F}\left[0.143 + \sqrt{0.0203 - 0.6427(0.889 - C_T)}\right] \tag{2.38}$$

if $a \leq 0.4$

$$a = \frac{1}{\left[1 + \frac{4Fsin(\phi)^2}{\sigma C_l cos(\phi) + C_d sin(\phi)}\right]} \tag{2.39}$$

5. Calculate a',

$$a' = \frac{1}{\left[-1 + \frac{4Fsin(\phi)cos(\phi)}{\sigma C_l sin(\phi) - C_d cos(\phi)}\right]} \tag{2.40}$$

6. Update a and a' values and repeat the steps starting from step 2.

7. Stop when error value is less than the defined error.

CHAPTER 3

WIND TURBINE DYNAMIC MODEL

In this chapter, the dynamic model for a horizontal axis wind turbine with upwind configuration is derived. Firstly, coordinate systems used in this thesis and transformation matrices between them are defined in Section 3.1 and 3.2. Then, aerodynamic and gravitational forces and their resulting moments affecting the rotor are derived and the rotor torque, which creates rotation, is calculated in Section 3.3. Finally, performance parameters of the turbine, power and power coefficient, are calculated in Section 3.4.

3.1 Coordinate System Definitions

Coordinate system definition is an important part of a dynamic model since displacements, velocities, forces and moments are represented using them. First, coordinate systems used in this thesis are described.

3.1.1 Hub Fixed Coordinate System

Hub coordinate system has an origin located on the origin of the hub. Its X axis points upwards from the ground. First blade is assumed to be positioned on X_{HUB}. Z axis, Z_{HUB}, is placed to point downwind. Finally, Y axis is found by the right hand rule. Hub coordinate system, $(OXYZ)_{HUB}$, is fixed to the hub and does not rotate with the rotor.

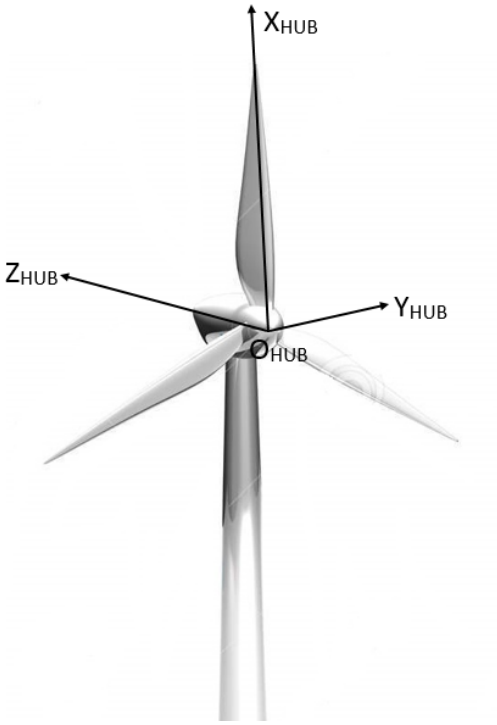

Figure 3.1: Hub Coordinate System

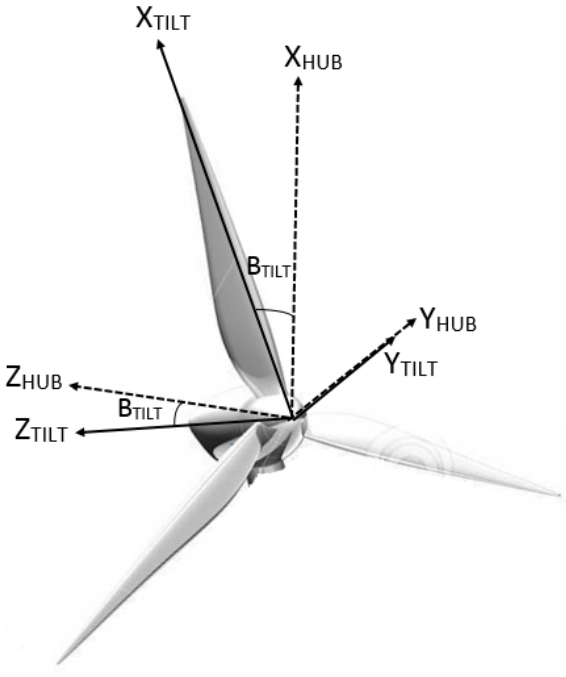

Figure 3.2: Relationship Between Hub Coordinate System and Tilt Coordinate System

3.1.2 Tilt Fixed Coordinate System

Tilt coordinate system, $(OXYZ)_{TILT}$, is obtained by rotating hub coordinate system around Y_{HUB} clockwise by an angle, β_{TILT}. For turbines with high blade radius, elastic blades might hit the tower at high winds. Therefore, tilt angle is added to increase the tower clearance.

3.1.3 Rotor Fixed Coordinate System

It is assumed that blades rotate around the hub with angular speed, Ω. They scan an angle called azimuth angle and the rotor coordinate system, $(OXYZ)_{ROTOR}$, is obtained by rotating the tilt coordinate system around Z_{TILT} counterclockwise by the azimuth angle, ψ. Relation between ψ and Ω after t seconds is found as;

$$\psi = \int_0^t \Omega dt \tag{3.1}$$

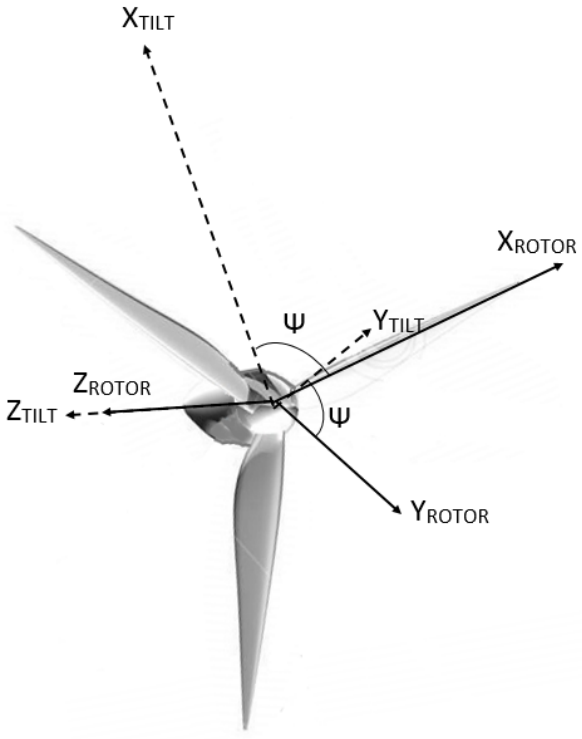

Figure 3.3: Relationship Between Tilt Coordinate System and Rotor Coordinate System

Aerodynamic torque is calculated in this coordinate system since the rotor shaft lies on Z_{ROTOR}.

3.1.4 Blade Fixed Coordinate System

When the rotor coordinate system is moved from the hub center to the blade root, blade coordinate system, $(OXYZ)_{BLADE}$, is obtained. The origin lies on X_{BLADE} and X_{ROTOR} is equal to zero when X_{BLADE} is equal to the hub radius.

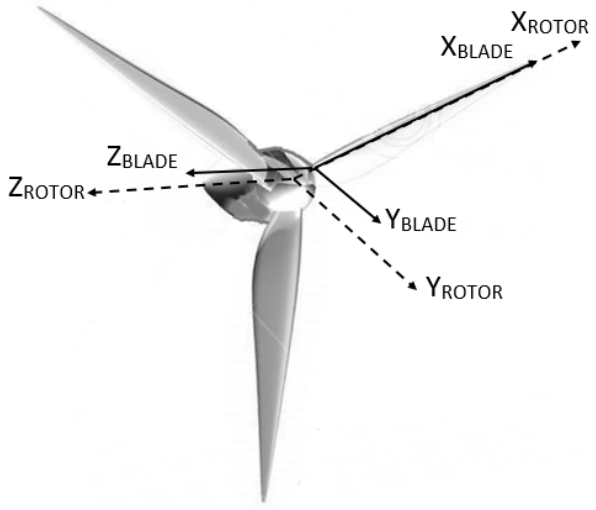

Figure 3.4: Relationship Between Rotor Coordinate System and Blade Coordinate System

3.1.5 Blade Fixed Coordinate System with Precone

Blade coordinate system is rotated around Y_{BLADE} counterclockwise by an angle named precone angle, β_p, and it forms blade precone coordinate system, $(OXYZ)_{BLADEPRECONE}$. Precone angle is positive when the blades are bended towards upwind. Besides the tilt angle, precone angle also increases the tower clearance.

3.1.6 Blade Section Fixed Coordinate System

Blade section coordinate system, $(OXYZ)_{BS}$, is needed since aerodynamic forces are calculated in this coordinate system. Its origin moves with r, for each blade element. Blade coordinate system is rotated around X_{BLADE} by the inflow angle ,which is defined as the angle between Y_{BLADE} and the relative velocity of the blade section.

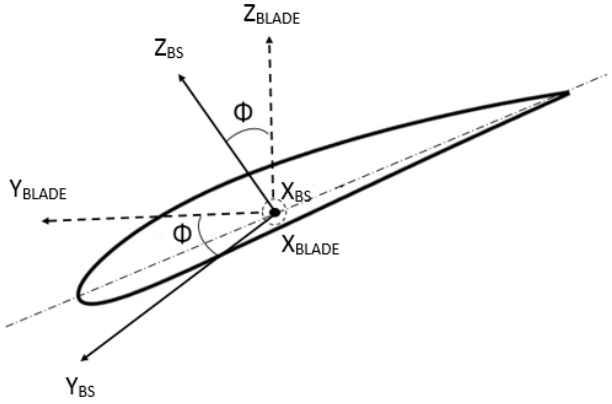

Figure 3.5: Relationship Between Blade Coordinate System and Blade Section Coordinate System

3.2 Transformation Matrices

Transformation matrices are used to transform a vector quantity calculated in one coordinate system to another coordinate system. Transformations used to define relation between coordinate systems used in thesis are explained in this section.

3.2.1 Hub Fixed Coordinate System to Tilt Fixed Coordinate System

Relationship between hub coordinate system and tilt coordinate system;

$$(OXYZ)_{TILT} = T(\beta_{TILT})(OXYZ)_{HUB} \tag{3.2}$$

or

$$(OXYZ)_{HUB} = T^{T}(\beta_{TILT})(OXYZ)_{TILT} \tag{3.3}$$

where transformation matrix could be calculated as;

$$T(\beta_{TILT}) = \begin{bmatrix} \cos(\beta_{TILT}) & 0 & \sin(\beta_{TILT}) \\ 0 & 1 & 0 \\ -\sin(\beta_{TILT}) & 0 & \cos(\beta_{TILT}) \end{bmatrix} \tag{3.4}$$

3.2.2 Tilt Fixed Coordinate System to Rotor Fixed Coordinate System

Relationship between tilt coordinate system and rotor coordinate system;

$$(OXYZ)_{ROTOR} = T(\psi)(OXYZ)_{TILT} \tag{3.5}$$

or

$$(OXYZ)_{TILT} = T^{T}(\psi)(OXYZ)_{ROTOR} \tag{3.6}$$

where

$$T(\psi) = \begin{bmatrix} \cos(\psi) & \sin(\psi) & 0 \\ -\sin(\psi) & \cos(\psi) & 0 \\ 0 & 0 & 1 \end{bmatrix} \tag{3.7}$$

3.2.3 Rotor Fixed Coordinate System to Blade Fixed Coordinate System

Relationship between rotor coordinate system and blade coordinate system with pre-cone angle;

$$(OXYZ)_{BLADE} = T(\beta_{PRECONE})(OXYZ)_{ROTOR} \tag{3.8}$$

or

$$(OXYZ)_{ROTOR} = T^{T}(\beta_{PRECONE})(OXYZ)_{BLADE} \tag{3.9}$$

where

$$T(\beta_{PRECONE}) = \begin{bmatrix} \cos(\beta_{PRECONE}) & 0 & -\sin(\beta_{PRECONE}) \\ 0 & 1 & 0 \\ \sin(\beta_{PRECONE}) & 0 & \cos(\beta_{PRECONE}) \end{bmatrix} \tag{3.10}$$

3.2.4 Blade Fixed Coordinate System with Precone to Blade Section Fixed Coordinate System

Relationship between precone coordinate system and blade section coordinate system;

$$(OXYZ)_{BS} = T(\phi)(OXYZ)_{BLADE} \tag{3.11}$$

or

$$(OXYZ)_{BLADE} = T^{T}(\phi)(OXYZ)_{BS} \tag{3.12}$$

where

$$T(\phi) = \begin{bmatrix} 1 & 0 & 0 \\ 0 & \cos(\phi) & -\sin(\phi) \\ 0 & \sin(\phi) & \cos(\phi) \end{bmatrix} \tag{3.13}$$

3.3 Forces and Moments

Forces acting on the rotor blades of the wind turbine are divided mainly into two categories; aerodynamic forces and gravitational forces. These forces form the rotor torque, which makes the rotor rotate around the hub. Derivations of these forces and moments are explained in this section.

3.3.1 Aerodynamic Forces

Wind passing through the blades of the turbine creates aerodynamic forces and these forces are the main reason behind the produced rotational kinetic energy. Aerodynamic forces are easier to inspect on the blade section coordinate system since lift and drag occurs tangential and parallel, respectively to the relative velocity of the blade as seen from Figure 3.6.

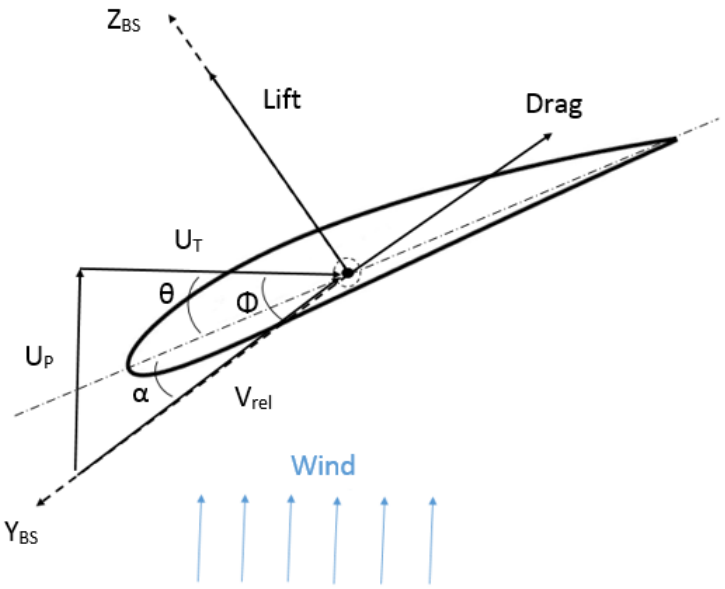

Figure 3.6: Aerodynamic Forces and Velocities on Blade Section Coordinate System

In order to calculate velocity and acceleration of a blade element, displacement vector is written as;

$$\vec{r} = \begin{bmatrix} r \\ 0 \\ 0 \end{bmatrix} \tag{3.14}$$

Then, velocity and acceleration of an element is found as;

$$\frac{d\vec{r}}{dt} = \dot{r} + \Omega \times r \tag{3.15}$$

$$\frac{d}{dt}\left(\frac{d\vec{r}}{dt}\right) = \vec{a} = \ddot{r} + 2(\Omega \times \dot{r}) + \dot{\Omega} \times r + \Omega \times (\Omega \times r) \tag{3.16}$$

where Ω represents the rotational velocity of the rotor.
Wind velocity is defined at the hub coordinate system as;

$$V_{wind-HUB} = [u, v, w]^T \tag{3.17}$$

In order to calculate the relative wind velocity on the blade, the wind velocity should be transformed to the blade coordinate system from the hub coordinate system as;

$$V_{wind-BLADE} = T(\beta_{PRECONE})T(\psi)T(\beta_{TILT})V_{wind-HUB} \tag{3.18}$$

Total velocity of an element is then;

$$V_{BLADE} = V_{wind-BLADE} + \frac{dr}{dt} = \begin{Bmatrix} U_r \\ U_t \\ U_p \end{Bmatrix} \tag{3.19}$$

Finally, U_r, U_t and U_p are found as;

$$\begin{bmatrix} U_r \\ U_t \\ U_p \end{bmatrix} = \begin{bmatrix} sin(\beta_P)sin(\beta_T) + cos(\beta_P)cos(\psi)cos(\beta_T) \\ -cos(\beta_T)sin(\psi) \\ -(cos(\beta_P)sin(\beta_T) - cos(\psi)cos(\beta_T)sin(\beta_P)) \end{bmatrix} u + \begin{bmatrix} cos(\beta_P)sin(\psi) \\ cos(\psi) \\ -(cos(\beta_P)sin(\beta_T) - cos(\psi)cos(\beta_T)sin(\beta_P))u + sin(\beta_P)sin(\psi) \end{bmatrix} v + \begin{bmatrix} -(cos(\beta_T)sin(\beta_P) - cos(\beta_P)cos(\psi)sin(\beta_T)) \\ sin(\psi)sin(\beta_T) \\ cos(\beta_P)cos(\beta_T) + cos(\psi)sin(\beta_P)sin(\beta_T) \end{bmatrix} w + \begin{bmatrix} 0 \\ \Omega r \\ 0 \end{bmatrix} \tag{3.20}$$

where $\beta_P = \beta_{PRECONE}$ and $\beta_T = \beta_{TILT}$.
Lift and drag forces are derived in Equations 2.16 and 2.17. The relative velocity with the effects of axial and tangential induction factors now calculated as;

$$V_{rel} = \sqrt{U_R^2 + U_T(1-a)^2 + U_P(1+a')^2} \tag{3.21}$$

Finally, aerodynamic forces on a blade element in the Blade Section coordinate system is written as;

$$dF_{AERO-BS} = \begin{bmatrix} 0 \\ -dD \\ dL \end{bmatrix} \tag{3.22}$$

3.3.2 Gravitational Forces

Gravitational forces are firstly written in the hub coordinate system since the gravitational acceleration is on -X_{HUB} direction. Weight of each blade section is different since properties such as chord, airfoil and thickness varies with r. Sectional mass, dm, on the Figure 3.7 has a unit of kg/m. Therefore, gravitational force on an element at

hub coordinate system is written as;

$$dF_{GRAV-HUB} = \begin{bmatrix} -dm * dr * g \\ 0 \\ 0 \end{bmatrix} \tag{3.23}$$

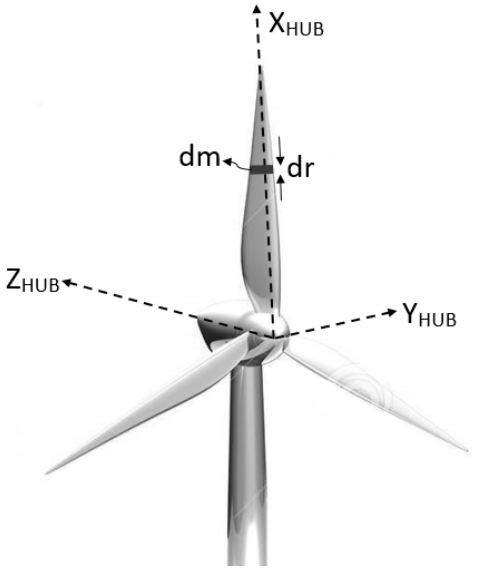

Figure 3.7: Gravitational Forces on Hub Coordinate System

3.3.3 Moments

The total torque on the rotor shaft affects the rotational speed of the rotor. If the net torque is positive, it accelerates the rotor but if it is negative the rotor decelerates. Aerodynamic forces on the rotor create aerodynamic torque. At Section 3.3.1, aerodynamic forces on a blade element are written in the blade section coordinate system. However, the torque is calculated at the rotor coordinate system since the rotor shaft lies in Z_{ROTOR}. Using necessary transformation matrices, aerodynamic forces are carried to the rotor coordinate system as follows;

$$dF_{AERO-ROTOR} = T^T(\beta_{PRECONE})T^T(\phi)dF_{AERO-BS} \tag{3.24}$$

Since the torque is calculated on the rotor coordinate system, $dF_{GRAV-HUB}$ also needed to be transformed to that coordinate system as;

$$dF_{GRAV-ROTOR} = T(\psi)T(\beta_{TILT})dF_{GRAV-HUB} \tag{3.25}$$

Then the total force acting on a blade element on the rotor coordinate system is found as;

$$dF_{ROTOR} = dF_{AERO-ROTOR} + dF_{GRAV-ROTOR} \tag{3.26}$$

Displacement vector in Equation 3.14 written in the blade coordinate system is carried to the rotor coordinate system as following;

$$r_{ROTOR} = T^T(\beta_{PRECONE}) r_{BLADE} \tag{3.27}$$

Finally, moments affecting a blade element in rotor coordinate system are calculated as;

$$dM_{ROTOR} = r_{ROTOR} \times dF_{ROTOR} = \begin{Bmatrix} dM_x \\ dM_y \\ dM_z \end{Bmatrix} \tag{3.28}$$

where dM_z represents the torque created by a blade element, dQ.
Then, the total torque acting on the rotor is found by integration;

$$Q = N \int dQ \tag{3.29}$$

where N represents the number of blades.

3.4 Power Calculations

Power shows the efficiency of the turbine.
Power generated at each blade element is calculated as;

$$dP = \Omega dQ \tag{3.30}$$

Total aerodynamic power created by rotor is as follows;

$$P = \Omega Q \tag{3.31}$$

Power coefficient is defined as the ratio between energy produced by the wind turbine and the total energy available in the wind. It is formulized as;

$$C_p = \frac{P}{\frac{1}{2}\rho A U^3} \tag{3.32}$$

CHAPTER 4

CONTROLLER DESIGN

The main goal of a variable-speed wind turbine control system is to increase the efficiency. Variable-speed turbines should be controlled for whole operation. In this chapter, a controller for a variable speed HAWT is designed. Firstly, operating regions of variable speed turbine are explained in Section 4.1. Then, a generator torque controller is designed for whole operating regions in Section 4.2. In Section 4.3, a pitch controller that will regulate the rotational speed at the above rated region is added to model.

4.1 Operating Regions

Variable speed wind turbines typically have three main operating regions as shown in Figure 4.1 in terms of the generator speed. Operating regions figure can be considered as a more detailed version of an ideal power curve which is shown previously in Figure 1.3.

When there is enough wind to produce energy, the supervisory controller changes the pitch angle from full feather to the run-pitch position. Once the generator speed reaches to a value, dependent on the wind turbine design, enough to compensate energy loss, the generator torque steps in. The operating region where the generator torque is equal to zero is called region 1.

Region 1-1/2 is a transition region between regions 1 and 2. The generator torque value is increased rapidly to catch desired value for a defined generator speed close to start-up.

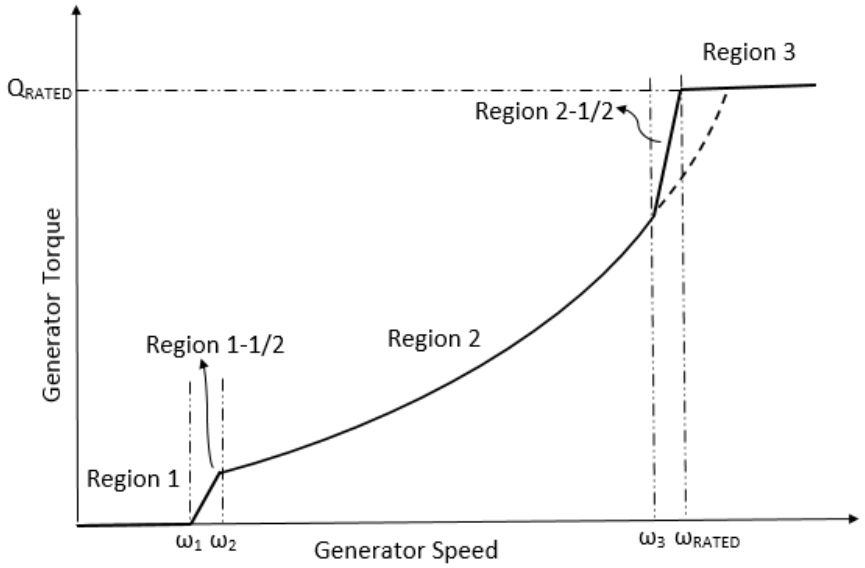

Figure 4.1: Wind Turbine Operating Regions

In region 2, the pitch angle is kept constant at run-pitch value and the generator torque increases with increasing wind speed up to the rated generator torque value which is also turbine dependent. In this region the generator torque controller is active.
For most of the wind turbines, the generator rated speed is achieved at the generator torque values lower than the rated value [48]. This causes low power production at region 3. In order to prevent this situation, in region 2-1/2 the generator torque value increases linearly to reach the rated generator torque at the rated generator speed.
After reaching the rated generator torque value, the generator torque is kept constant. In region 3, the pitch controller gets on the stage to regulate the generator rotational speed. Hence, aerodynamic loads on the turbine do not exceed their safe limits.

4.2 Generator Torque Controller

The purpose of the generator torque controller is to maximize power production for the below rated regions. Power equation is written as following from Equation 3.32;

$$P = \frac{1}{2}\rho C_p A U^3 \tag{4.1}$$

where,

$$A = \pi R^2 \tag{4.2}$$

Tip speed ratio, λ is defined as;

$$\lambda = \frac{\Omega R}{U} \tag{4.3}$$

Inserting Equations 4.3 and 4.2 into Equation 4.1 power equation is rewritten as;

$$P = \frac{1}{2}\rho C_p \pi R^5 \frac{\Omega^3}{\lambda^3} \tag{4.4}$$

Power equation derived above is expressed in terms of the rotor rotational speed, Ω. In order to express it in terms of the generator speed, Equation 4.4 is rearranged as following;

$$P = \frac{1}{2}\rho C_p \pi R^5 \frac{\Omega_{gen}^3}{N_{gear}^3 \lambda^3} \tag{4.5}$$

where N_{gear} is the gearbox ratio and defined as;

$$N_{gear} = \frac{\Omega}{\Omega_{gen}} \tag{4.6}$$

In order to extract maximum power from wind, power coefficient should be at its maximum value during the below rated operation. Power coefficient, C_p, is a function of both the tip speed ratio and the pitch angle. Optimum value of λ at which C_p is maximum is found and used in Equation 4.5 and the pitch angle is kept constant at the optimum value to obtain maximum power.

$$P_{max} = \frac{1}{2}\rho C_{p_{max}} \pi R^5 \frac{\Omega_{gen}^3}{N_{gear}^3 \lambda_{opt}^3} \tag{4.7}$$

The generator torque needed to maintain maximum power is calculated using Equations 3.31 and 4.7 as;

$$Q_{gen} = \frac{P_{max}}{\Omega_{gen}} = \frac{1}{2}\rho C_{p_{max}} \pi R^5 \frac{\Omega_{gen}^2}{N_{gear}^3 \lambda_{opt}^3} \tag{4.8}$$

The generator torque controller uses the generator speed as input and gives the generator torque value needed to maximize power, i.e. maintain the optimum tip speed ratio, as output.

$$Q_{gen} = k\Omega_{gen}^2 \tag{4.9}$$

where,

$$k = \frac{1}{2}\rho C_{p_{max}} \pi R^5 \frac{1}{N_{gear}^3 \lambda_{opt}^3} \tag{4.10}$$

However, $Q_{gen} = k\Omega_{gen}^2$ curve reaches the rated generator speed below the rated generator torque. Since wind turbines are not allowed to exceed the rated speed,

the rated power of the turbine would be low. This problem is solved by inserting a transition region, region 2-1/2, between regions 2 and 3. The aim of region 1-1/2 is similar with region 2-1/2. At these regions, the generator torque increases linearly with the generator speed.

The generator torque at region 1-1/2;

$$Q_{gen} = \frac{Q_2}{\Omega_2 - \Omega_1}(\Omega_{gen} - \Omega_1) \tag{4.11}$$

where

$$Q_2 = k\Omega_2^2 \tag{4.12}$$

The generator torque at region 2-1/2;

$$Q_{gen} = Q_3 + \frac{Q_{RATED} - Q_3}{\Omega_{RATED} - \Omega_3}(\Omega_{gen} - \Omega_3) \tag{4.13}$$

where

$$Q_3 = k\Omega_3^2 \tag{4.14}$$

Ω_1, Ω_2 and Ω_3 values are seen in Figure 4.1 and they are turbine dependent values.

The generator torque value is kept constant at the rated value in region 3.

Finally, the generator controller can be summarized in a scheme as seen in Figure 4.2;

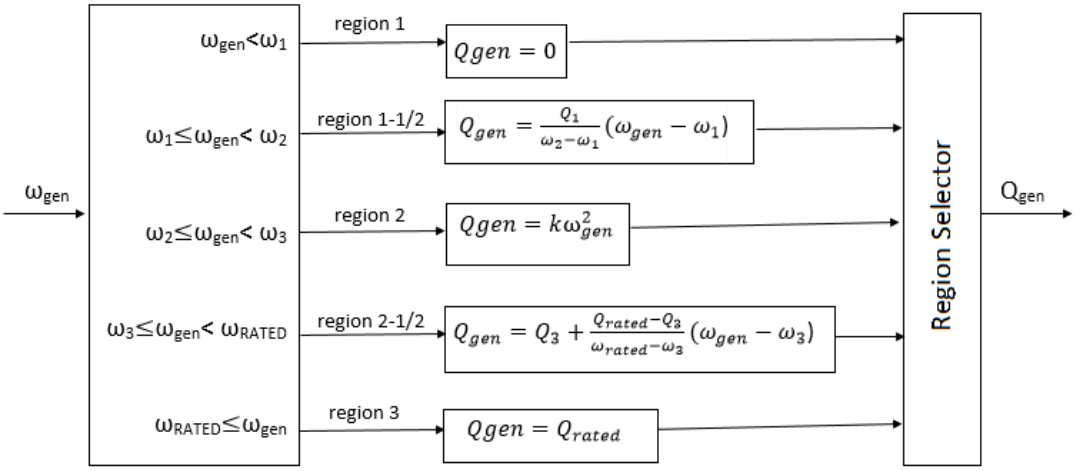

Figure 4.2: Generator Torque Controller Scheme

The generator torque acts in opposite direction to the aerodynamic torque. Thus, the net torque on the wind turbine shaft is found as;

$$Q_{net} = Q_{aero} - N_{gear}Q_{gen} \tag{4.15}$$

Relation between the torque and the rotational acceleration is written as;

$$Q_{net} = I_{total}\dot{\Omega} \tag{4.16}$$

where I_{total} is the total rotational inertia of the turbine and calculated as;

$$I_{total} = I_{rotor} + N_{gear}^2 I_{gen} \tag{4.17}$$

When Q_{net} is positive, $\dot{\Omega}$ is positive and the rotational speed increases to reach the optimum tip speed ratio. On the contrary, negative total torque causes a decrease in the rotational speed in order to maintain the optimum tip speed ratio.

4.3 Pitch Controller

Pitch controller proposed in this thesis keeps the generator speed at its rated value for the above rated regions. It is active in region 3. The pitch angle is constant for other regions at its optimum value which gives maximum power coefficient.
Increasing the pitch angle decreases the angle of attack, as a result the aerodynamic forces are decreased. Relationship between the pitch angle and the angle of attack is seen in Figure 3.6. Aerodynamic forces are the dominant factor creating the rotor torque. By decreasing them both the rotational speed and the aerodynamic loads are limited.
The linear model used for the pitch controller design contains only the rotor rotational speed as the single degree of freedom. The rotational acceleration is found as following from Equation 4.16;

$$\dot{\Omega} = \frac{Q_{net}}{I_{total}} \tag{4.18}$$

Aerodynamic torque term used to calculate Q_{net} is a function of the wind speed, U, the rotor speed, Ω, and the pitch angle, β. It can be expanded using Taylor Series neglecting higher order terms as following;

$$Q_{aero} = Q_{aero}(U_0, \Omega_0, \beta_o) + \frac{\partial Q_{aero}}{\partial U}\delta U + \frac{\partial Q_{aero}}{\partial \Omega}\delta\Omega + \frac{\partial Q_{aero}}{\partial \beta}\delta\beta \tag{4.19}$$

where U_0, Ω_0, β_o are nominal values at the equilibrium and δU, $\delta\Omega$, $\delta\beta$ are perturbations. Perturbations are assumed to present small deviations of these variables away

from their equilibrium values at steady state. Perturbed aerodynamic torque is defined as following;

$$\delta Q_{aero} = Q_{aero}(U, \Omega, \beta) - Q_{aero}(U_0, \Omega_0, \beta_0) \tag{4.20}$$

Using Equations 4.18, 4.20 and 4.15 and assuming the rotational acceleration, $\dot{\Omega}$, at the equilibrium is zero, perturbed rotational acceleration is found as;

$$\delta\dot{\Omega} = \frac{1}{I_{total}} \left(Q_{aero}(U_0, \Omega_0, \beta_0) + \delta Q_{aero} - N_{gear} Q_{gen} \right) \tag{4.21}$$

Since at the equilibrium there is no rotational acceleration then;

$$Q_{aero}(U_0, \Omega_0, \beta_0) - N_{gear} Q_{gen} = 0 \tag{4.22}$$

Finally, the linear model used for the pitch controller design is found as;

$$\delta\dot{\Omega} = \frac{1}{I_{total}} \left(\frac{\partial Q_{aero}}{\partial U}\delta U + \frac{\partial Q_{aero}}{\partial \Omega}\delta\Omega + \frac{\partial Q_{aero}}{\partial \beta}\delta\beta \right) \tag{4.23}$$

For simplicity A_U, A_Ω and A_β abbreviations will be used to define the derivatives of aerodynamic torque. Where,

$$A_U = \frac{1}{I_{total}} \frac{\partial Q_{aero}}{\partial U} \tag{4.24}$$

$$A_\Omega = \frac{1}{I_{total}} \frac{\partial Q_{aero}}{\partial \Omega} \tag{4.25}$$

$$A_\beta = \frac{1}{I_{total}} \frac{\partial Q_{aero}}{\partial \beta} \tag{4.26}$$

and

$$\delta\dot{\Omega} = A_U \delta U + A_\Omega \delta\Omega + A_\beta \delta\beta \tag{4.27}$$

Proportional Integral Derivative (PID) controller will be used to regulate the turbine speed. The pitch perturbation is related to the rotational speed perturbation by PID controller as;

$$\delta\beta(t) = K_p \delta\Omega(t) + K_i \int \delta\Omega(t)dt + K_d \delta\dot{\Omega}(t) \tag{4.28}$$

where K_p, K_i and K_d represents proportional, integral and derivative gains respectively. Inserting Equation 4.28 into Equation 4.23, the rotational acceleration in time domain is found as;

$$\delta\dot{\Omega}(t) = A_U \delta U(t) + A_\Omega \delta\Omega(t) + A_\beta \left(K_p \delta\Omega(t) + K_i \int \delta\Omega(t)dt + K_d \delta\dot{\Omega}(t) \right) \tag{4.29}$$

Rewriting Equation 4.29 in Laplace domain, the rotational speed is found as;

$$s\delta\Omega(s) = A_U\delta U(s)+A_\Omega\delta\Omega(s)+A_\beta\left(K_p\delta\Omega(s) + K_i\frac{1}{s}\delta\Omega(s) + K_d s\delta\Omega(s)\right) \quad (4.30)$$

Collecting all $\delta\Omega(s)$ terms on the right hand side and rearranging s terms considering their orders, the linear model is written as;

$$\left[\left(1 - A_\beta K_d\right)s^2 + \left(-A_\Omega - A_\beta K_p\right)s + \left(-A_\beta K_i\right)\right]\delta\Omega(s) = sA_U\delta U(s) \quad (4.31)$$

Closed-loop transfer function, TF_c, between the output, $\delta\Omega(s)$, and the input, $\delta U(s)$ is obtained from Equation 4.31 as following;

$$TF_c = \frac{\delta\Omega(s)}{\delta U(s)} = \frac{sA_U}{\left(1 - A_\beta K_d\right)s^2 + \left(-A_\Omega - A_\beta K_p\right)s + \left(-A_\beta K_i\right)} \quad (4.32)$$

Denominator of the transfer function gives the characteristic equation of the system. Stability analysis are done using this equation. To have a stable system, all roots of the characteristic equation should have negative real parts. To find the roots of the characteristic equation, it is written as;

$$\left(1 - A_\beta K_d\right)s^2 + \left(-A_\Omega - A_\beta K_p\right)s + \left(-A_\beta K_i\right) = 0 \quad (4.33)$$

For an equation written in the form of $as^2 + bs + c$, all roots have negative real parts if constants a, b, c are all positive [36]. Therefore, for a stable system, conditions to be ensured are given as;

$$\begin{aligned} 1 - A_\beta K_d &> 0 \\ -A_\Omega - A_\beta K_p &> 0 \\ -A_\beta K_i &> 0 \end{aligned} \quad (4.34)$$

Moreover, Equation 4.33 can be written in the form of the system damping ratio, ξ, and the natural frequency, ω as;

$$s^2 + 2\xi\omega s + \omega^2 = 0 \quad (4.35)$$

where

$$2\xi\omega = \frac{-A_\Omega - A_\beta K_p}{1 - A_\beta K_d} \quad (4.36)$$

and

$$\omega^2 = \frac{-A_\beta K_i}{1 - A_\beta K_d} \quad (4.37)$$

Gain values are found as;

$$K_p = \frac{2\xi\omega\left(A_\beta K_d - 1\right) - A_\Omega}{A_\beta} \tag{4.38}$$

$$K_i = \frac{\omega^2\left(A_\beta K_d - 1\right)}{A_\beta} \tag{4.39}$$

Values of ξ and ω affect the turbine performance. Some studies suggest that choosing ξ value between 0.6 to 0.7 and ω value 0.6 gives good performance [17]. However, these values are turbine dependent and performance should be examined for different values.

K_d value should be decided considering conditions given in Equation 4.34 to calculate K_p and K_i values. So choosing $K_d = 0$, K_p and K_i are found as;

$$K_p = \frac{-2\xi\omega - A_\Omega}{A_\beta} \tag{4.40}$$

$$K_i = \frac{-\omega^2}{A_\beta} \tag{4.41}$$

In order to find A_Ω, A_β, and A_U values, firstly an operation point at region 3 is chosen. Then, small perturbations are applied to that operating point to calculate partial derivatives. Give small perturbations to the pitch angle and calculate $\partial Q_{aero}/\partial\beta$ and repeat this for other variables. Partial derivative is calculated using Taylor series as follows;

$$Q_{aero_{i+1}} = Q_{aero_i} + \frac{\partial Q_{aero}}{\partial\beta}\delta\beta \tag{4.42}$$

where i shows point before perturbation and $i+1$ shows point after perturbation.

After calculating A_Ω, A_β, and A_U and deciding ξ and ω values, K_p and K_i values are calculated. Since K_d value is chosen as zero, the controller is now called proportional-integral (PI) controller. The controller scheme applied to pitch to regulate the rotational speed is seen in Figure 4.3.

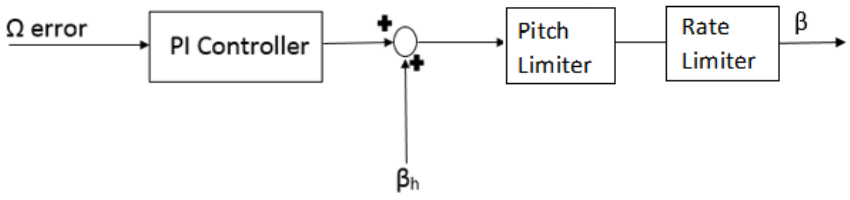

Figure 4.3: Pitch Controller Scheme

β_h represents the pitch angle value at the point where linearization is done. It is added to the pitch value obtained from PI controller and this summation gives the total pitch command. The pitch command going to the dynamic model is limited. The lower limit is equal to region 2 optimum pitch angle and the upper limit is very close to full feathered blade pitch. Moreover, a rate limiter is added to avoid high pitch fluctuations.

CHAPTER 5

RESULTS AND DISCUSSIONS

5.1 Verification of the Model

Verification is essential in creating a dynamic model. In this thesis, a horizontal axis, upwind three-bladed wind turbine is modelled and verification is done by using the LMS Samtech, Samcef for Wind Turbines software [39]. Aerodynamic verification tutorial is followed for whole procedure [8].

In Samcef simulation, rotor blades are assumed rigid and wind shear is ignored in order to create a turbine model similar with the model designed in this thesis. Gravitational forces are not taken into consideration since they do not have any impact on aerodynamic results. Three different load cases are used in order to verify the model for its operational envelope. These load cases are below rated, rated and above rated load cases. Their wind speed, rotor speed and pitch angle configurations are given in Appendix A

Same model properties with S4WT are used in the model created in MATLAB/Simulink. Blade section properties such as distance from root, chord and twist angle are given in Appendix A. Airfoils used in these sections and their lift and drag coefficient distributions are also shown.

Lift and drag coefficients of three airfoils used in blades are given in tutorial for some angle of attack values. In order to make them available for all angle of attack values from -180 degree to 180 degree, interpolation is done in Matlab. The accuracy of interpolation results are shown in Figures 5.1, 5.2 and 5.3. For inner three sections, cylindrical cross sections with constant lift and drag coefficients are used.

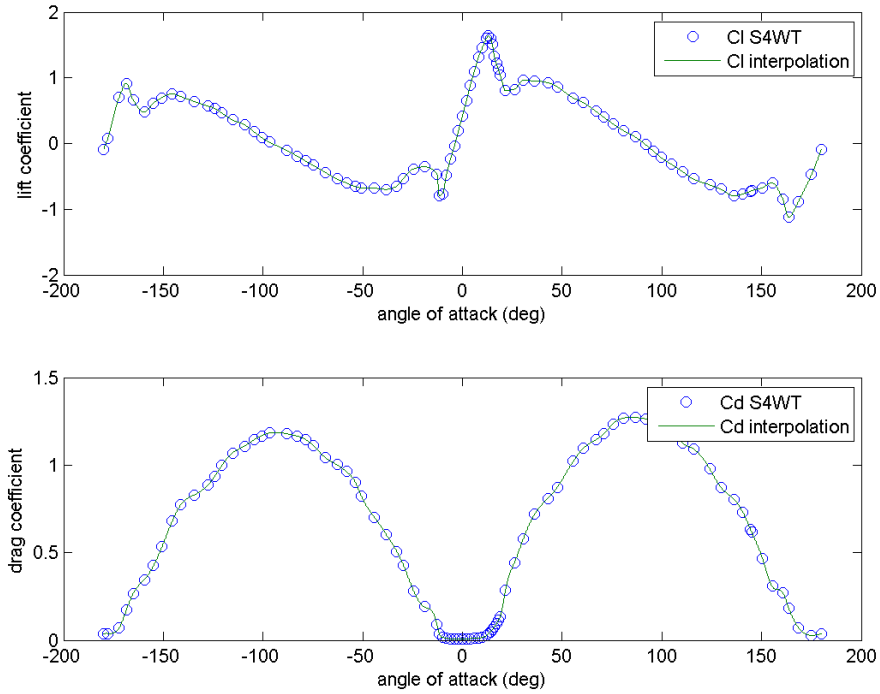

Figure 5.1: Cl and Cd Data and Interpolated Values for Airfoil LS1m13

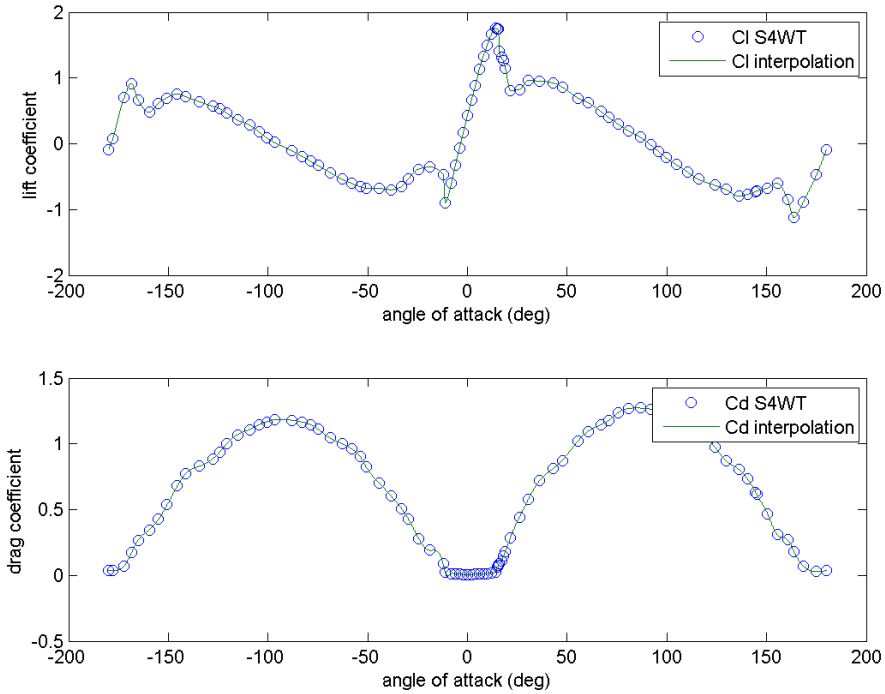

Figure 5.2: Cl and Cd Data and Interpolated Values for Airfoil LS1m17

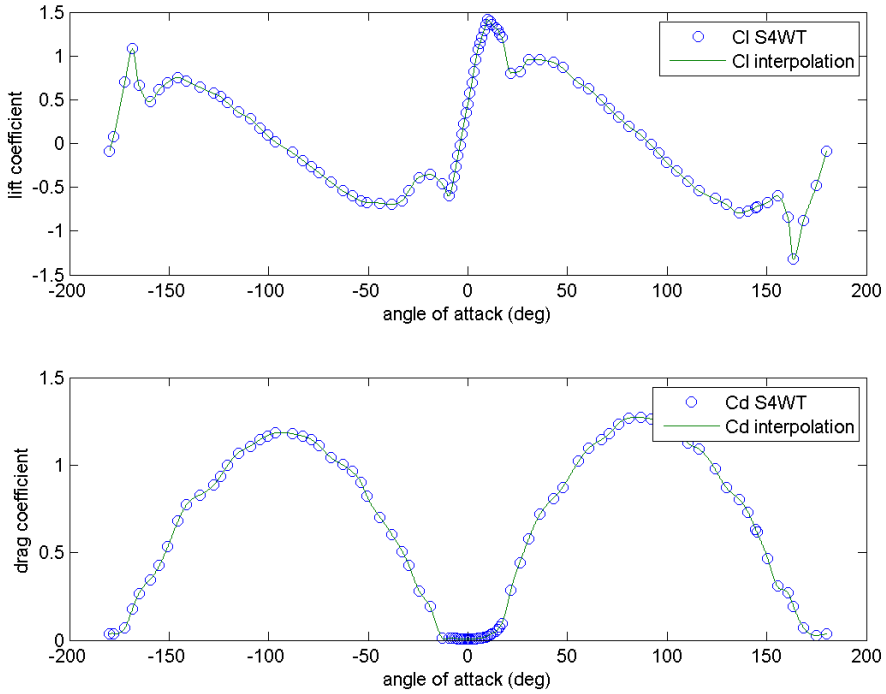

Figure 5.3: Cl and Cd Data and Interpolated Values for Airfoil LS1m21

The axial and the tangential induction factors are calculated by iteration as explained in Section 2.3.4. The iteration is stopped when the defined error is less than a limit value hence convergence is ensured. The tip-hub loss factor is also calculated in this iteration. After a and a' calculated, the inflow angle angle, the angle of attack values and the velocities are found. By using the angle of attack value, lift and drag coefficients are obtained from interpolated data of the airfoil used in that section. Lift and drag values are calculated using velocities and coefficients. Finally, the tangential and the normal forces, and torque are found. This process is repeated for each section along the blade span. Moments created in each section are summed to find the total moment on a blade. Properties of each blade is calculated by changing the azimuth angle. Aerodynamic torque on the rotor is calculated by summation of torque values of each blade. Power and power coefficients are calculated from the total torque as explained in Section 3.4.

5.1.1 Below Rated Loading Case

For the below rated load case, wind speed of 8 m/s and constant rotational speed of 13 rpm are applied. The pitch angle is kept zero since for the below rated wind speeds, pitch is not an active control strategy.

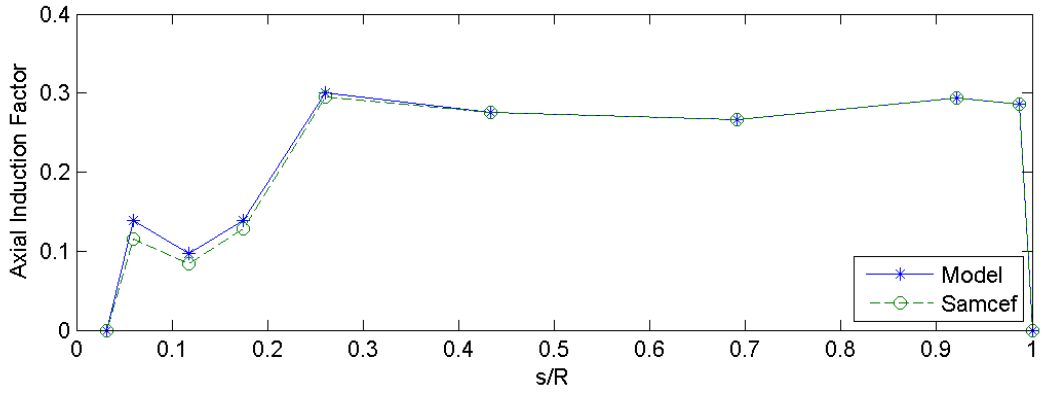

Figure 5.4: Below Rated Loading Case Axial Induction Factors

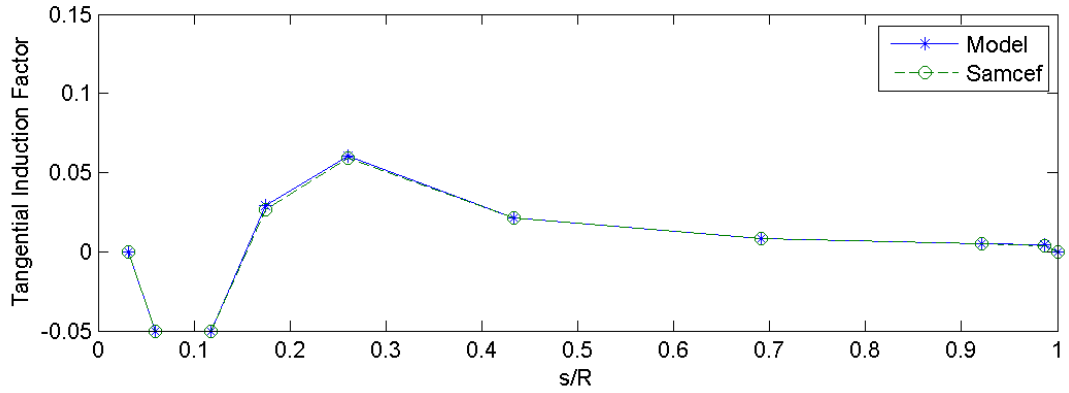

Figure 5.5: Below Rated Loading Case Tangential Induction Factors

Figures 5.4 and 5.5 show a comparison of axial and tangential induction factor between the model and the Samcef outputs, separately. It is seen that there is a small difference at axial induction factor value at sections close to the hub. Difference is caused by the tip-hub loss factor difference seen in Figure 5.6. Since the model has a smaller F, it has a bigger a. Relation between them can be seen in Chapter 2. Difference might be caused by the use of a different correction for hub loss in the Samcef.

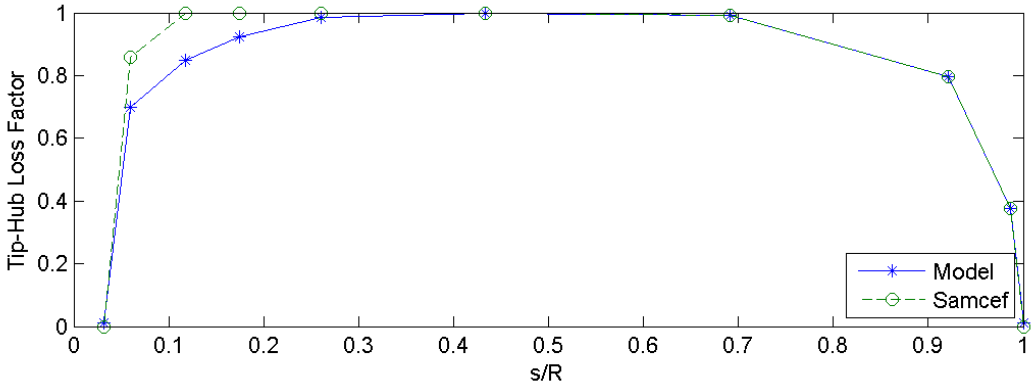

Figure 5.6: Below Rated Loading Case Tip-Hub Loss Factor

The perpendicular velocity component is directly affected from the axial induction factor (see Figure 5.8.

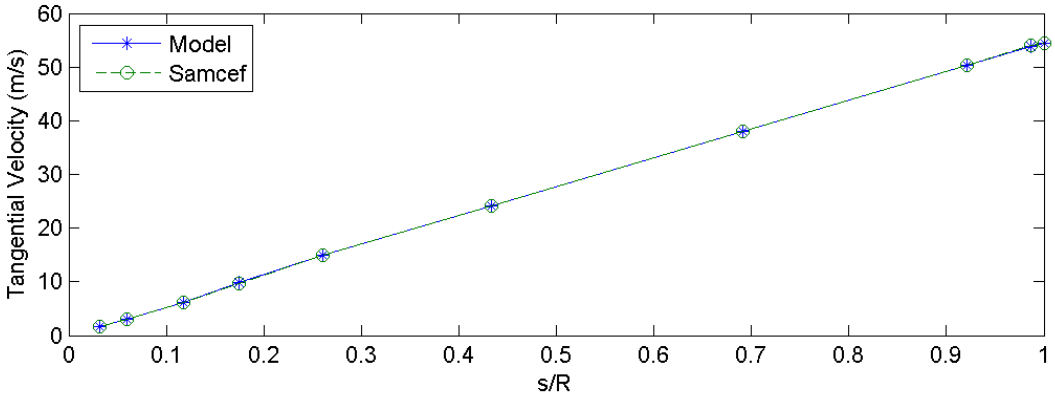

Figure 5.7: Below Rated Loading Case Tangential Velocity Component

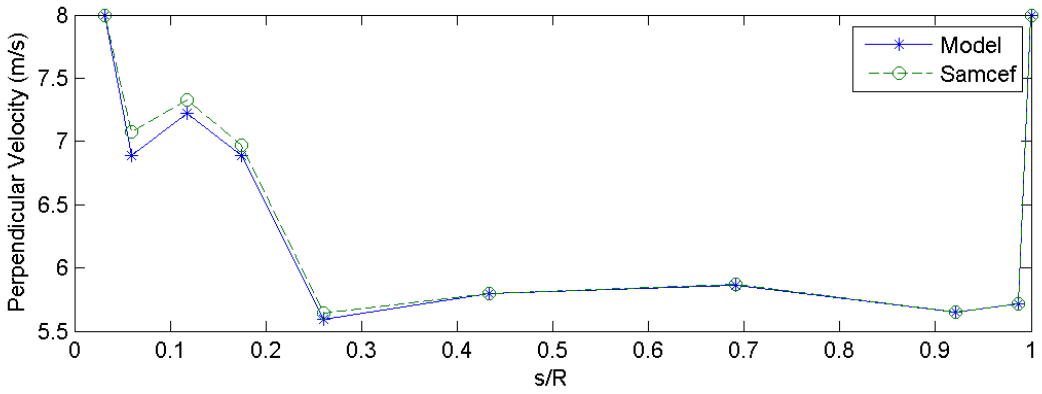

Figure 5.8: Below Rated Loading Case Perpendicular Velocity Component

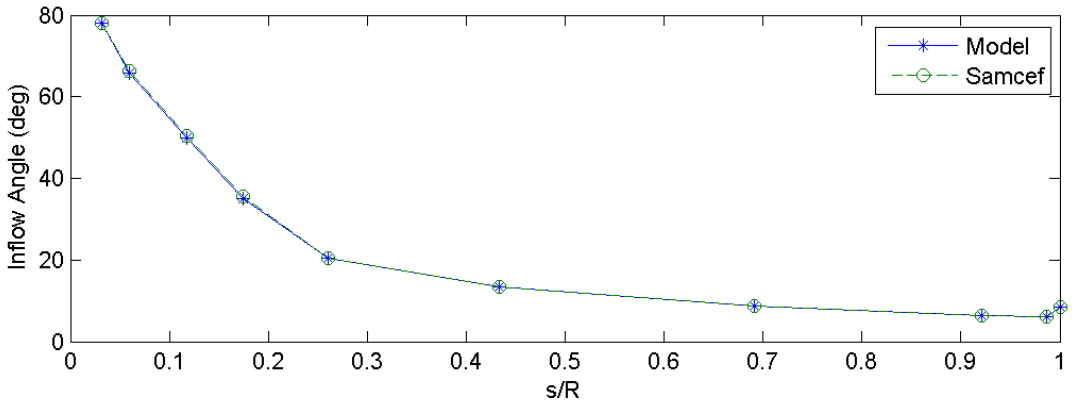

Figure 5.9: Below Rated Loading Case Inflow Angle

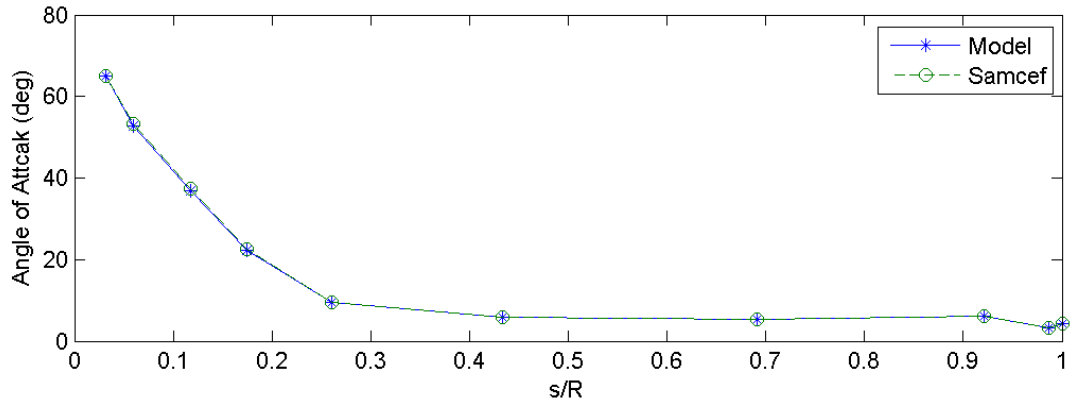

Figure 5.10: Below Rated Loading Case Angle of Attack

Difference in sections close to the hub does not affect the performance of the wind turbine. First three sections of the blade are not airfoil shaped. They are cylindrical sections with constant lift and drag coefficients. As seen from Figures 5.11 and 5.12, hub loss coefficient has no effect on lift and drag coefficients hence sectional lift and drag forces.

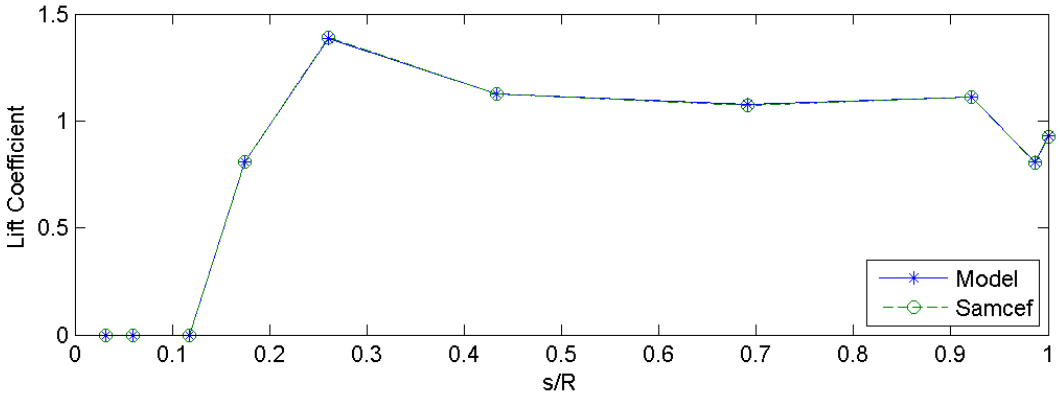

Figure 5.11: Below Rated Loading Case Lift Coefficient

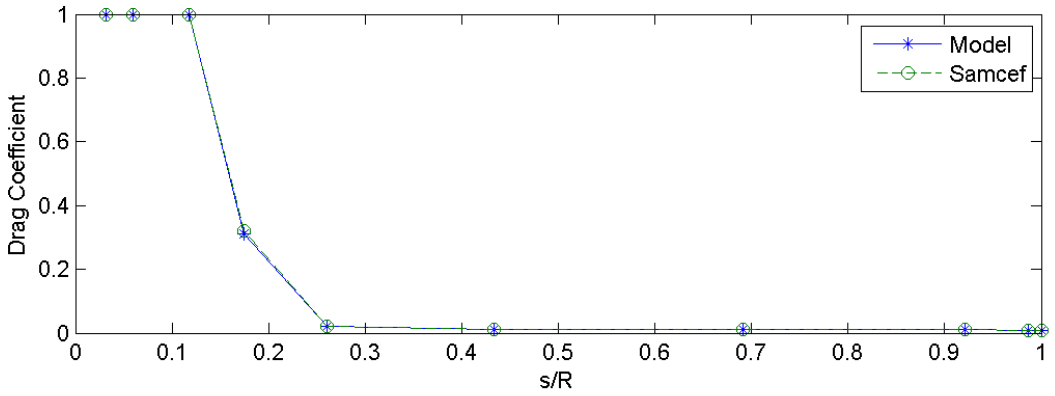

Figure 5.12: Below Rated Loading Case Drag Coefficient

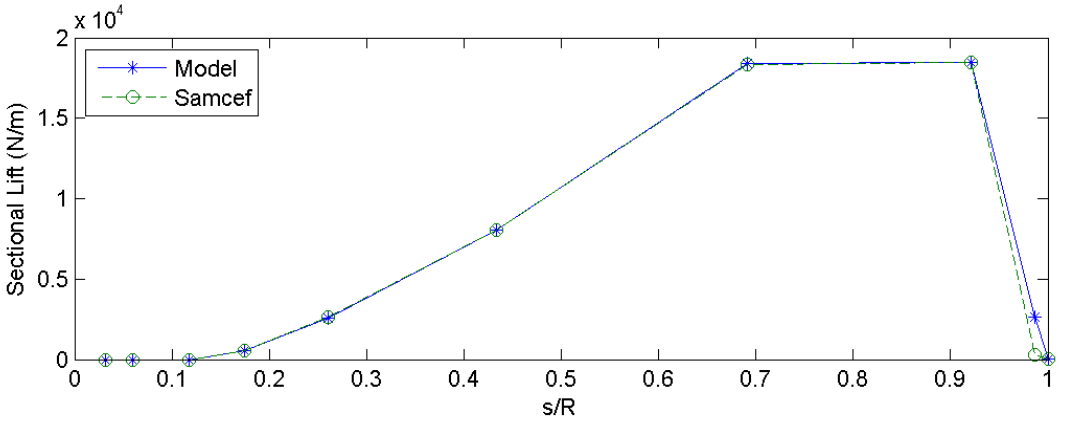

Figure 5.13: Below Rated Loading Case Sectional Lift

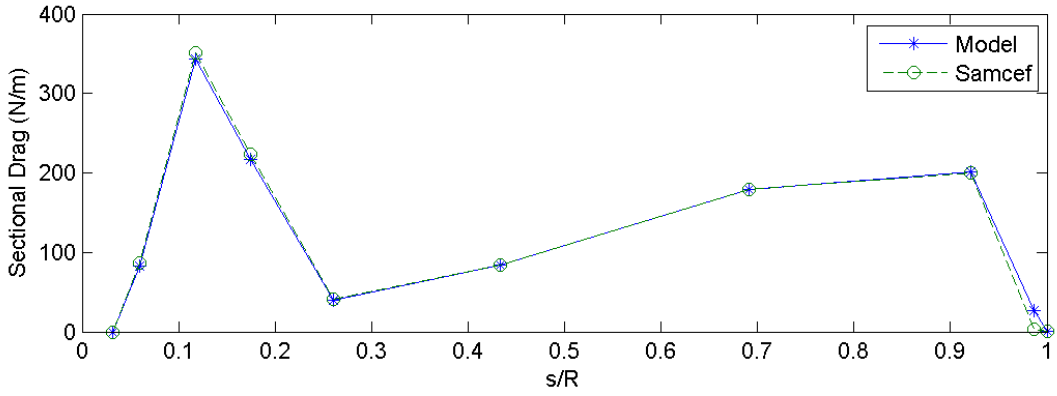

Figure 5.14: Below Rated Loading Case Sectional Drag

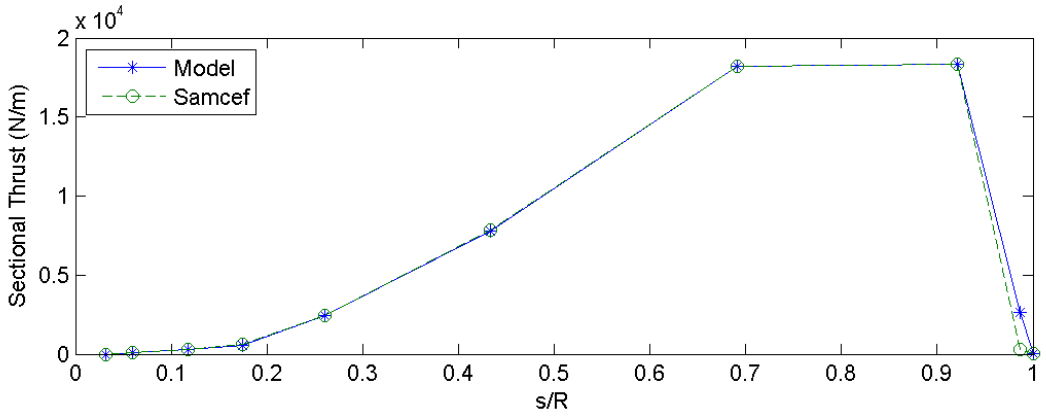

Figure 5.15: Below Rated Loading Case Sectional Thrust

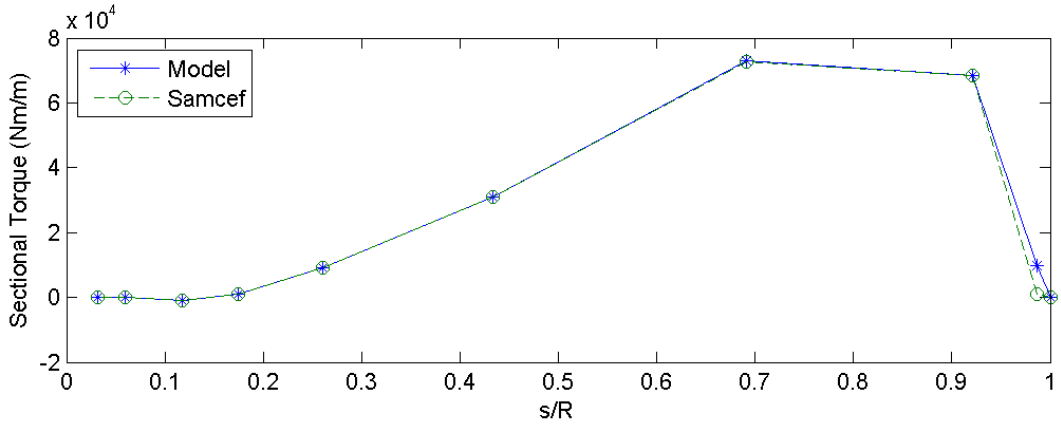

Figure 5.16: Below Rated Loading Case Sectional Torque

Finally, for the below rated load case, all outputs are quite similar with the Samcef. Only difference occurs at sections where hub loss correction is implemented.

5.1.2 Rated Loading Case

For the rated load case, wind speed is 12 m/s, and rotational speed is 15 rpm. The pitch angle is still zero since the pitch controller becomes active the when wind speed passes the rated value.

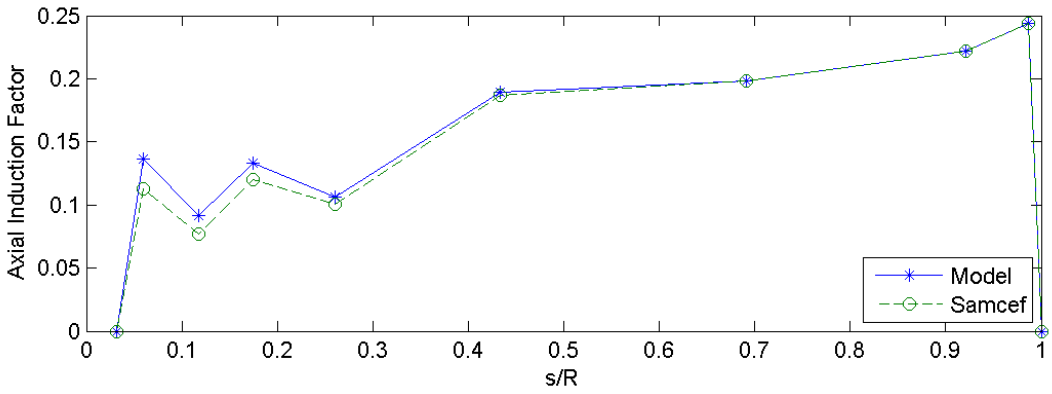

Figure 5.17: Rated Loading Case Axial Induction Factors

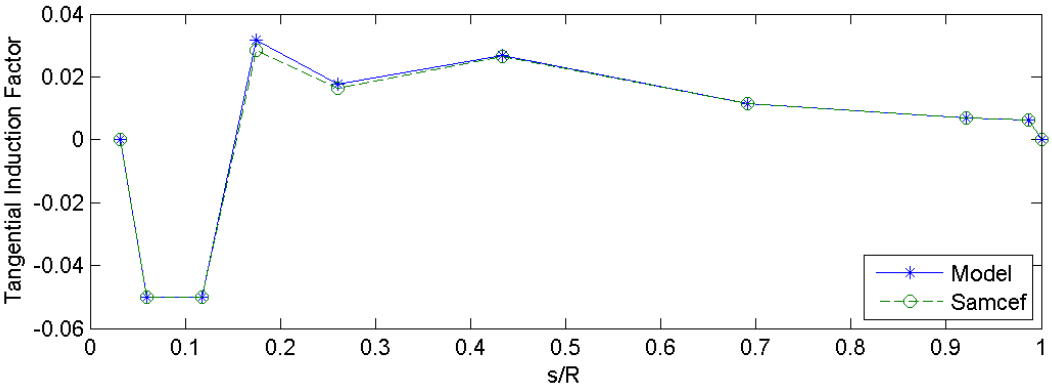

Figure 5.18: Rated Loading Case Tangential Induction Factors

Difference in both the axial and the tangential induction factors (see Figures 5.17 and 5.18) are caused by the hub loss factor (see Figure 5.19).

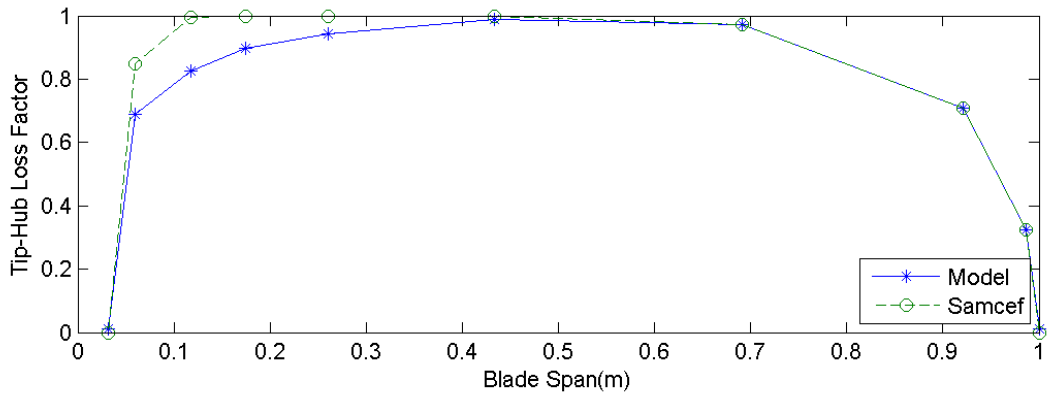

Figure 5.19: Rated Loading Case Tip-Hub Loss Factor

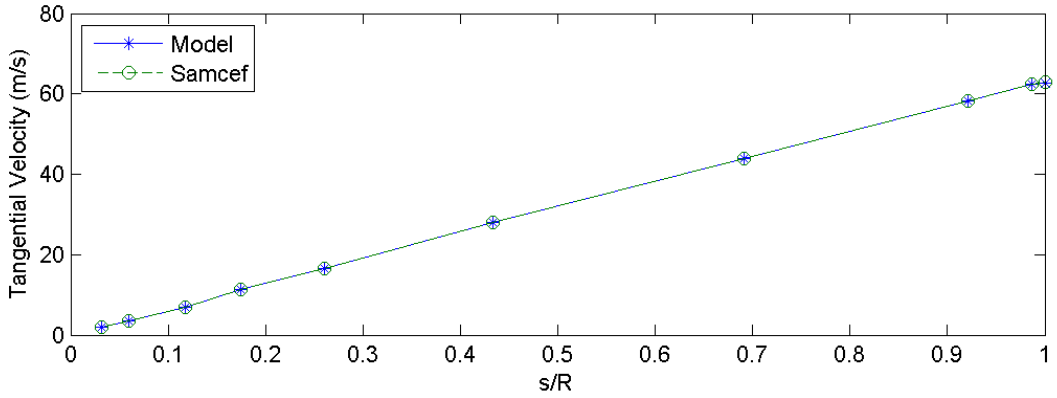

Figure 5.20: Rated Loading Case Tangential Velocity Component

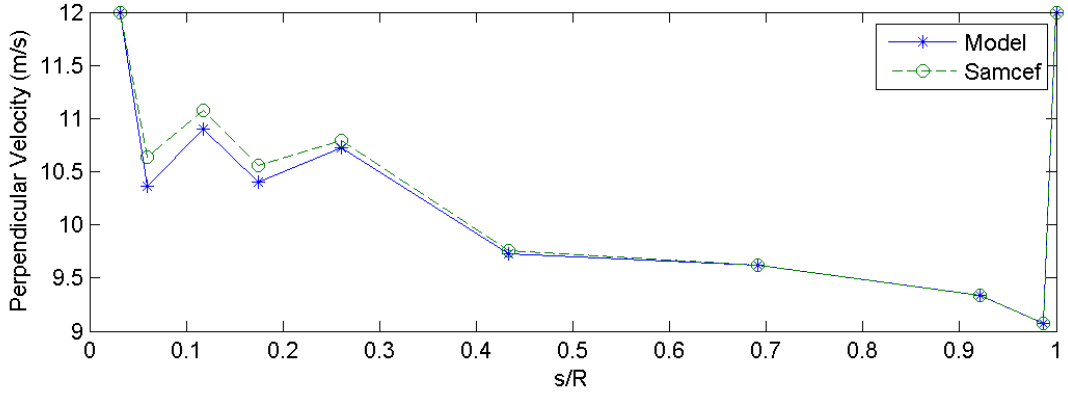

Figure 5.21: Rated Loading Case Perpendicular Velocity Component

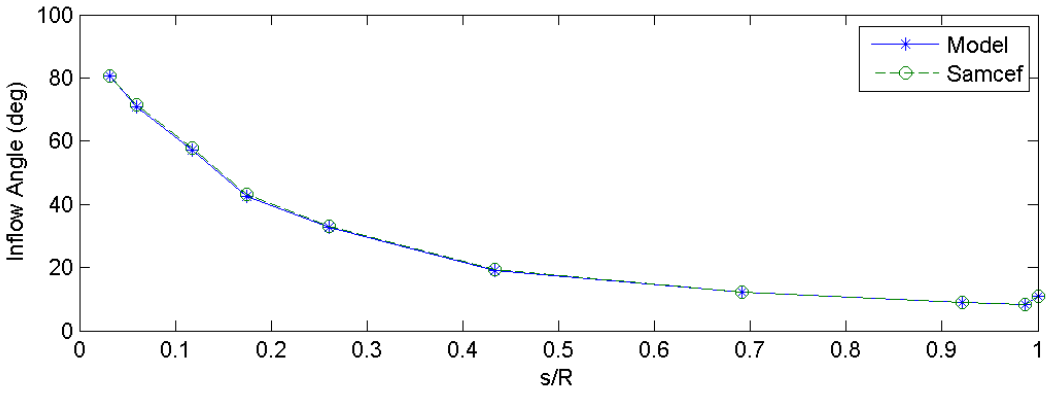

Figure 5.22: Rated Loading Case Inflow Angle

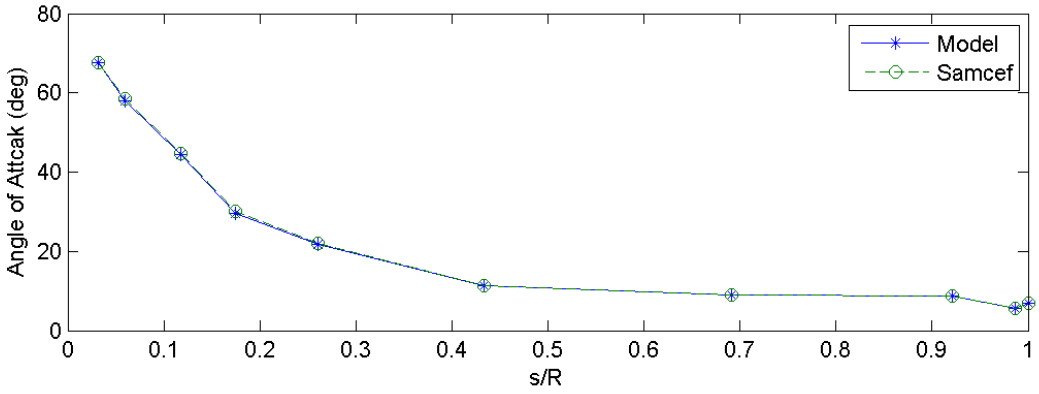

Figure 5.23: Rated Loading Case Angle of Attack

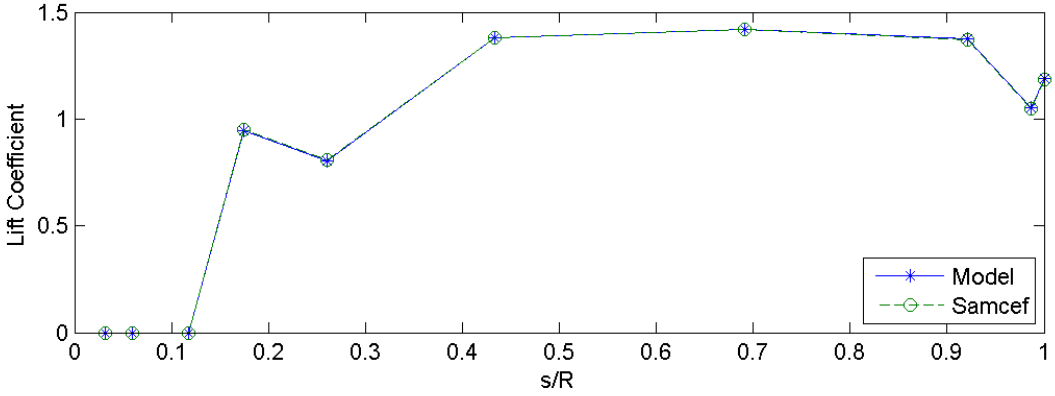

Figure 5.24: Rated Loading Case Lift Coefficient

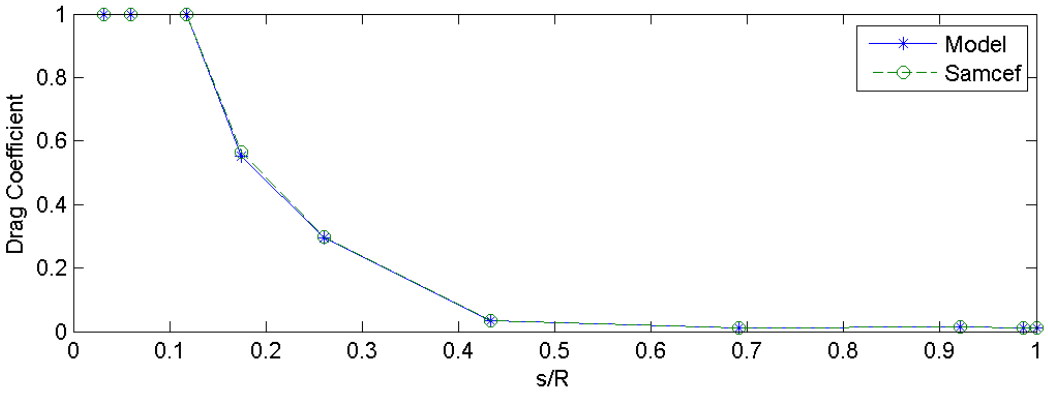

Figure 5.25: Rated Loading Case Drag Coefficient

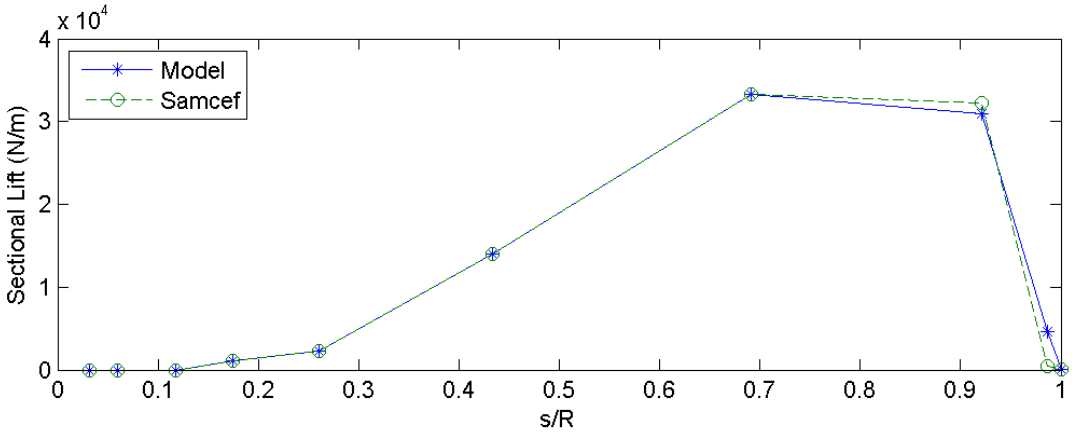

Figure 5.26: Rated Loading Case Sectional Lift

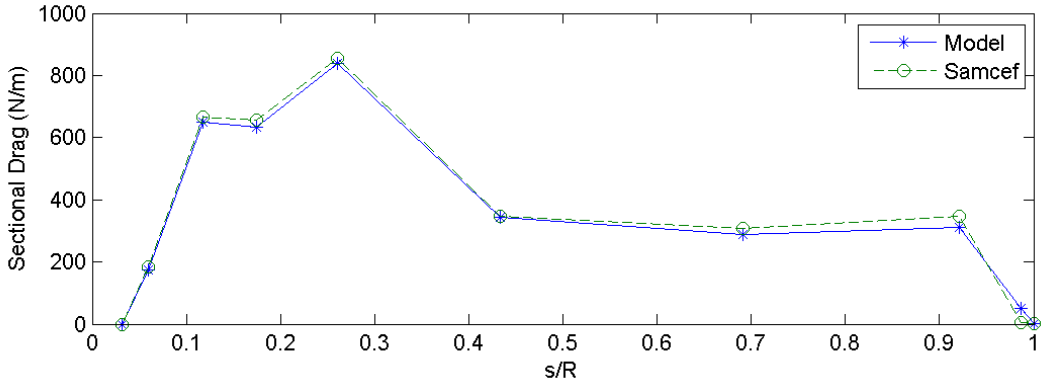

Figure 5.27: Rated Loading Case Sectional Drag

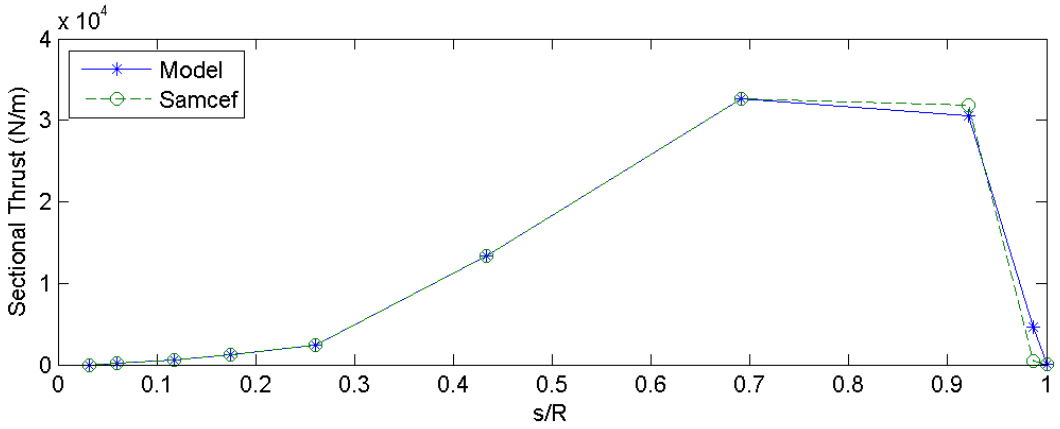

Figure 5.28: Rated Loading Case Sectional Thrust

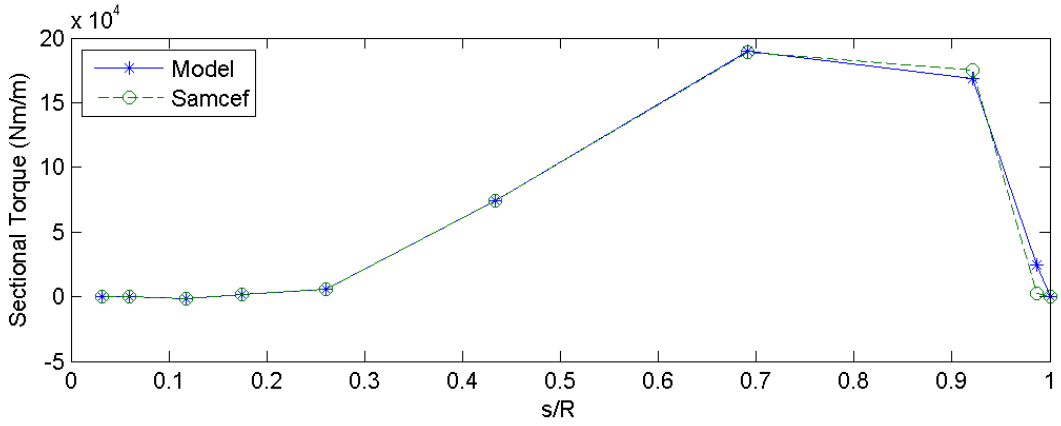

Figure 5.29: Rated Loading Case Sectional Torque

Simulation results of both the Samcef and the model are almost matched for the rated load case. Small differences occur due to the tip-hub loss calculation variation whose effect is seen at last steps; sectional thrust and torque values as seen in Figures 5.28 and 5.29.

5.1.3 Above Rated Loading Case

For the rated load case, wind speed is 18 m/s, and rotational speed is 15 rpm. There is a constant 10 degree pitch angle in order to keep the rotational speed constant for the given wind speed.

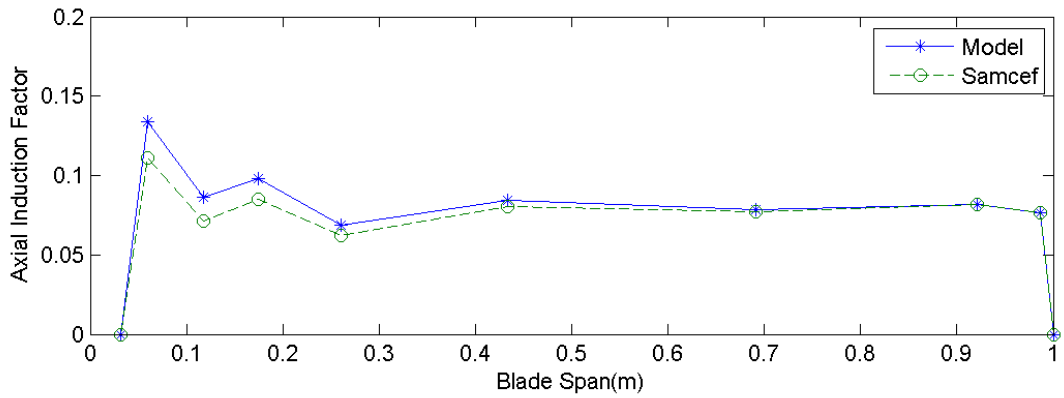

Figure 5.30: Above Rated Loading Case Axial Induction Factors

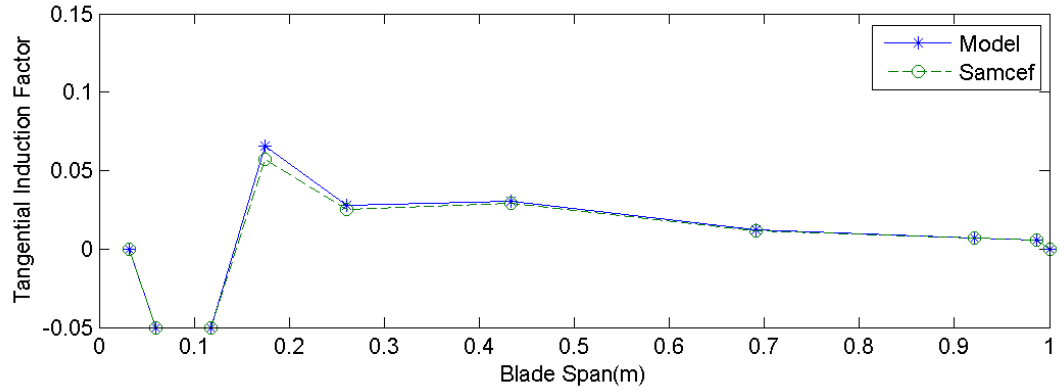

Figure 5.31: Above Rated Loading Case Tangential Induction Factors

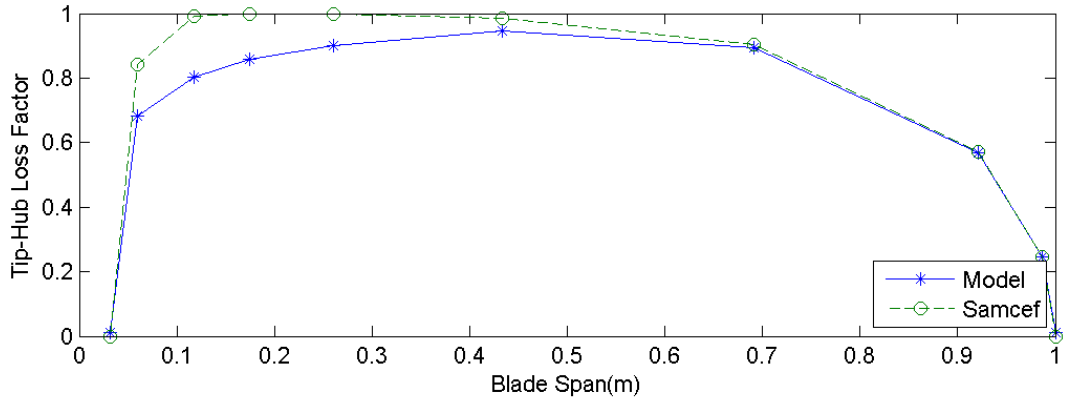

Figure 5.32: Above Rated Loading Case Tip-Hub Loss Factor

Difference between the tip-hub loss factors increases with the increasing wind speed,

which can be seen comparing Figures 5.6, 5.19 and 5.32. The tip-hub loss correction factor used in this thesis is not directly related to the wind speed but it is related with the inflow angle. Despite the inflow angle outputs are very similar (see Figure 5.35) the tip-hub loss factors are resulted differently. And most of this variation occurs at sections close to the hub. The possible reasons the use of a different correction factor the hub loss by the Samcef.

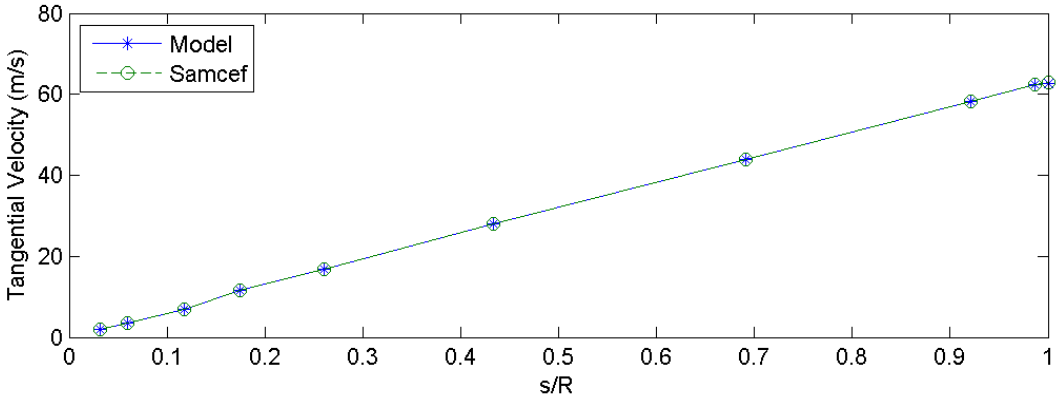

Figure 5.33: Above Rated Loading Case Tangential Velocity Component

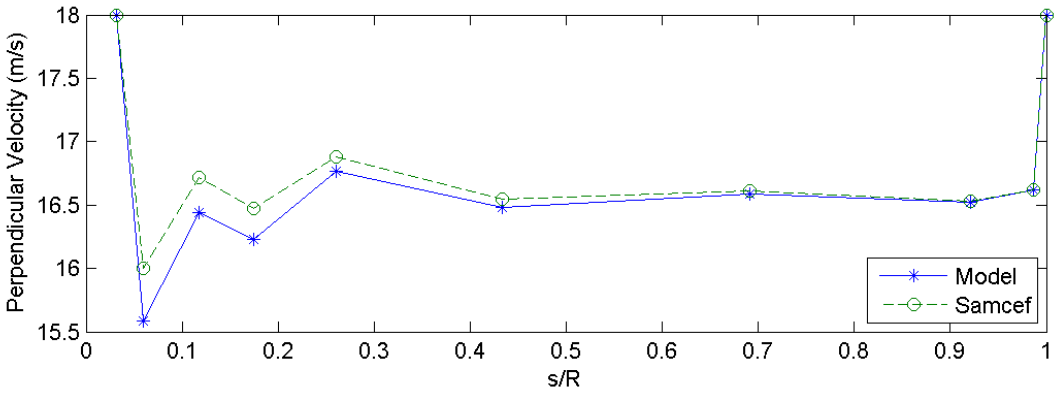

Figure 5.34: Above Rated Loading Case Perpendicular Velocity Component

Difference in the hub loss factors affect the axial induction factor and hence the perpendicular velocity component as seen in Figure 5.34.

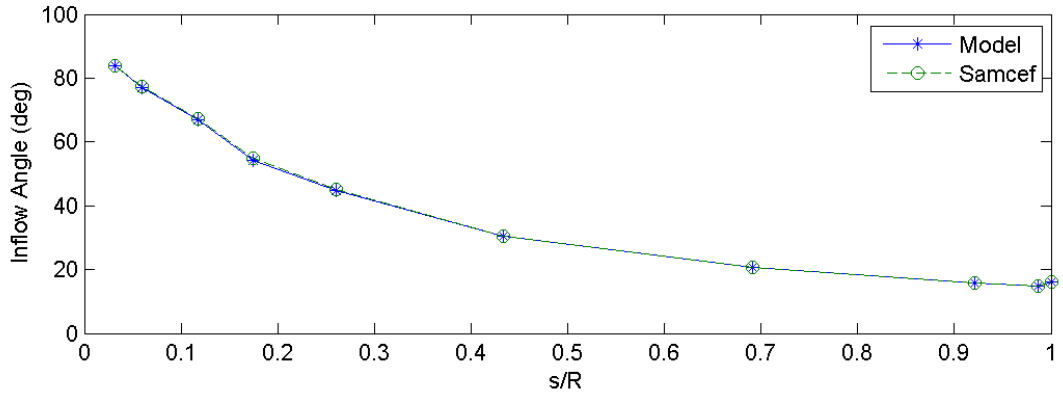

Figure 5.35: Above Rated Loading Case Inflow Angle

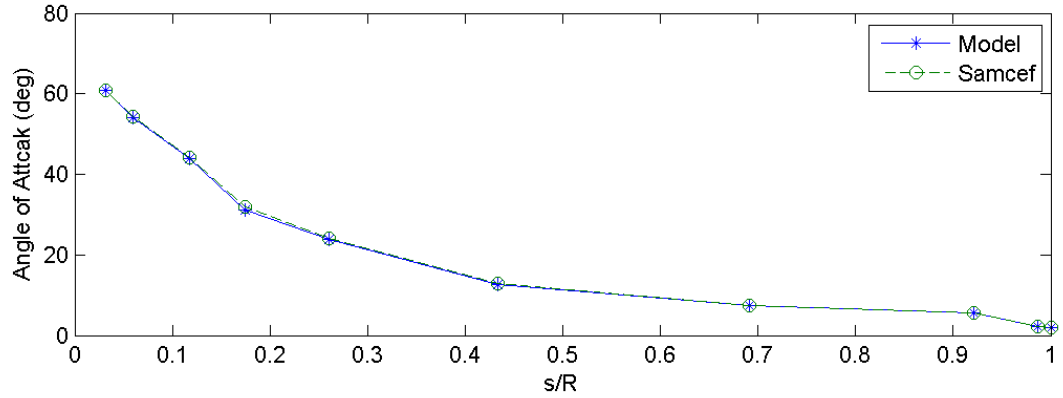

Figure 5.36: Above Rated Loading Case Angle of Attack

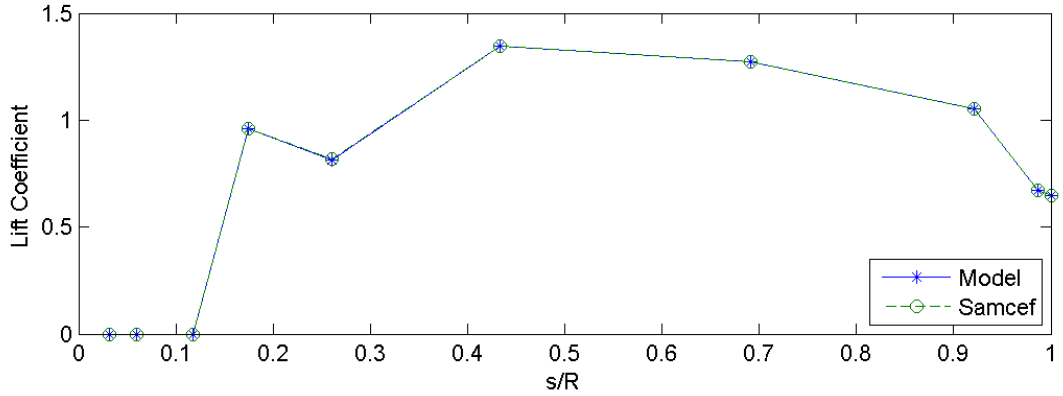

Figure 5.37: Above Rated Loading Case Lift Coefficient

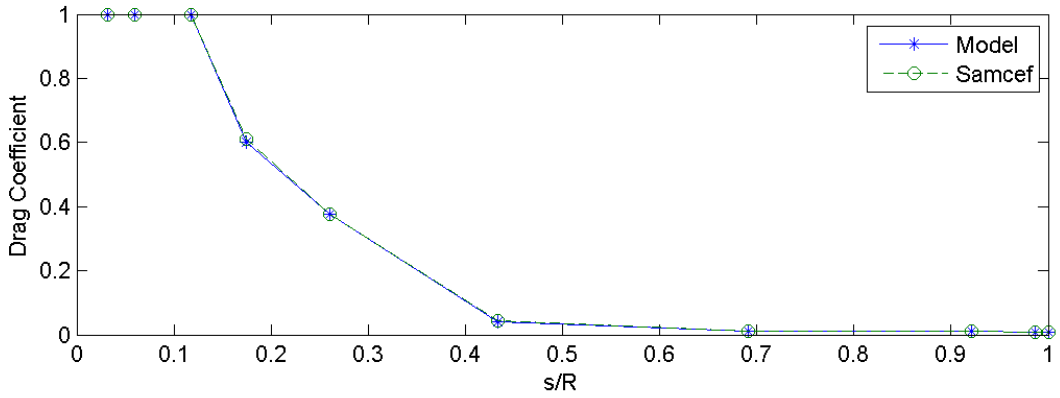

Figure 5.38: Above Rated Loading Case Drag Coefficient

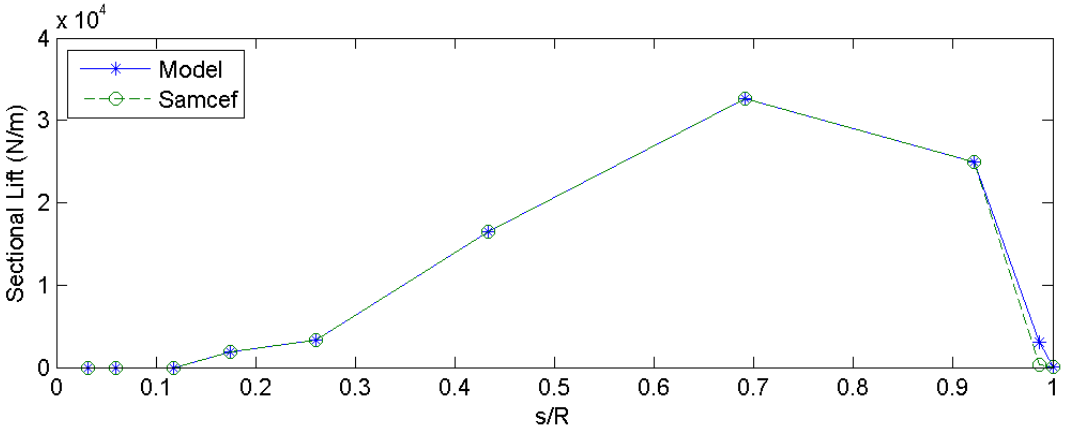

Figure 5.39: Above Rated Loading Case Sectional Lift

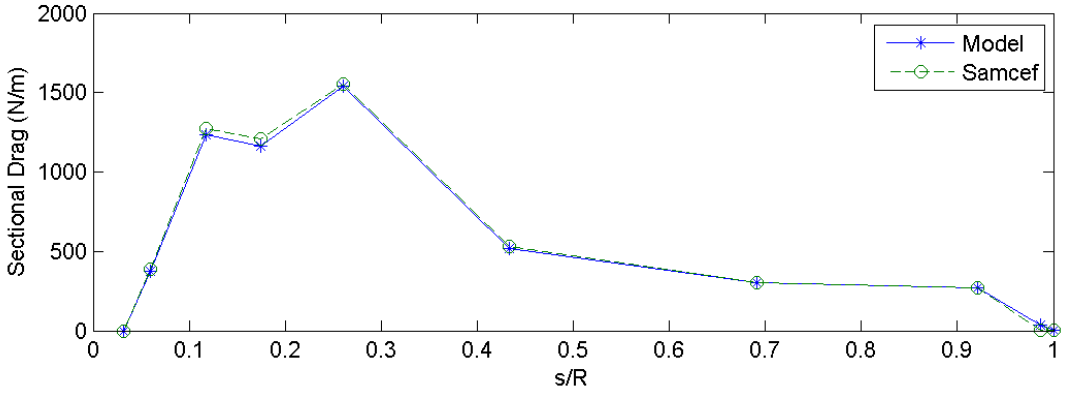

Figure 5.40: Above Rated Loading Case Sectional Drag

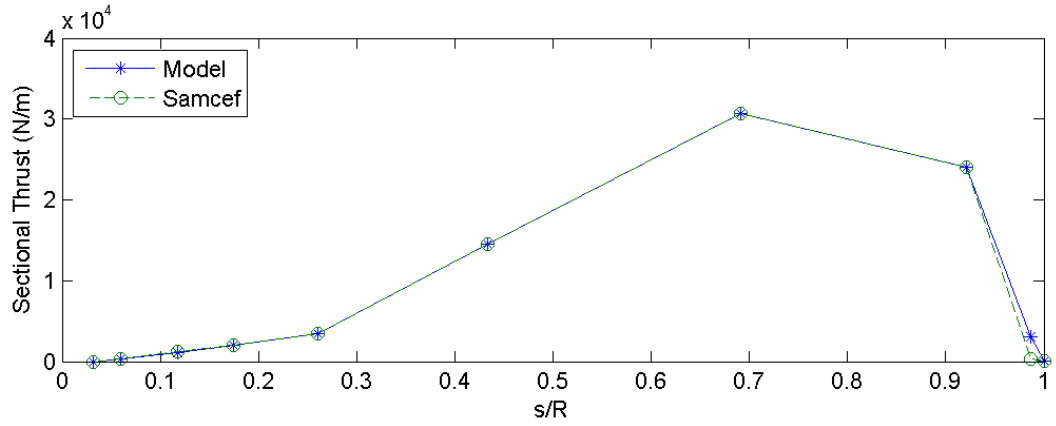

Figure 5.41: Above Rated Loading Case Sectional Thrust

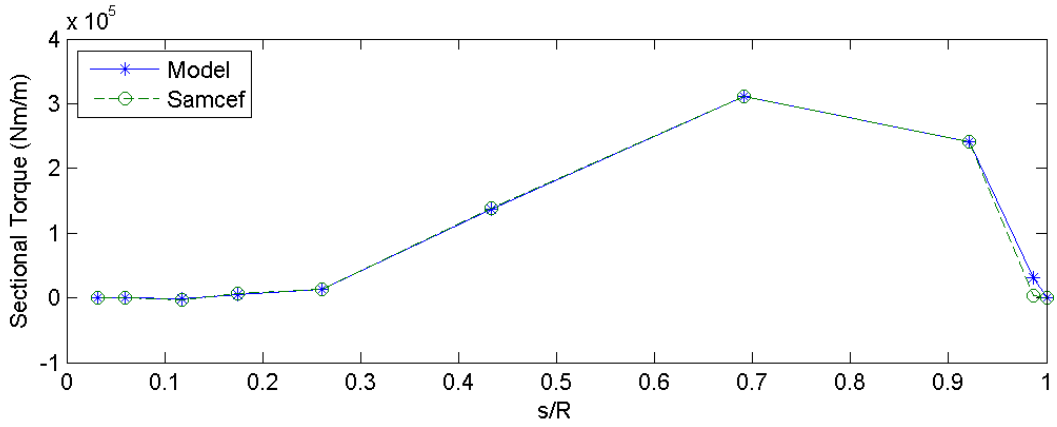

Figure 5.42: Above Rated Loading Case Sectional Torque

Like the rated load case, the above rated load case outputs are quite similar with the Samcef simulation.

For all three load cases, the tangential induction factor is limited to -0.05 for minimum value since the Samcef does not allow smaller values. The results are not realistic for the first three sections near the hub. However, as explained before the first three sections of the blade are not airfoil shaped. Circular-shaped blade is used near the hub and pure drag forces are acting these sections. Therefore, aerodynamic analysis in these sections are less important then other sections.

Table 5.1 shows the comparison of the aerodynamic torque, the power and the power coefficient outputs between the Samcef and the model for three different load cases. It is seen that the biggest difference between C_p values occur in the below rated load case which is about 5 %. With increasing wind speed, error between the Samcef and the model decreases. For above rated load case it is only 1 %.

Table 5.1: Torque, Power and Power Coefficient Comparison

	Below Rated		**Rated**		**Above Rated**	
	Samcef	*Model*	*Samcef*	*Model*	*Samcef*	*Model*
Torque(Nm)	5.47e+5	5.74e+5	1.34e+6	1.39e+6	2.13e+6	2.21e+6
Power(W)	7.44e+5	7.81e+5	2.11e+6	2.18e+6	3.34e+6	3.46e+6
Cp	0.472	0.496	0.395	0.410	0.186	0.1937

Overall, the simulation results of both the S4WT and the model are matching satisfactorily. Differences occur due to the use of different corrections for tip-hub loss factors.

5.1.4 Rigid and Aeroelastic Blades Comparison

After verification of the model is done by comparing the rigid rotor results with the Samcef, rigid and aeroelastic results are also compared. Three loading cases are repeated with aeroelastic blades in Samcef software. Figures shown below represent the results of the model with rigid rotor and the Samcef with aeroelastic rotor.
Material and stiffness properties used in Samcef are given in Appendix A.

Table 5.2: Torque, Power and Power Coefficient Comparison between the Samcef with Aeroelastic Blades and the Model with Rigid Blades

	Below Rated		**Rated**		**Above Rated**	
	Samcef	*Model*	*Samcef*	*Model*	*Samcef*	*Model*
Torque(Nm)	5.509e+5	5.74e+5	1.344e+6	1.39e+6	2.19e+6	2.21e+6
Power(W)	7.49e+5	7.81e+5	2.11e+6	2.18e+6	3.44e+6	3.46e+6
Cp	0.475	0.496	0.396	0.410	0.191	0.193

By comparing Figures 5.46, 5.50 and 5.54, it is seen that differences in sectional thrust and torque values are increasing with increasing wind speed as expected. However, even for the worst case, above rated loading case, results look quite similar. It can be deduced that the rigid model developed in this thesis gives appropriate results compared to an aeroelastic rotor with stiffness and blade properties specified in Appendix A. This situation can not be generalized for all rotors since deformation of the blades depends on blade radius, material choice and stiffness properties.

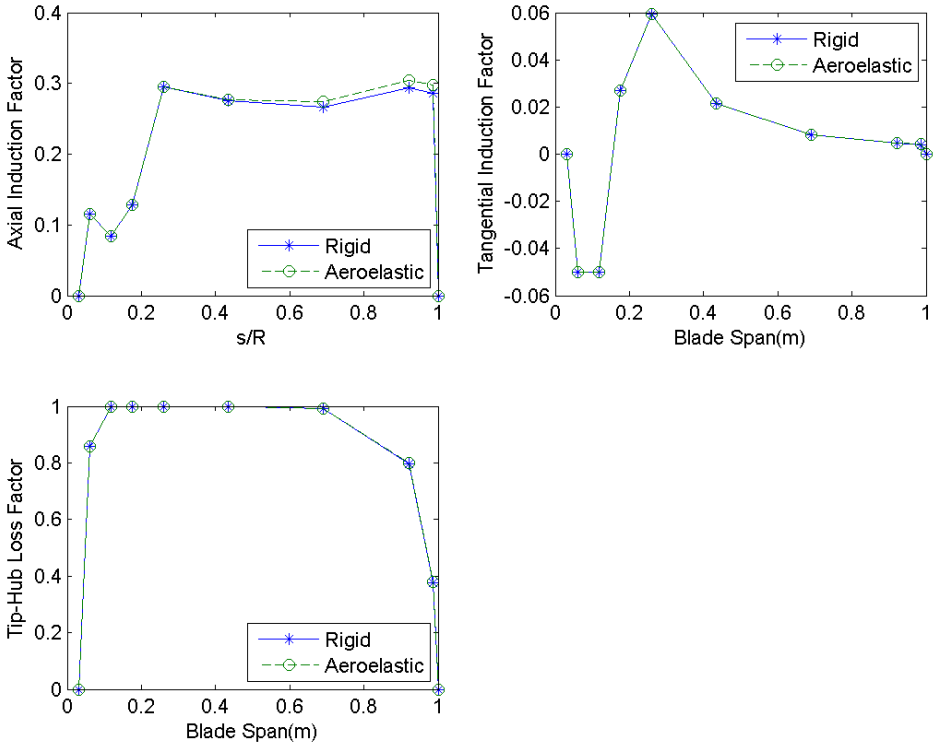

Figure 5.43: Below Rated Loading Case-Part 1

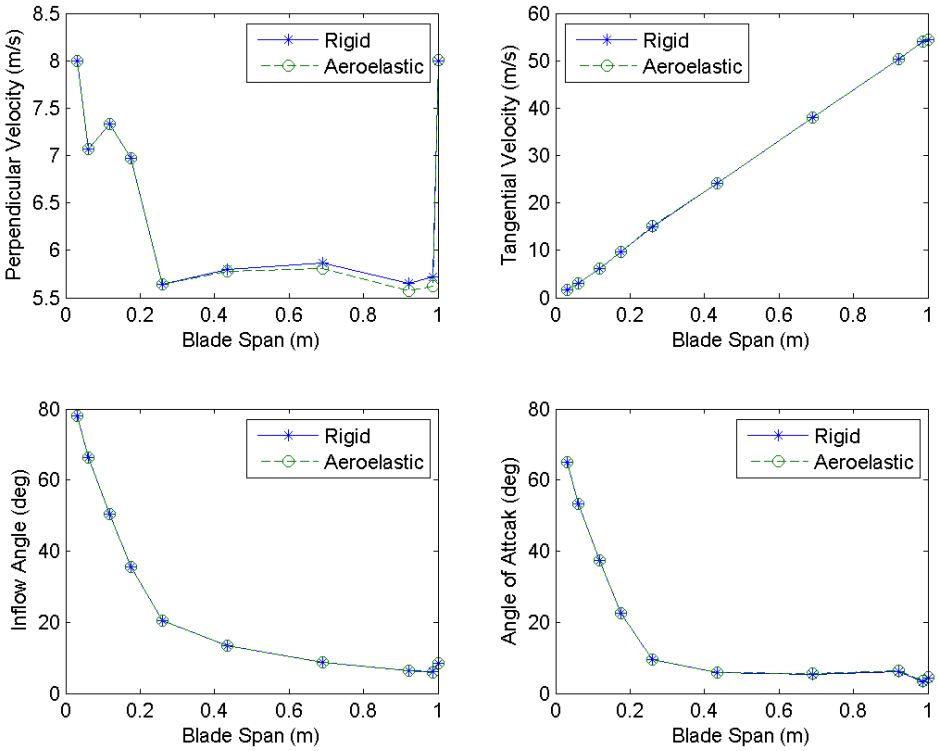

Figure 5.44: Below Rated Loading Case-Part 2

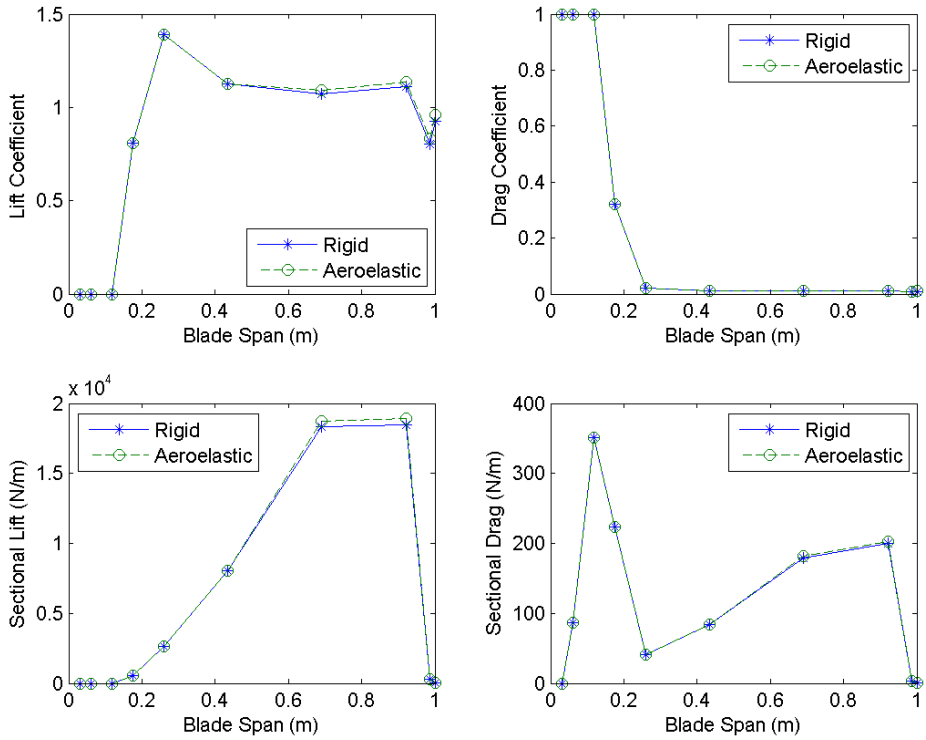

Figure 5.45: Below Rated Loading Case-Part 3

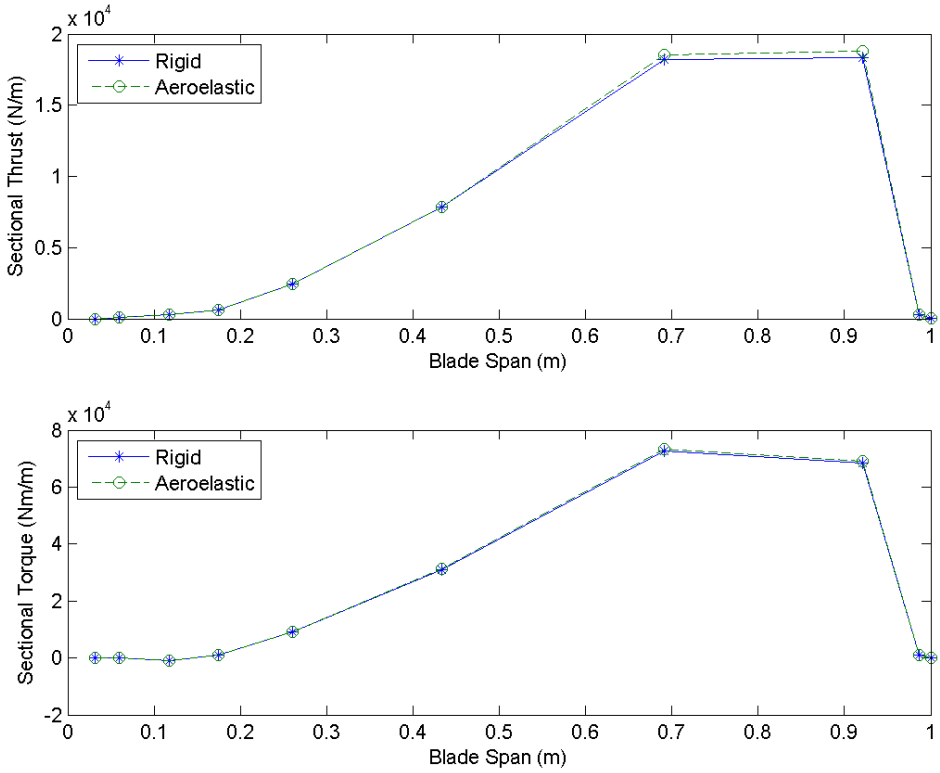

Figure 5.46: Below Rated Loading Case-Part 4

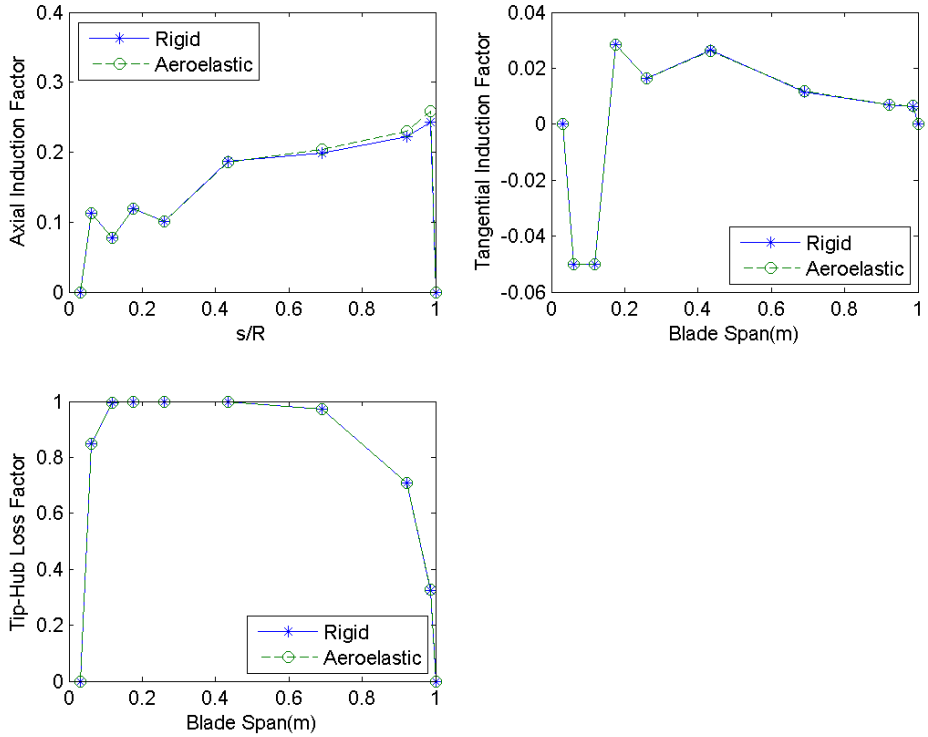

Figure 5.47: Rated Loading Case-Part 1

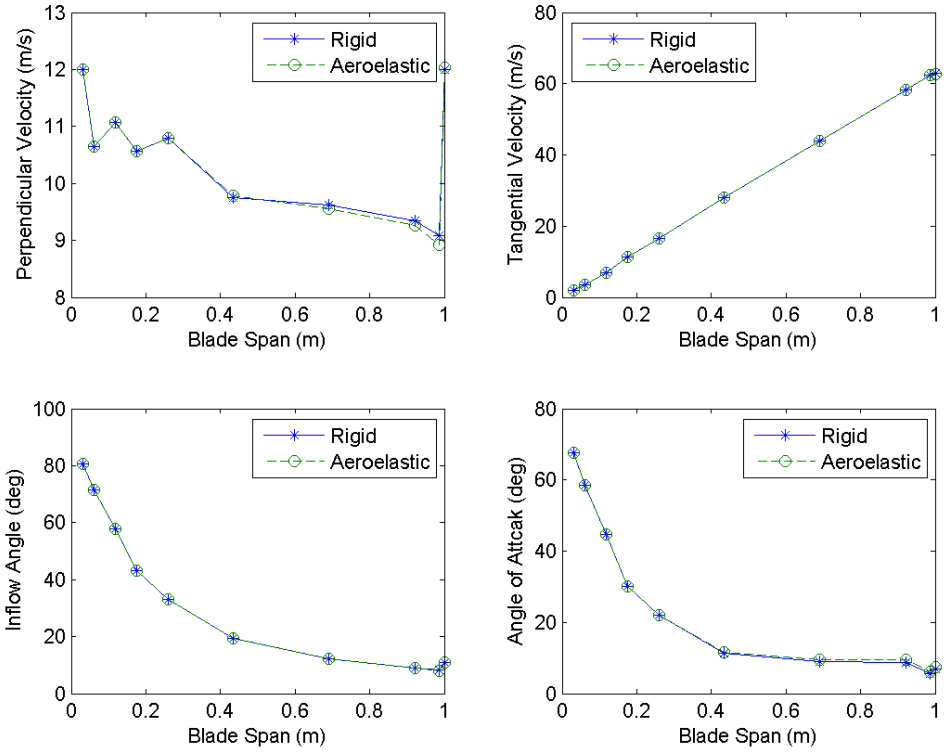

Figure 5.48: Rated Loading Case-Part 2

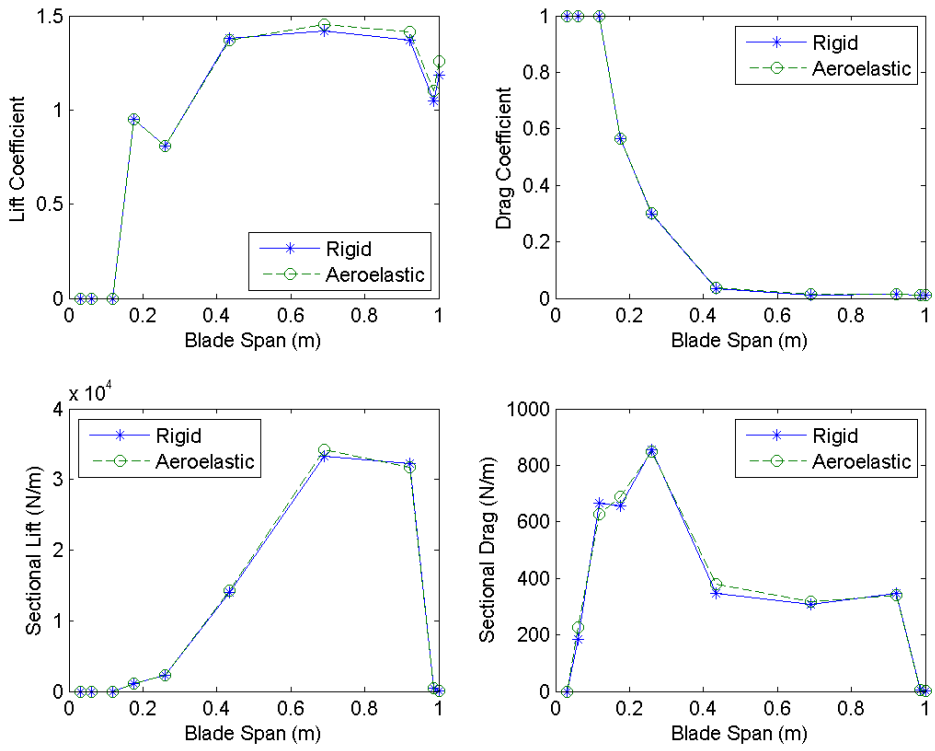

Figure 5.49: Rated Loading Case-Part 3

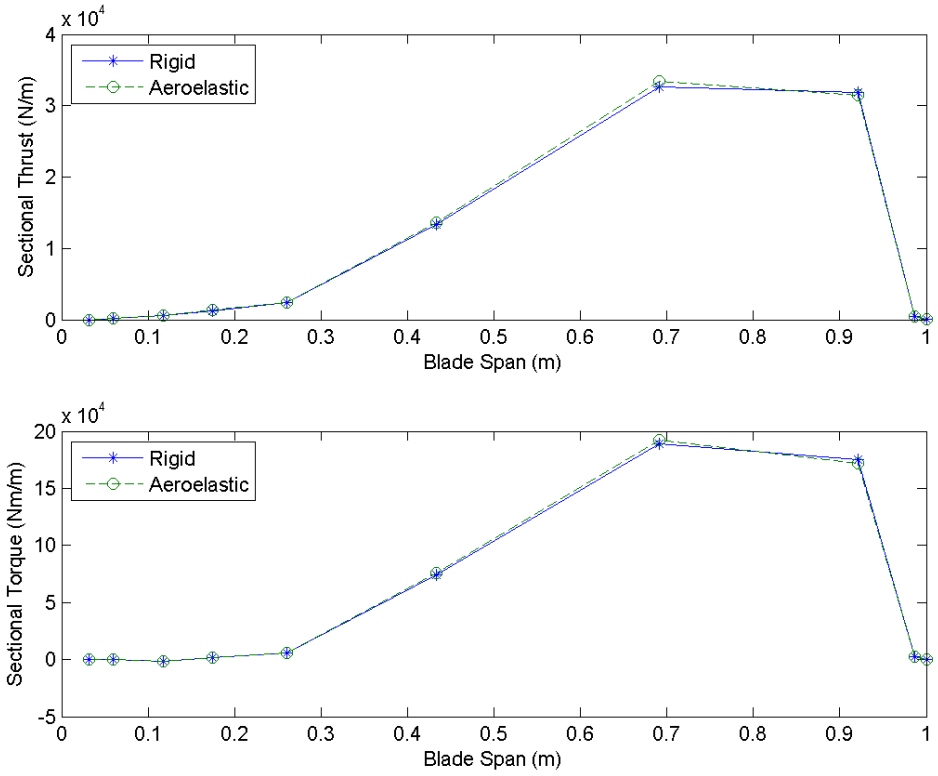

Figure 5.50: Rated Loading Case-Part 4

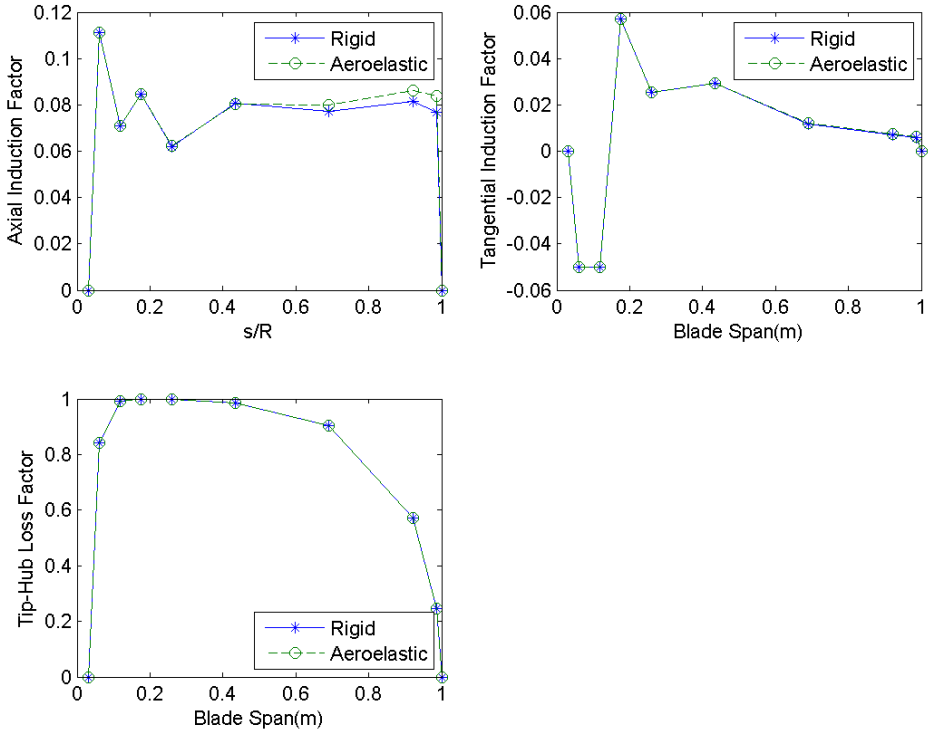

Figure 5.51: Above Rated Loading Case-Part 1

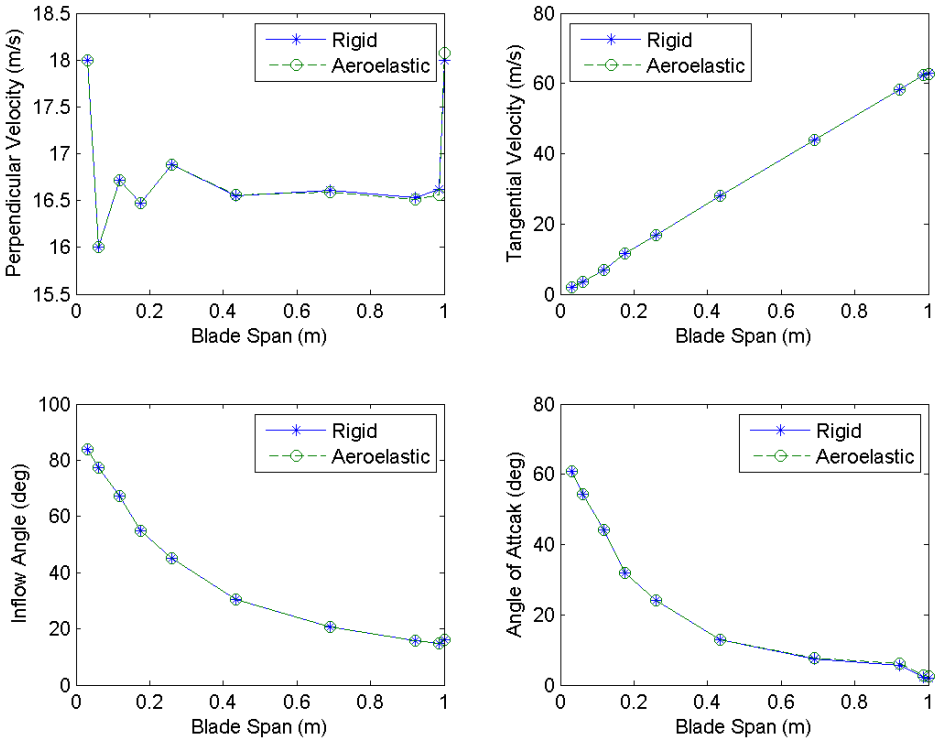

Figure 5.52: Above Rated Loading Case-Part 2

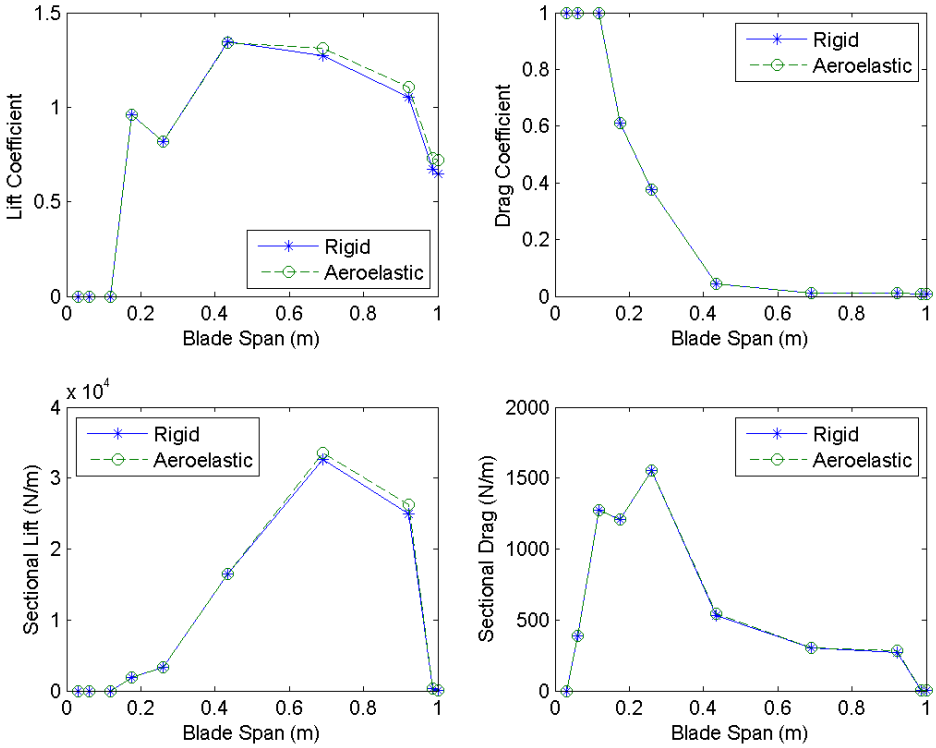

Figure 5.53: Above Rated Loading Case-Part 3

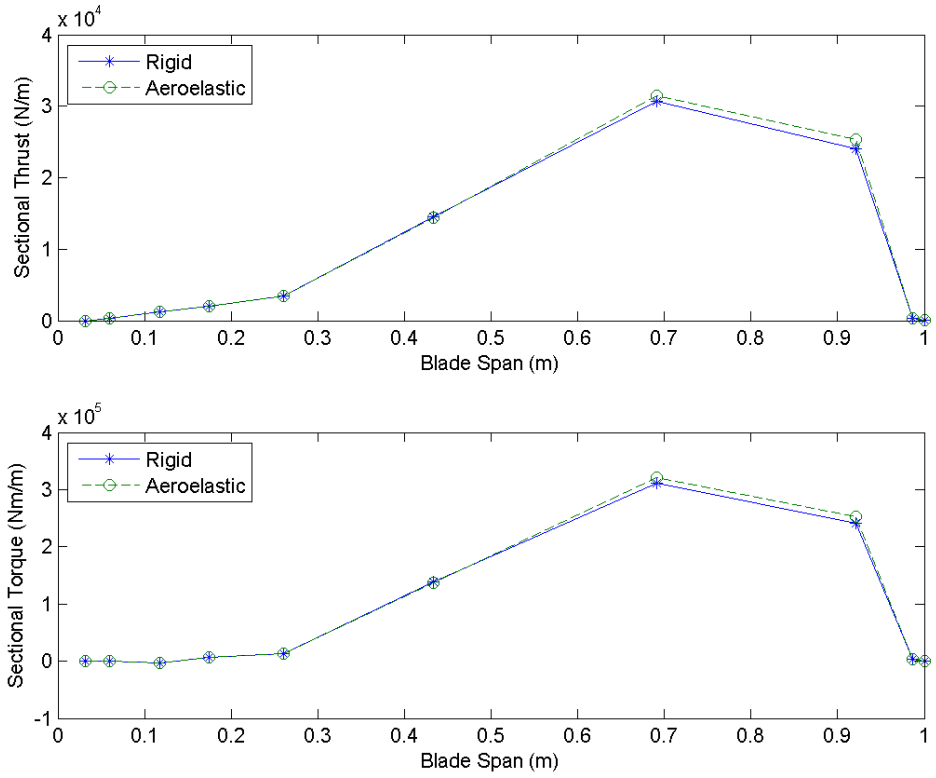

Figure 5.54: Above Rated Loading Case-Part 4

5.2 Controller Design of the Model

For the controller design the NREL 5MW reference wind turbine model is used. Its data are given in Appendix B. The reason behind this choice is that, NREL wind turbine has a more complex model with tilt and precone angle. Moreover, it is an open source and its data are more detailed.

Time step used in the simulation is chosen to be 0.01s.

The NREL 5MW wind turbine uses six different airfoils to form the blades. First three sections are cylindrical shaped sections with pure drag forces. Lift and drag coefficients are found by interpolation for given angle of attack values. The accuracy of the interpolated values are shown in Figures 5.55, 5.56, 5.57, 5.58, 5.59 and 5.60.

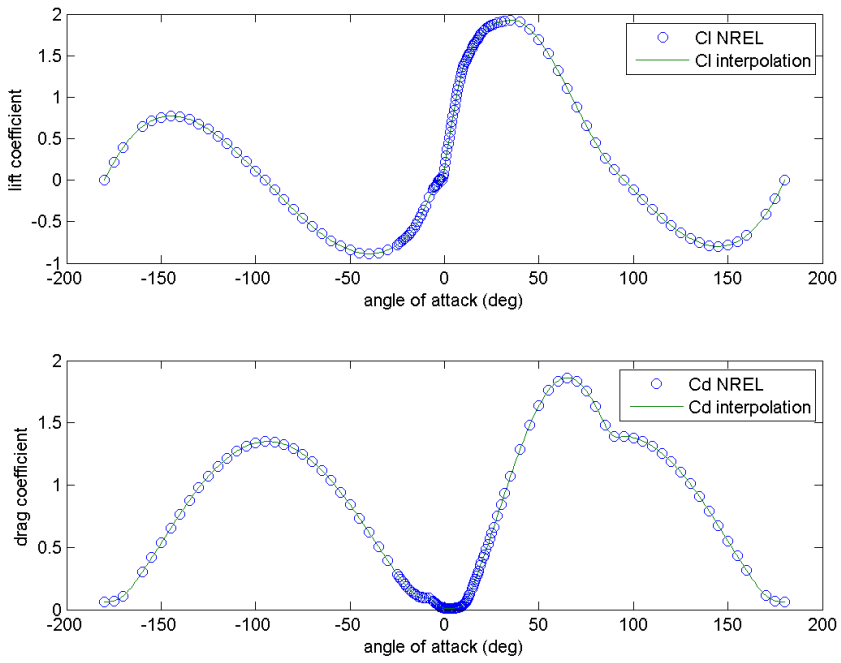

Figure 5.55: Cl and Cd Data and Interpolated Values for Airfoil DU40

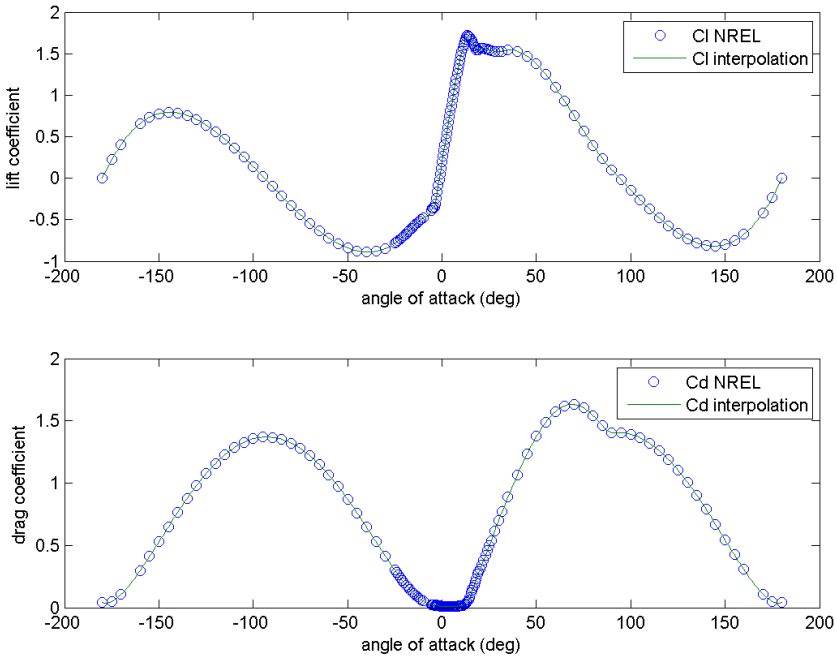

Figure 5.56: Cl and Cd Data and Interpolated Values for Airfoil DU35

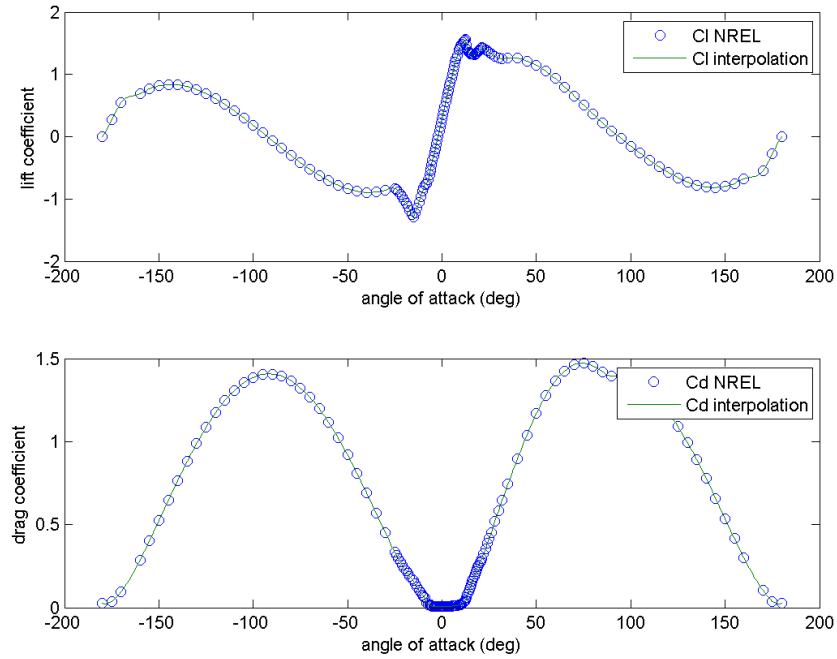

Figure 5.57: Cl and Cd Data and Interpolated Values for Airfoil DU30

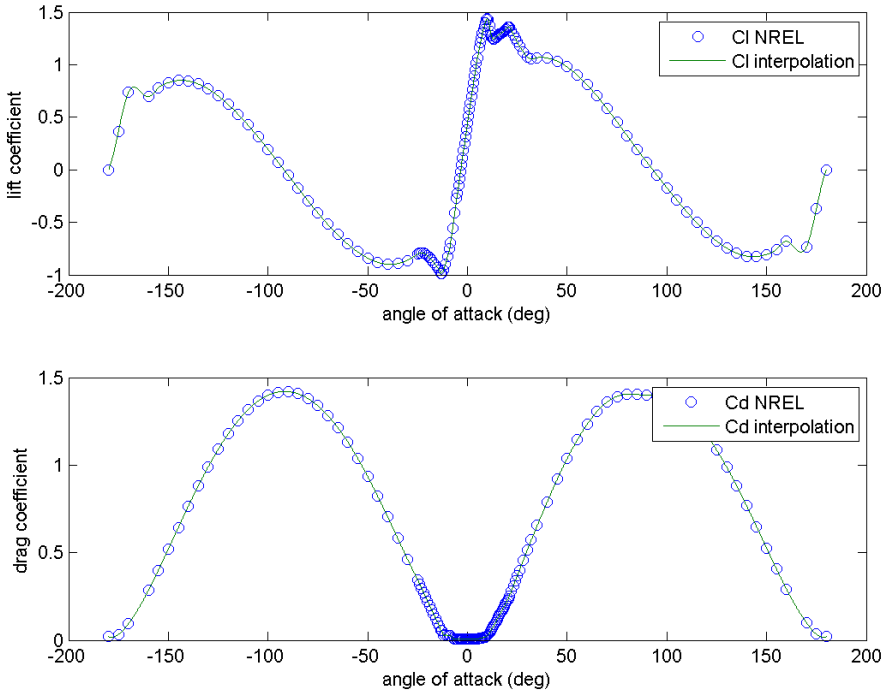

Figure 5.58: Cl and Cd Data and Interpolated Values for Airfoil DU25

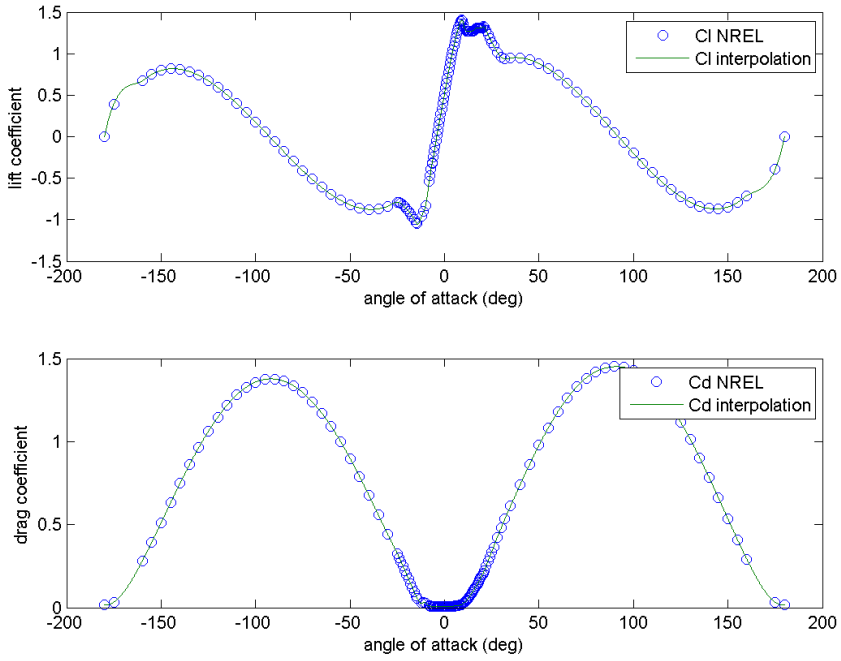

Figure 5.59: Cl and Cd Data and Interpolated Values for Airfoil DU21

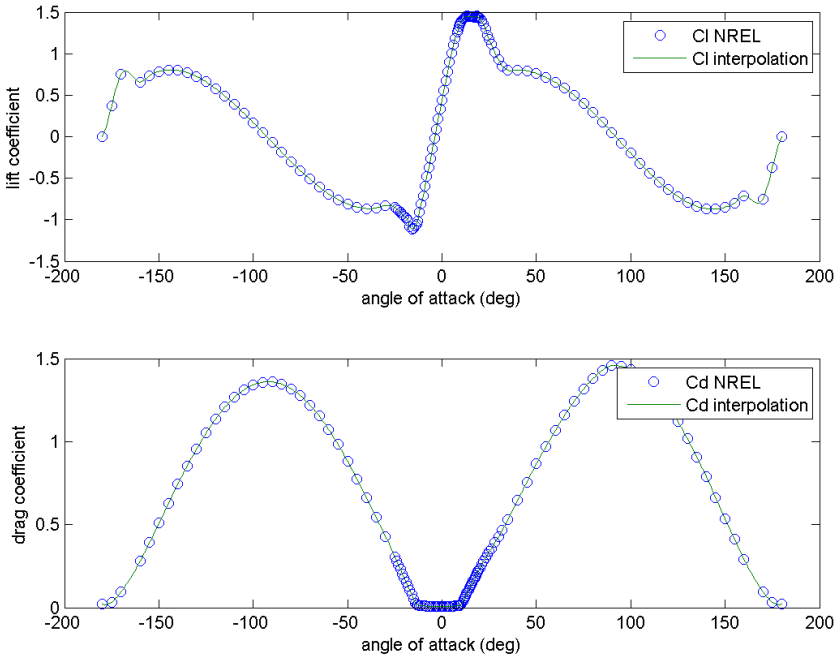

Figure 5.60: Cl and Cd Data and Interpolated Values for Airfoil NACA64

5.2.1 Generator Torque Controller

As stated in Section 4.2, maximum power production is aimed for the generator torque controller. For this purpose, maximum power coefficient which is a function of both the tip speed ratio and the pitch angle is found. C_p versus tip speed ratio and pitch angle surface for the NREL 5MW wind turbine is shown in Figure 5.61. The maximum power coefficient is calculated as 0.4751. The optimum tip speed ratio and the pitch angle values are 7.4 and -0.4 degree, respectively. Proportional gain for the generator torque controller is calculated as;

$$k = \frac{1}{2}(1.19)(0.4751)\pi(63)^5 \frac{1}{(97)^3(7.4)^3} = 2.383 \tag{5.1}$$

Finally, region 2 generator torque controller is found as;

$$Q_{gen} = 2.383\Omega_{gen}^2 \tag{5.2}$$

Ideal generator torque curve is shown in Figure 5.62. As seen, the rated generator torque value is not reached at the rated generator speed. Moreover, the generator torque starts to be applied when the cut-in generator speed is reached.

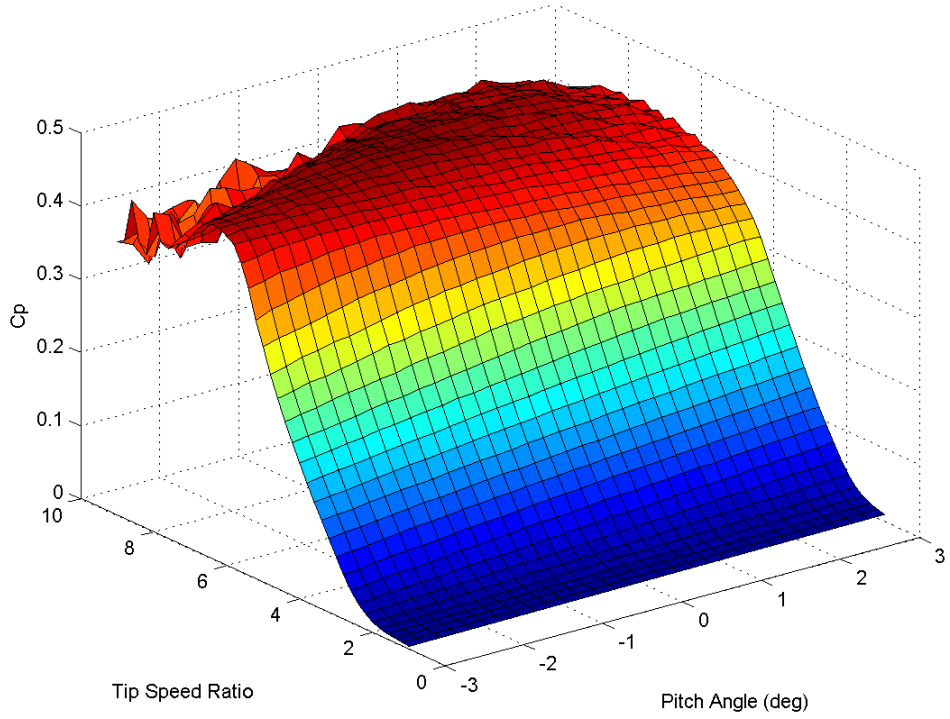

Figure 5.61: Power Coefficient Variation with Tip Speed Ratio and Pitch Angle

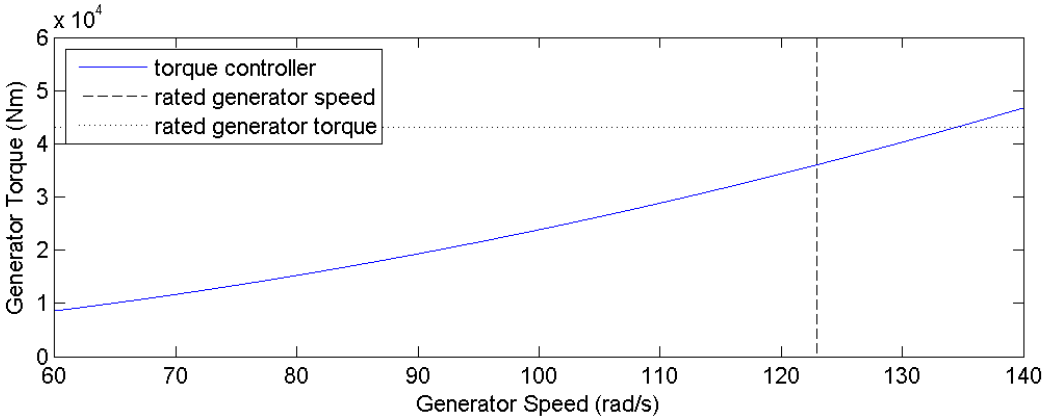

Figure 5.62: Generator Torque vs Generator Speed

Transition regions are defined to solve the problems stated above. Region 1-1/2 is added to make sure that the generator torque is started to be applied at the cut-in generator speed and reaches the optimum value quickly. Region 2-1/2 aims to reach to the rated generator torque value at the rated generator speed. Region 1-1/2 starts at

the cut-in generator speed, and ends 10 % above this value. Region 2-1/2 starts 5 % below the rated value, and ends at the rated generator speed. Region 2-1/2 is short to prevent power loss since turbine produces more power at the generator speeds close to the rated. Finally, overall generator torque implemented by the controller follows

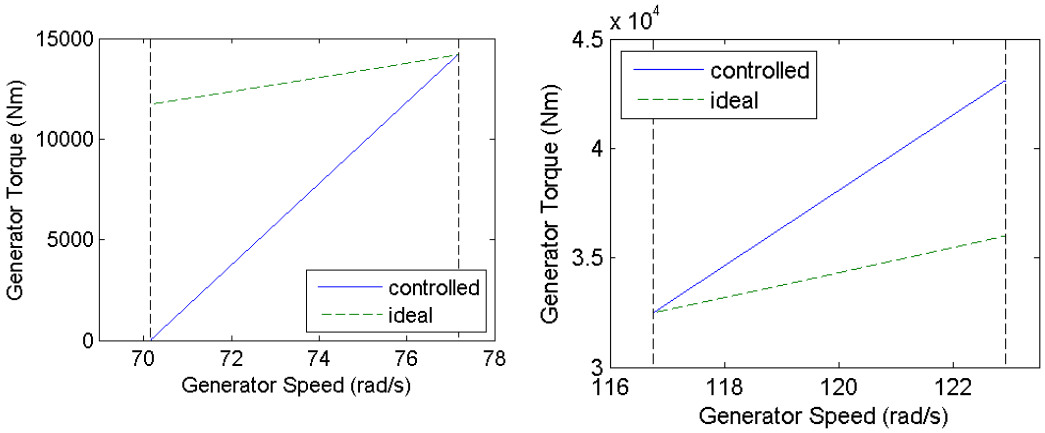

(a) Region 1-1/2

(b) Region 2-1/2

Figure 5.63: Ideal and Controlled Generator Torque

the path shown in Figure 5.64.

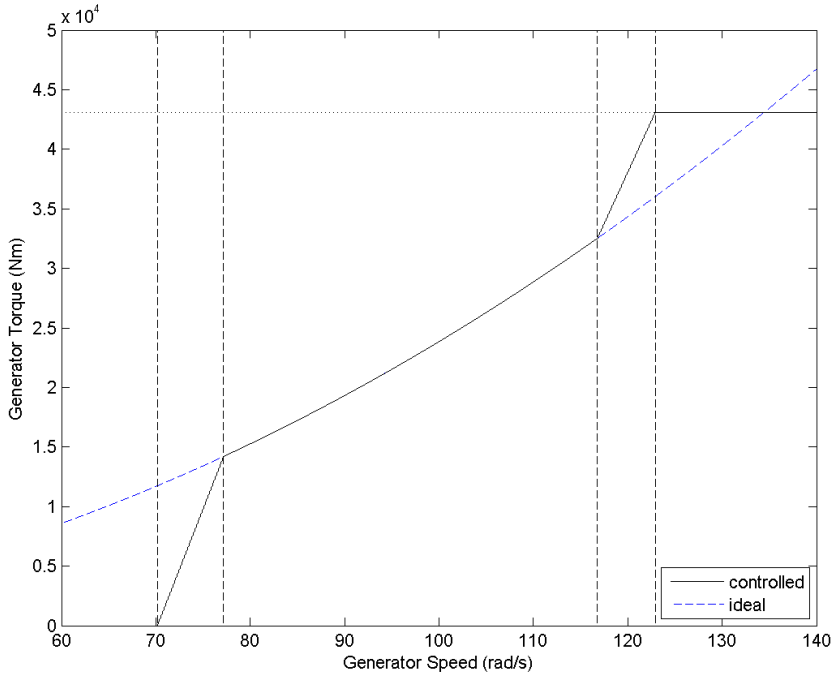

Figure 5.64: Generator Torque Controller Output

To test the generator torque controller at region 2, the tip speed ratio of the model is tracked to see whether it reaches and stays at the optimum tip speed ratio or not. Figures 5.65, 5.66 and 5.67 show responses to 7 m/s constant wind speed.

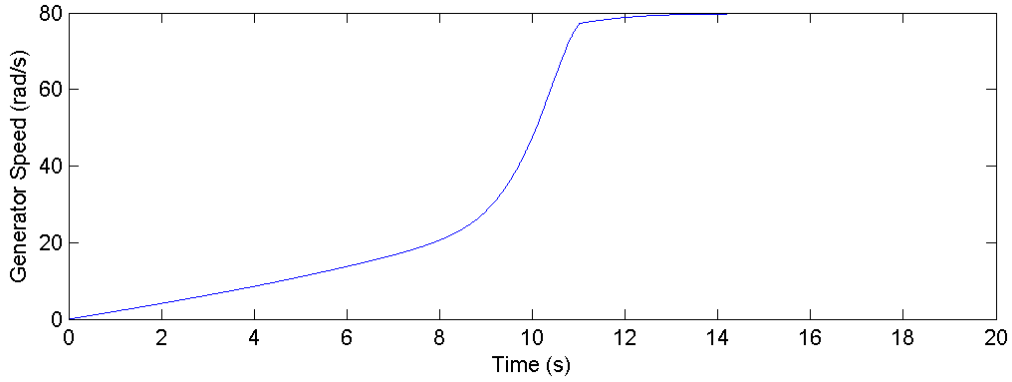

Figure 5.65: Generator Speed for 7 m/s Wind Speed

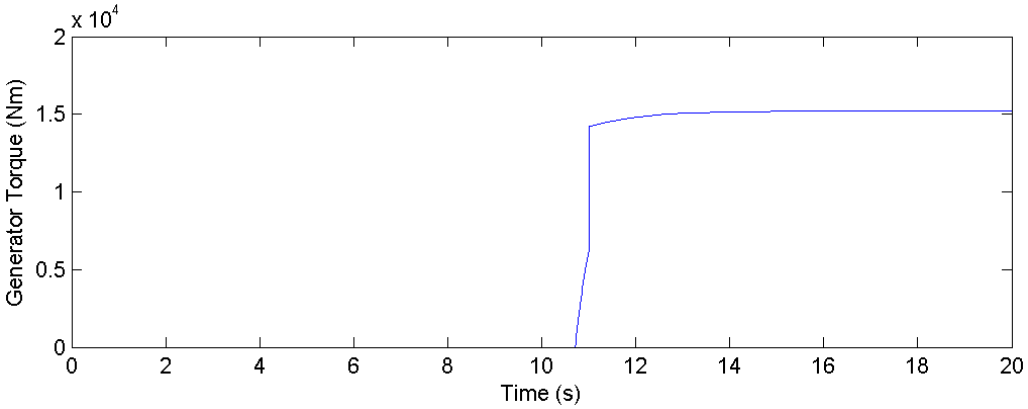

Figure 5.66: Generator Torque for 7 m/s Wind Speed

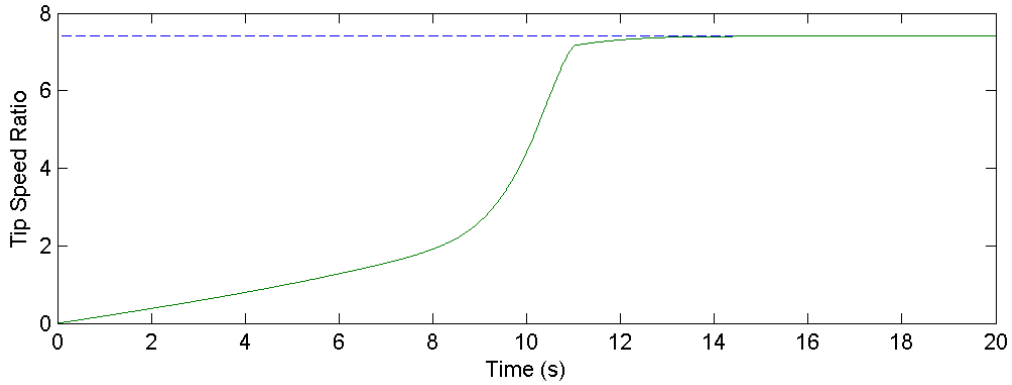

Figure 5.67: Tip Speed Ratio for 7 m/s Wind Speed

For 7 m/s wind speed, when the generator speed reaches the cut-in value, the generator torque starts to increase. Tip speed ratio is kept constant at the optimum value. If the wind speed increases, the optimum tip speed ratio is reached more quickly which can be seen from Figure 5.70.

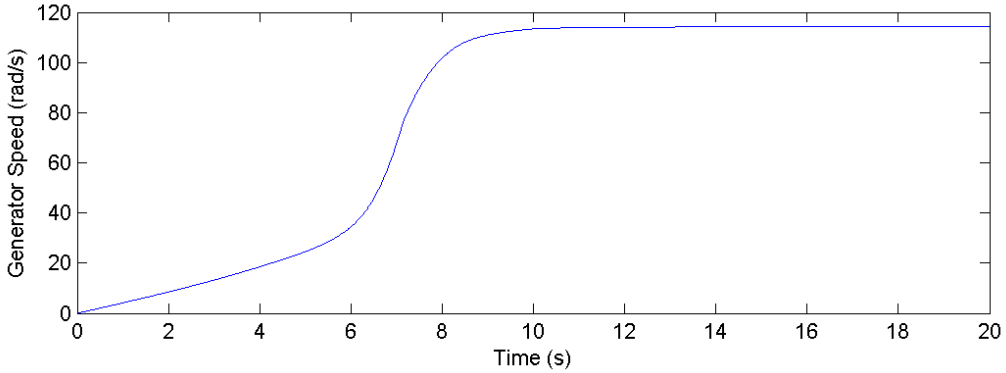

Figure 5.68: Generator Speed for 10 m/s Wind Speed

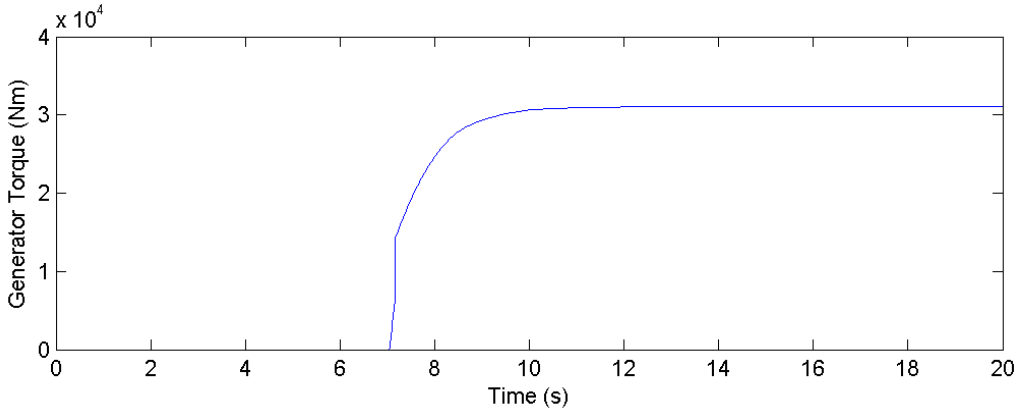

Figure 5.69: Generator Torque for 10 m/s Wind Speed

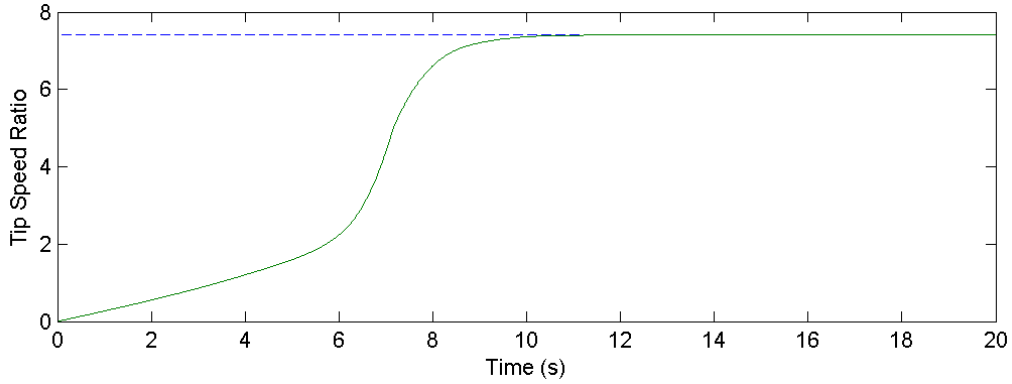

Figure 5.70: Tip Speed Ratio for 10 m/s Wind Speed

Responses for a step wind input are shown in Figures 5.71, 5.72 and 5.73. Wind speed is increases from 7 m/s to 8 m/s at 25th second.

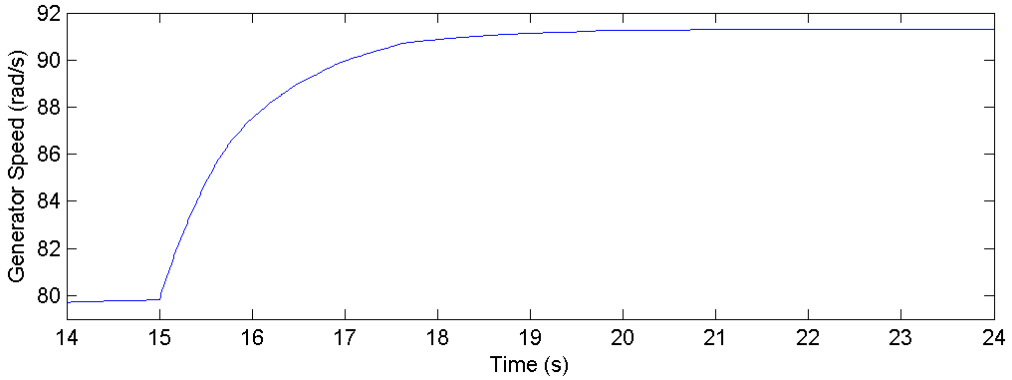

Figure 5.71: Generator Speed for 7 m/s to 8 m/s Step Input Wind Speed

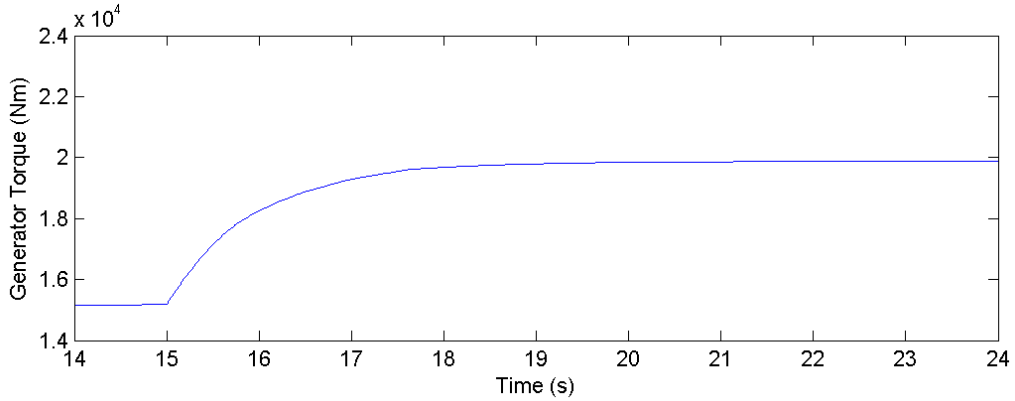

Figure 5.72: Generator Torque for 7 m/s to 8 m/s Step Input Wind Speed

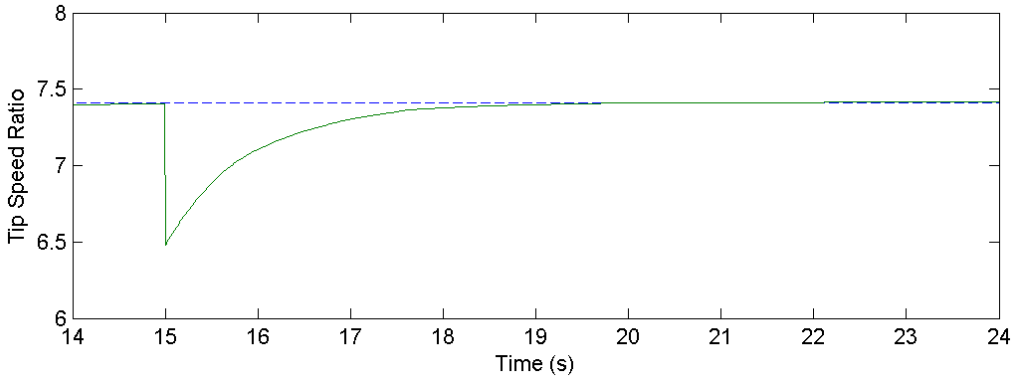

Figure 5.73: Tip Speed Ratio for 7 m/s to 8 m/s Step Input Wind Speed

As a result, it can be said that the generator torque controller accomplishes its purpose for region 2. It keeps the wind turbine at the optimum tip speed ratio which is desired for maximum power production.

5.2.2 Pitch Controller

The pitch controller is added to the model in order to limit the generator speed at region 3. At regions apart from region 3, pitch angle is kept constant at its optimum value which is calculated as -0.4 degree previously.

As given in 4 Section 4.3, proportional and integral gains are calculated as following;

$$K_p = \frac{2\xi\omega\left(A_\beta K_d - 1\right) - A_\Omega}{A_\beta} \tag{5.3}$$

$$K_i = \frac{\omega^2\left(A_\beta K_d - 1\right)}{A_\beta} \tag{5.4}$$

A_β and A_Ω values are calculated by giving small perturbations to the pitch angle and the rotational speed and using Taylor series. $A_\beta = -2.93$ and $A_\Omega = -0.536$ are obtained for the point where wind speed is 12 m/s, pitch angle is 0.5 degree and rotor speed is 1.267 rad/s. Natural frequency, ω, is chosen as 0.6 [17].

Different damping ratio values are tested for performance by giving unit step wind input at time 45s. At 45th second, wind speed changes from 15 m/s to 16 m/s. The rotor speed response to unit step wind input can be seen in Figure 5.74.

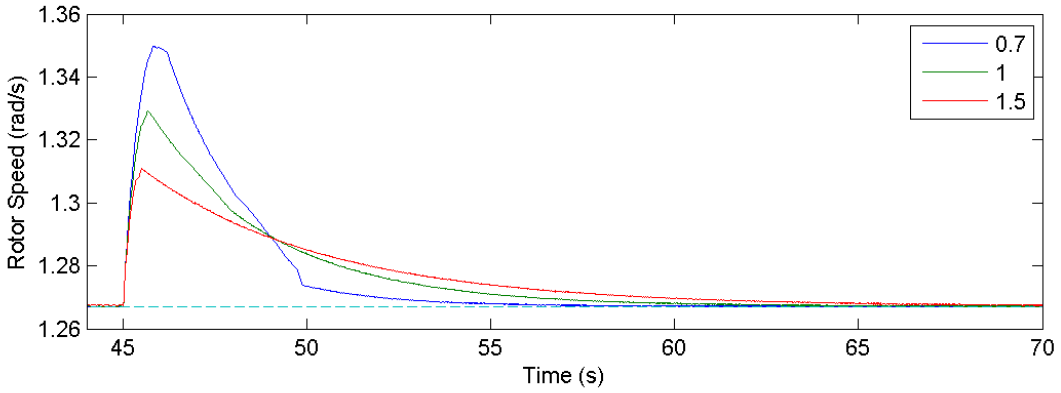

Figure 5.74: Response to a Step Wind Input for Various Damping Ratios

As seen from the figure above, with increasing damping ratio overshot decreases but settling time increases. $\xi = 1$ is chosen since it has a shorter settling time than $\xi = 1.5$ and a smaller overshoot value than $\xi = 0.7$.

Different derivative gains are tested to decrease overshoot. Unit step wind input is given at 40th second. Wind speed is increased from 15 m/s to 16 m/s .The rotor speed response can be seen in Figure 5.75.

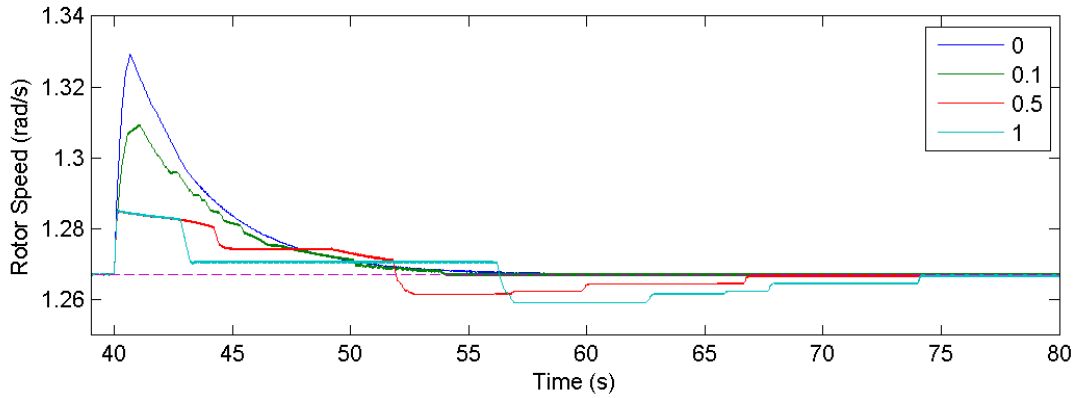

Figure 5.75: Response to a Step Wind Input for Various Derivative Gains

As seen from Figure 5.75, increasing K_d decreases overshoot. However, there occurs a small oscillation. In order to avoid that oscillation 0.1 is chosen as derivative gain. Proportional and integral gains are calculated for $\xi = 1$ and $K_d = 0.1$ as following; $K_p = 0.346$, $K_i = 0.158$. Rate limiter is added to the pitch controller in order to

avoid high pitch fluctuations. The blade pitch rate is set to 10 deg/s.

The pitch controller has to keep the generator speed at the rated value at region 3. Constant wind speeds are applied to the model. Responses to 13 m/s wind speed are shown in Figures 5.76, 5.77 and 5.78. Increasing pitch angle manages to keep the rotor speed at the rated value. Generator torque value is kept constant at the rated value after rotor speed exceeds its rated value.

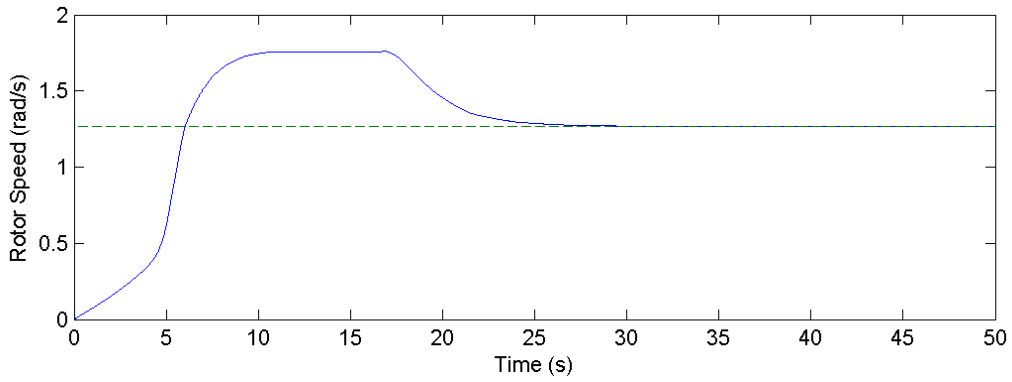

Figure 5.76: Generator Speed for 13 m/s Wind Speed

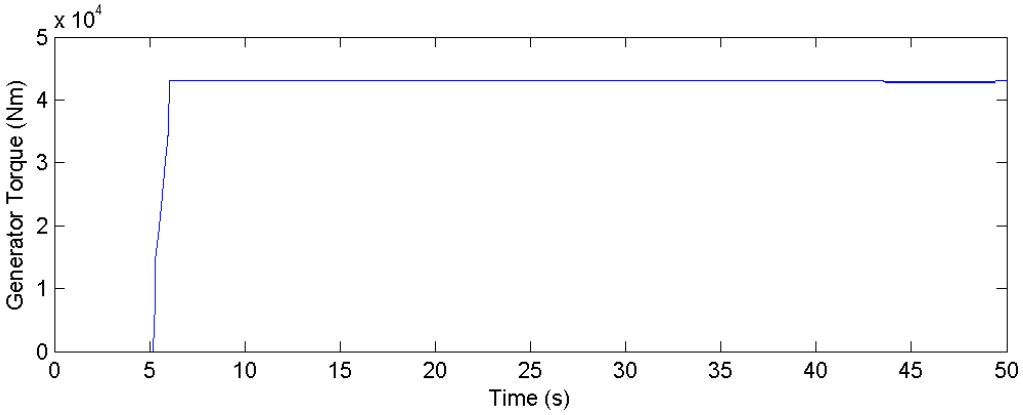

Figure 5.77: Generator Torque for 13 m/s Wind Speed

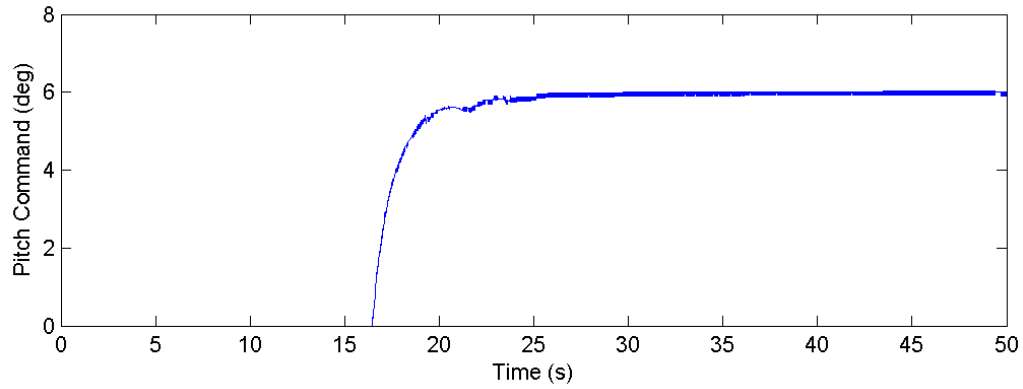

Figure 5.78: Pitch Angle for 13 m/s Wind Speed

For a higher wind speed, 17 m/s, maximum overshoot increases but settling time decreases. The rated rotor speed is still preserved.

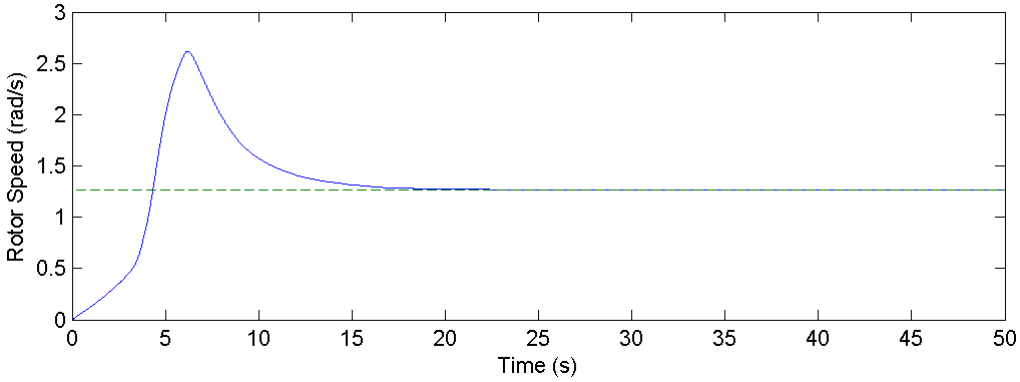

Figure 5.79: Generator Speed for 17 m/s Wind Speed

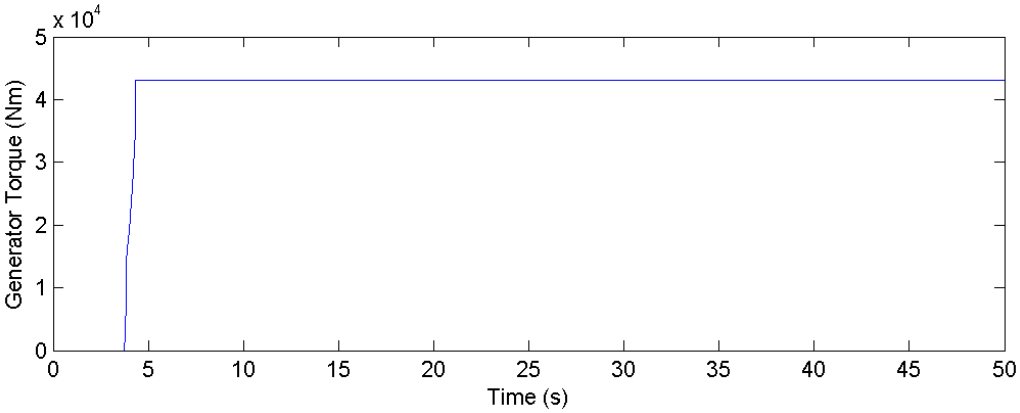

Figure 5.80: Generator Torque for 17 m/s Wind Speed

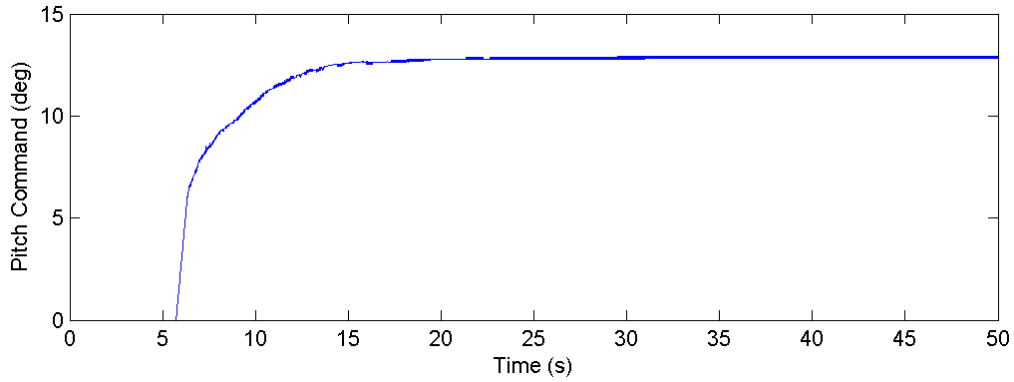

Figure 5.81: Pitch Angle for 17 m/s Wind Speed

The generator speed responses for different step wind inputs are shown in Figure 5.82. The wind speed increases from 15 m/s to 16 m/s for the first disturbance and from 19 m/s to 20 m/s for the second disturbance at 35th second.

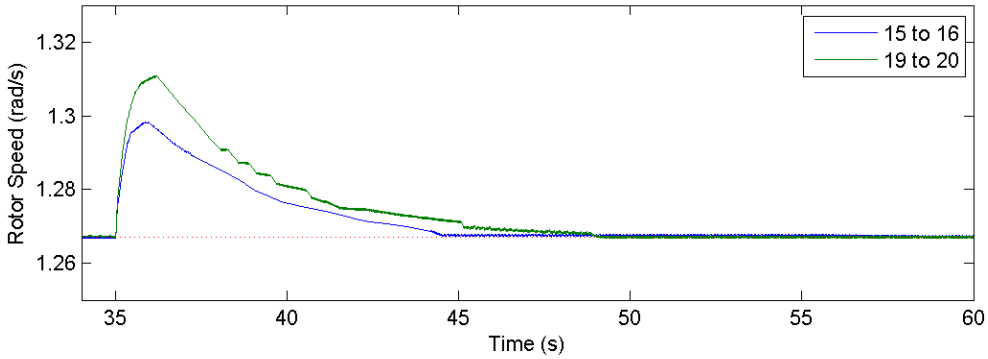

Figure 5.82: Rotor Speed for Various Unit Step Wind Speeds

The designed pitch controller succeeds to hold the generator speed at the rated value chosen for the wind turbine model.

5.2.3 Non-uniform Wind Input

Until now, controllers designed are tested only for uniform wind inputs. For more realistic simulations, non-uniform wind inputs are considered. Wind inputs are created using turbulence block from aerosim blockset in Simulink. Two different load cases are tested; below rated and above rated.

For below rated load case, wind speed is chosen as 8 m/s. Wind speed components are shown in Figures 5.83,5.84 and 5.85.

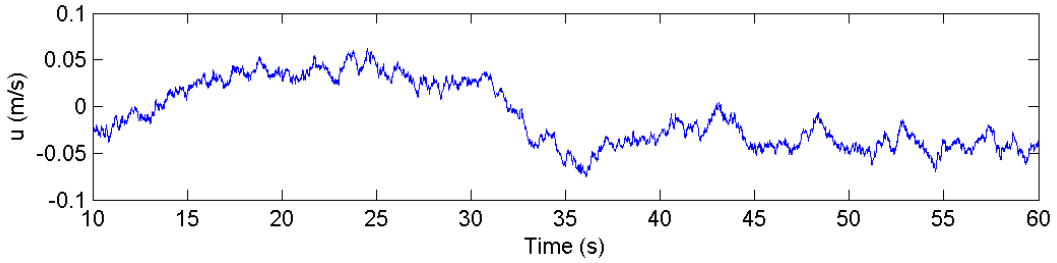

Figure 5.83: Wind Speed X Component for Below Rated Case

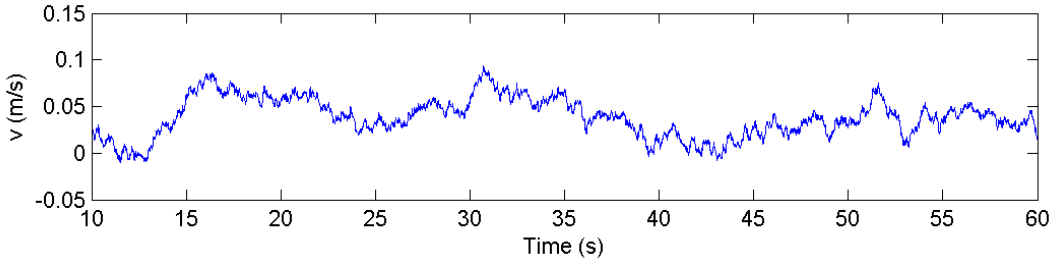

Figure 5.84: Wind Speed Y Component for Below Rated Case

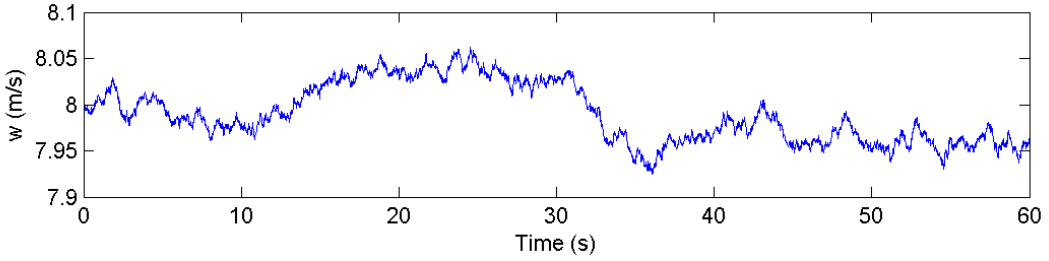

Figure 5.85: Wind Speed Z Component for Below Rated Case

As seen from Figure 5.86, oscillations in wind speed cause oscillation in rotor speed. However, overall performance of the generator controller is enough to keep the tip speed ratio at its optimum value (see Figure 5.88).

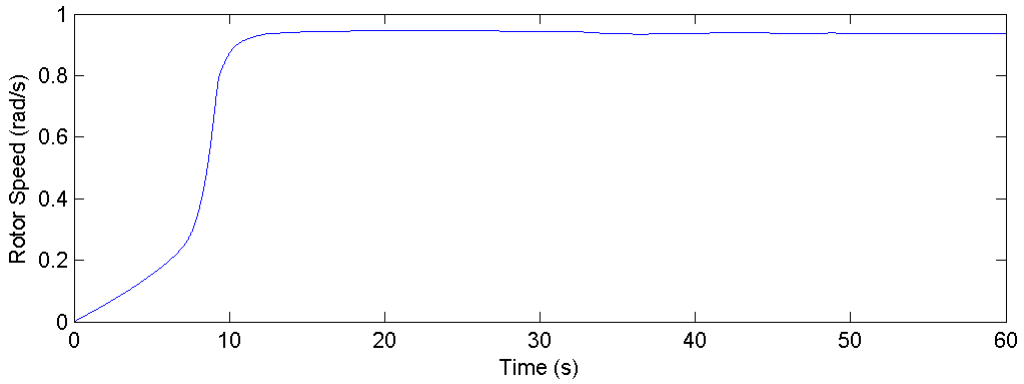

Figure 5.86: Rotor Speed for Below Rated Load Case

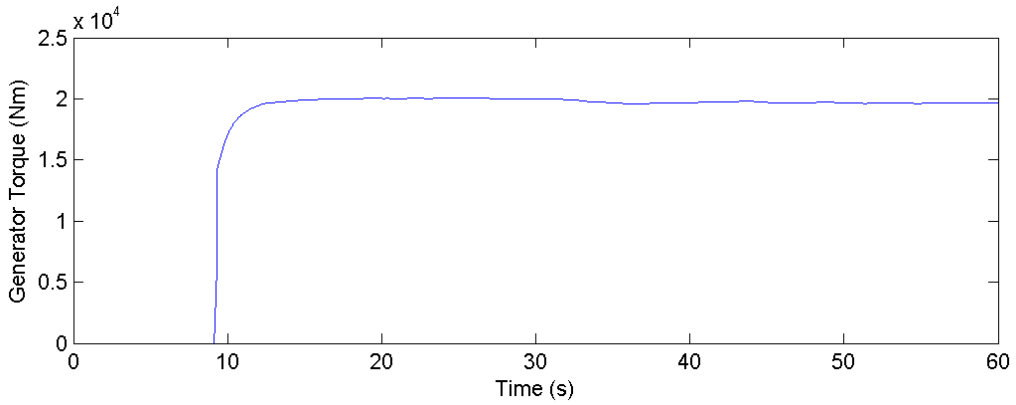

Figure 5.87: Generator Torque for Below Rated Load Case

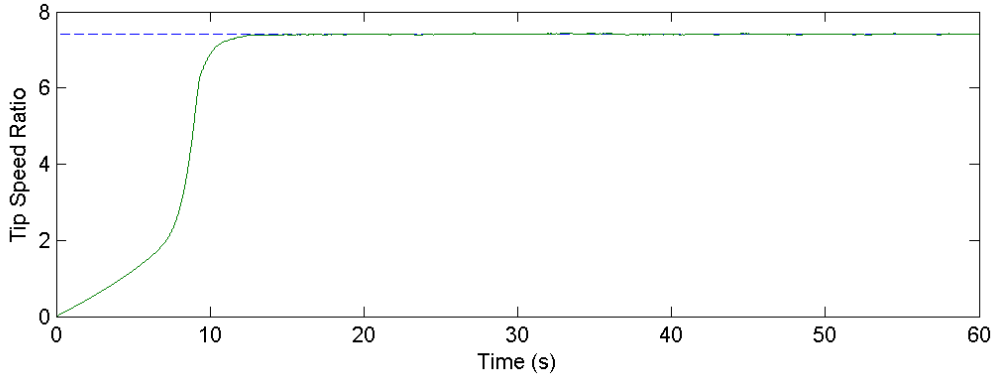

Figure 5.88: Tip Speed Ratio for Below Rated Load Case

For above rated load case, wind speed is chosen as 18 m/s. Wind speed components are shown in Figures 5.89,5.90 and 5.91.

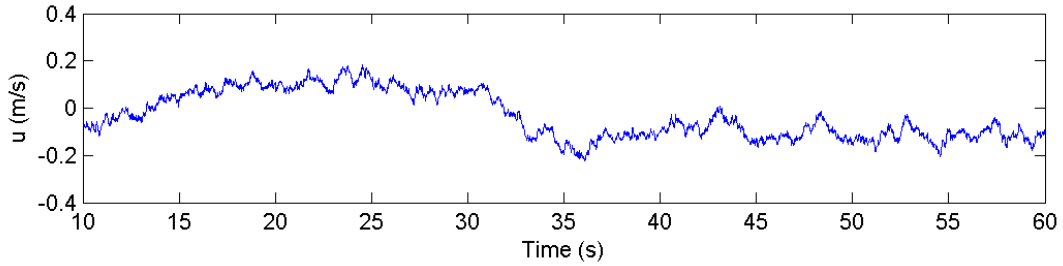

Figure 5.89: Wind Speed X Component for Above Rated Case

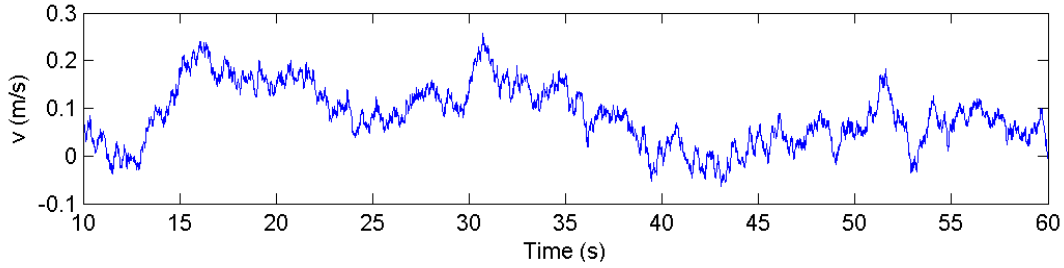

Figure 5.90: Wind Speed Y Component for Above Rated Case

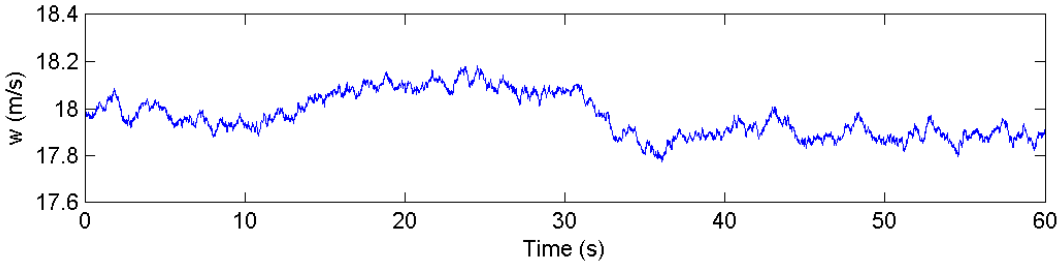

Figure 5.91: Wind Speed Z Component for Above Rated Case

For the above rated loading case, oscillations in wind speed cause oscillations at both pitch command and generator torque command (see Figure 5.93 and 5.94). From Figure 5.92, it is seen that pitch controller succeeds to hold the rotor speed at the rated value.

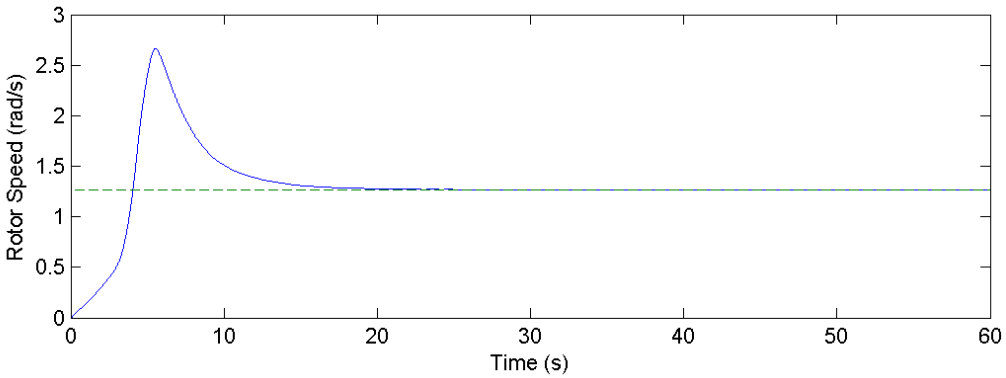

Figure 5.92: Rotor Speed for Above Rated Load Case

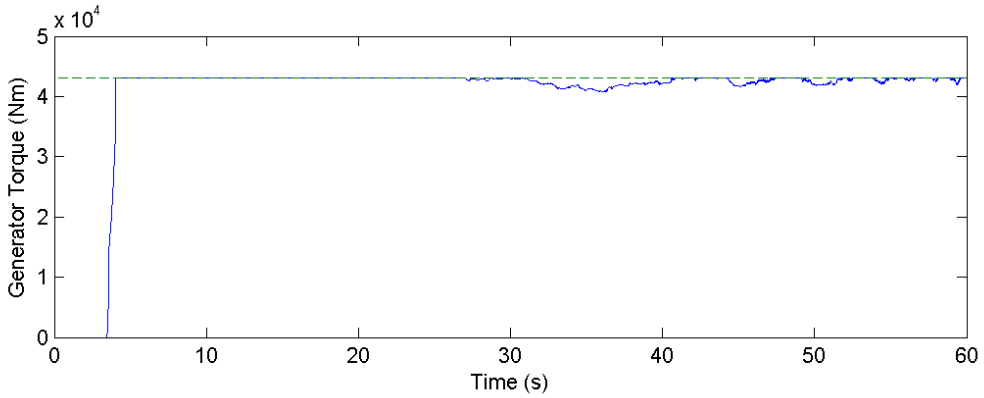

Figure 5.93: Generator Torque for Above Rated Load Case

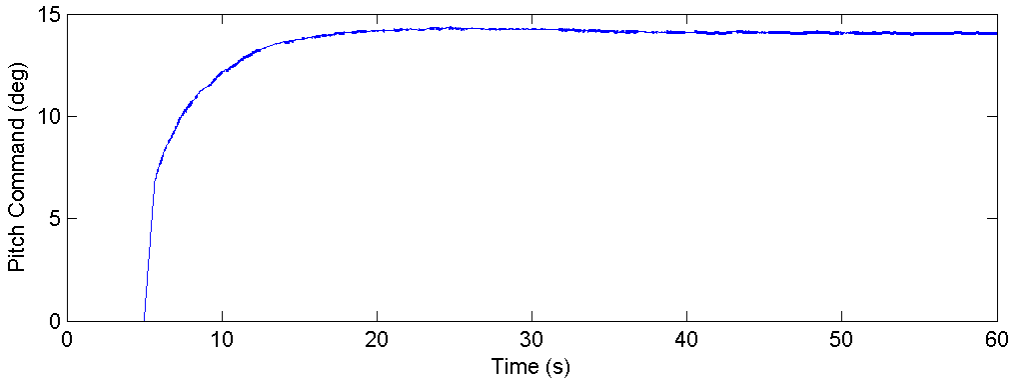

Figure 5.94: Pitch Command for Above Rated Load Case

It can be concluded that, both controllers do their duty properly also for non-uniform wind inputs.

5.2.4 Steady State Performance

Overall steady state behaviours of the model are shown for various properties. Dashed lines indicate the region borders.

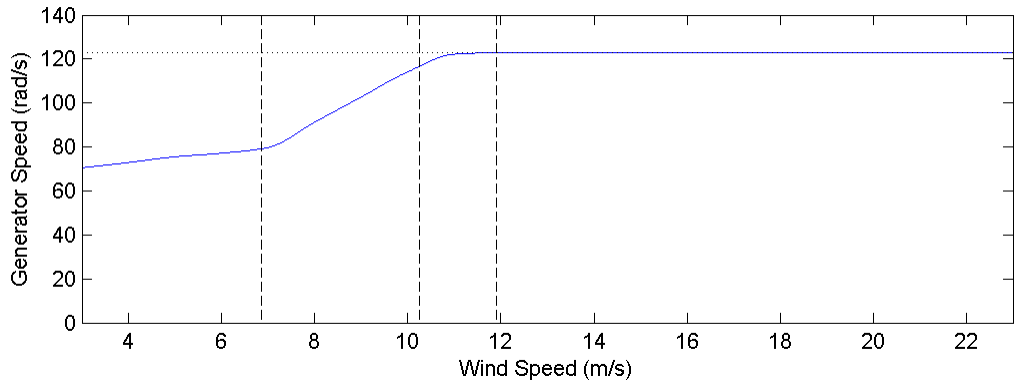

Figure 5.95: Generator Speed as a Function of Wind Speed

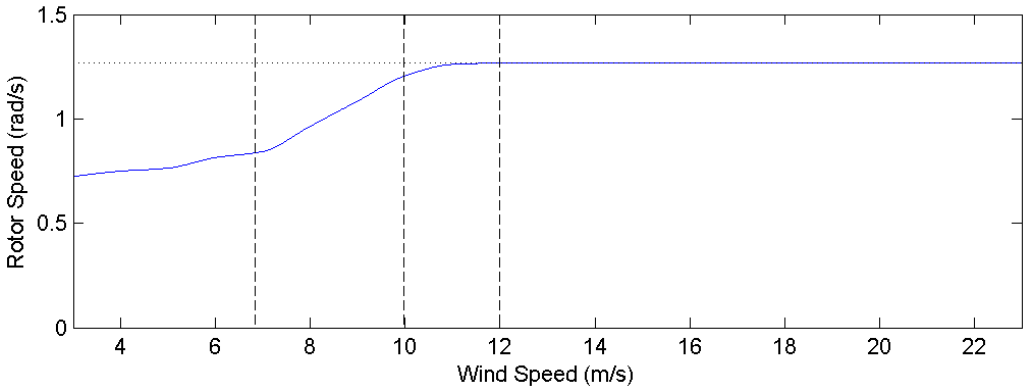

Figure 5.96: Rotor Speed as a Function of Wind Speed

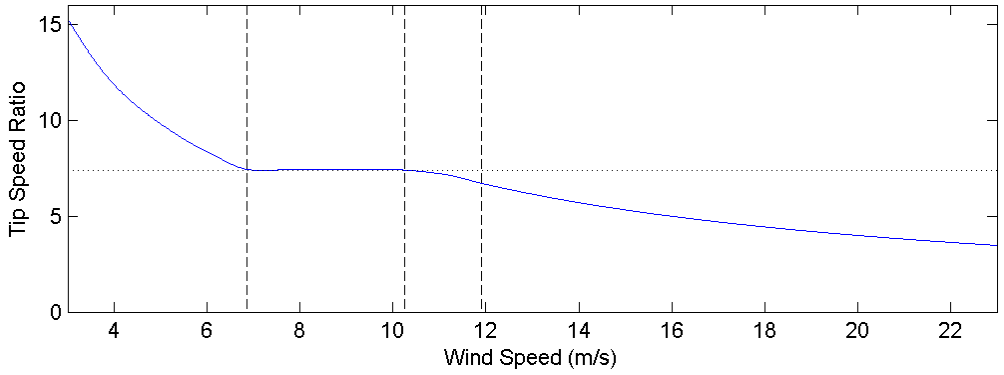

Figure 5.97: Tip Speed Ratio as a Function of Wind Speed

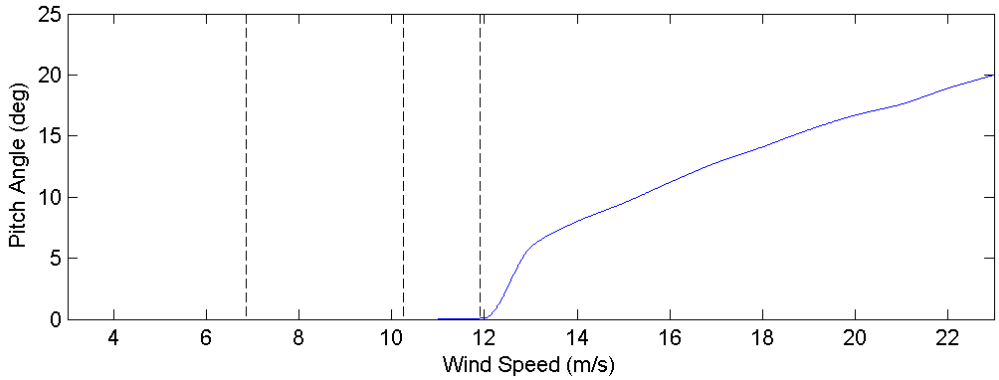

Figure 5.98: Pitch Angle as a Function of Wind Speed

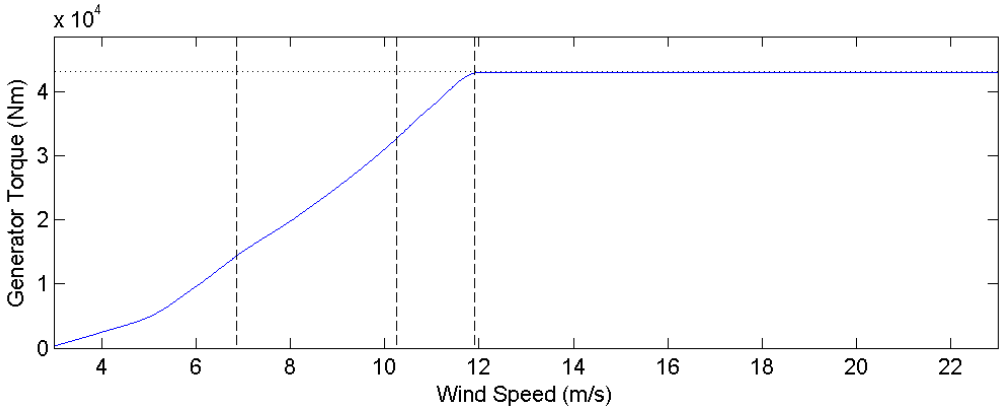

Figure 5.99: Generator Torque as a Function of Wind Speed

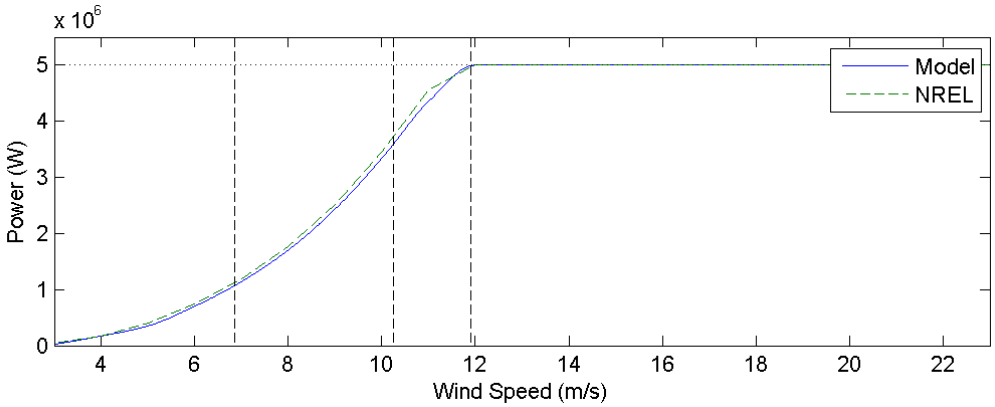

Figure 5.100: Power as a Function of Wind Speed

It is seen that the dynamic model and the controllers designed in this thesis work as desired. In region 2, the generator controller holds the tip speed ratio at the optimum

value hence maximum power is extracted from wind. In region 2-1/2, the generator torque increases more rapidly than the one in region 2. In this way the generator torque reaches the rated value at the same time the generator speed reaches its rated value. In region 3, the pitch controller starts to send pitch commands to the model to limit the generator speed. While the pitch angle increases, the generator speed and the torque values are constant in this region.

The power output is found by multiplying the generator speed and the generator torque outputs. Generator efficiency is taken as 94.4 % as indicated in Appendix B. The model produces 5MW power at the region 3 just like the NREL 5MW reference wind turbine. Moreover as seen in Figure 5.100, power curve of the model follows almost the same pattern with the NREL at below rated regions.

CHAPTER 6

CONCLUSION

The goal of this thesis is to create a dynamic model for a horizontal axis wind turbine. The wind turbine is chosen to be variable speed, upwind configuration and three-bladed. The MATLAB/Simulink environment is used to create the model and to run simulations. The rotor which is assumed rigid is modelled by Blade Element Momentum Theory.

Throughout the thesis, first, aerodynamic properties of the wind turbine rotor is introduced. Momentum Theory and Blade Element Theory are introduced as building blocks of the Blade Element Momentum Theory. Aerodynamic forces are modelled as distributed loads. They are the main reason behind the rotation of the rotor. In order to obtain these forces sectional velocities, inflow angles and angle of attacks are calculated. The axial and the tangential factors are calculated by iteration. Glauert correction factor is implemented to these factors for the axial induction factors higher than 0.4. The tip and hub loss effects are added to get more realistic results. Rotors with tilt and precone angles are treated as minor cases. Their effects on wind turbine aerodynamics are added later.

After aerodynamic forces are obtained gravitational forces are added to them. Coordinate systems used to define forces, velocities and angles, and transformations between them are explained. Sectional moments are calculated using sectional forces. They are summed to find total moments on a blade. The torque component of these moments are calculated for each blade. The rotor torque caused from aerodynamic and gravitational forces is obtained. The power output of the model is calculated using the torque and the rotational speed.

Verification of the model is done by using the LMS Samtech, Samcef for Wind Tur-

bines software. The same wind turbine properties with the Samcef are implement to the model. Three different load cases are used for verification; below rated load case, rated load case and above rated load case. Aerodynamic properties of the blade sections and rotor performance parameters are calculated for each load case. It is observed that the model and the Samcef simulations give quite similar results. The only difference is seen at the tip-hub loss factors at sections close to the hub. The possible reason is the use of different correction factor. Apart from sections near the hub, aerodynamic properties are very similar except some minor differences. The maximum error of the performance parameters is 5%. It is observed that performance outputs of the model are higher than the Samcef since the hub loss of the model is smaller. In order to observe the effect of aeroelasticity, simulations in the Samcef are repeated with aeroelastic blades. It is seen that for the wind turbine model given in the Samcef verification tutorial, the rigid model developed in this thesis gives also appropriate results for aeroelastic blades.

Controllers are designed to make sure the model is valid for its operational envelope. Operational regions and their control objectives are defined. Data of the NREL 5MW reference wind turbine is used since it has tilt and precone angle. Two different controllers are designed to meet these objectives. Firstly, a standard generator torque controller is designed for the below rated regions. The model is simulated of various tip speed ratios and pitch angles. Optimum pitch angle and tip speed ratio which give the maximum power coefficient are found. Using the maximum power coefficient and the optimum tip speed ratio, ideal generator torque curve is found for maximum power production. Two transient regions are added to the model. First one is for the start up and the second one is for arranging the rated generator speed and the generator torque relation. It is seen that the generator torque maintains the optimum tip speed ratio for various wind speeds as desired.

The pitch controller is added to the model for the above rated regions. A PID controller is designed as the pitch controller to hold generator speed at its rated value. The performance of the controller is examined for various damping ratios and derivative gains. Pitch rate limiter is added to the model for avoidance of high pitch fluctuations. It is seen that the pitch controller hold the generator speed at the rated value for different wind speeds as expected.

Moreover, non-uniform wind inputs are tried for a more realistic simulations. Below

rated and above rated non-uniform wind speeds are tried to test the controllers. It is seen that controllers do their duty successfully.

Finally, the overall steady state behaviour of the model is obtained. The power curve of the dynamic model gives realistic and satisfactory results compared to the NREL 5 MW reference wind turbine power curve.

The next step could be the improvement of the model in terms of aeroelasticity. Comparison between aeroelastic and rigid model is done. However, generalization from these results is not possible. Aeroelastic blades could be added to the dynamical model. Deformations in flapping, lead-lag and feathering axis could be added. Moreover, the tower is an important factor affecting aerodynamics of wind turbines. Its effects could be considered during simulations. Moreover, different oncoming turbulent winds and wind gust could be considered to create more realistic atmospheric conditions. More complex controller could be designed to increase the turbine's performance. Structural loads on the blades became an important issue. In order to avoid them individual pitch controller could be implemented to the model. Other similar improvements for both the model and the controllers could be explored. The dynamic model designed in this thesis is just a start to examine wind turbines.

REFERENCES

[1] A. Abdullah and A. Fekih. Pitch control design for optimum energy capture in variable-speed wind turbines. In *Systems, Signals & Devices (SSD), 2013 10th International Multi-Conference on*, pages 1–6. IEEE, 2013.

[2] X. Anjun, X. Hao, H. Shuju, and X. Honghua. Pitch control of large scale wind turbine based on expert pid control. In *Electronics, Communications and Control (ICECC), 2011 International Conference on*, pages 3836–3839. IEEE, 2011.

[3] E. W. E. Association. Wind energy statics and targets. `http://www.ewea.org/uploads/pics/EWEA_Wind_energy_factsheet.png`.

[4] W. W. E. Association. New record in worldwide wind İnstallation. http://www.wwindea.org/new-record-in-worldwide-wind-installations/.

[5] O. Bauchau and J. Craig. Euler-bernoulli beam theory. In *Structural analysis*, pages 173–221. Springer, 2009.

[6] A. Baumgart. A mathematical model for wind turbine blades. *Journal of sound and vibration*, 251(1):1–12, 2002.

[7] F. D. Bianchi, H. De Battista, and R. J. Mantz. *Wind turbine control systems: principles, modelling and gain scheduling design*. Springer Science & Business Media, 2006.

[8] Bonnet. *SWT V3.302 Stationary Aerodynamics Validation*. 2013.

[9] E. Bossanyi. Further load reductions with individual pitch control. *Wind energy*, 8(4):481–485, 2005.

[10] M. L. Buhl. *A new empirical relationship between thrust coefficient and induction factor for the turbulent windmill state*. National Renewable Energy Laboratory Golden, CO, 2005.

[11] T. Burton, N. Jenkins, D. Sharpe, and E. Bossanyi. *Wind energy handbook*. John Wiley & Sons, 2011.

[12] P. Chaviaropoulos. Flap/lead–lag aeroelastic stability of wind turbine blade sections. *Wind Energy*, 2(2):99–112, 1999.

[13] G. W. E. Council. Wind in numbers. `http://www.gwec.net/global-figures/wind-in-numbers/`.

[14] W. P. Directory. The 10 biggest turbines in the word. http://www.windpowermonthly.com/10-biggest-turbines, 2014.

[15] W. E. Foundation. History. http://www.windenergyfoundation.org/about-wind-energy/historyl.

[16] M. M. Hand and M. Balas. Systematic controller design methodology for variable-speed wind turbines. *Wind Engineering*, 24(3):169–187, 2000.

[17] M. H. Hansen, A. D. Hansen, T. J. Larsen, S. Øye, P. Sørensen, and P. Fuglsang. *Control design for a pitch-regulated, variable speed wind turbine*. 2005.

[18] M. O. Hansen. *Aerodynamics of wind turbines*. Routledge, 2015.

[19] D. H. Hodges and E. Dowell. Nonlinear equations of motion for the elastic bending and torsion of twisted nonuniform rotor blades. 1975.

[20] J. C. Houbolt and G. W. Brooks. *Differential equations of motion for combined flapwise bending, chordwise bending, and torsion of twisted nonuniform rotor blades*. NACA, 1958.

[21] K. E. Johnson et al. *Adaptive torque control of variable speed wind turbines*. Citeseer, 2004.

[22] J. M. Jonkman, S. Butterfield, W. Musial, and G. Scott. *Definition of a 5-MW reference wind turbine for offshore system development*. National Renewable Energy Laboratory Golden, CO, 2009.

[23] B. S. Kallesøe. Equations of motion for a rotor blade, including gravity, pitch action and rotor speed variations. *Wind Energy*, 10(3):209–230, 2007.

[24] M. A. Lackner and G. van Kuik. A comparison of smart rotor control approaches using trailing edge flaps and individual pitch control. *Wind Energy*, 13(2-3):117–134, 2010.

[25] J. H. Laks, L. Y. Pao, and A. D. Wright. Control of wind turbines: Past, present, and future. In *American Control Conference, 2009. ACC'09.*, pages 2096–2103. IEEE, 2009.

[26] R. Lanzafame and M. Messina. Fluid dynamics wind turbine design: Critical analysis, optimization and application of bem theory. *Renewable energy*, 32(14):2291–2305, 2007.

[27] J. W. Larsen and S. R. Nielsen. Non-linear dynamics of wind turbine wings. *International Journal of Non-Linear Mechanics*, 41(5):629–643, 2006.

[28] L. Li, Y. Li, Q. Liu, and H. Lv. A mathematical model for horizontal axis wind turbine blades. *Applied Mathematical Modelling*, 38(11):2695–2715, 2014.

[29] M. Liao, L. Dong, L. Jin, and S. Wang. Study on rotational speed feedback torque control for wind turbine generator system. In *Energy and Environment Technology, 2009. ICEET'09. International Conference on*, volume 1, pages 853–856. IEEE, 2009.

[30] C.-W. Lim. Torque control methods for wind turbines and their responses. In *Control, Automation and Systems (ICCAS), 2012 12th International Conference on*, pages 1788–1790. IEEE, 2012.

[31] J. F. Manwell, J. G. McGowan, and A. L. Rogers. *Wind energy explained: theory, design and application*. John Wiley & Sons, 2010.

[32] A. Merabet, J. Thongam, and J. Gu. Torque and pitch angle control for variable speed wind turbines in all operating regimes. In *Environment and Electrical Engineering (EEEIC), 2011 10th International Conference on*, pages 1–5. IEEE, 2011.

[33] P. J. Moriarty and A. C. Hansen. *AeroDyn theory manual*. National Renewable Energy Laboratory Golden, Colorado, USA, 2005.

[34] P. Musgrove, P. Musgrove, P. Musgrove, and P. Musgrove. *Wind power*. Cambridge University Press Cambridge, 2010.

[35] NREL. Solar energy basics. `http://www.nrel.gov/learning/re_solar.html`, 2014.

[36] K. Ogata and Y. Yang. Modern control engineering. 2002.

[37] L. Y. Pao and K. E. Johnson. A tutorial on the dynamics and control of wind turbines and wind farms. In *American Control Conference, 2009. ACC'09.*, pages 2076–2089. IEEE, 2009.

[38] K. W. Project. Wind energy history. `http://learn.kidwind.org/learn/wind_basics_historyl`.

[39] S4WT. Lms samtech samcef wind turbines. `http://www.plm.automation.siemens.com/en_us/products/lms/samtech/samcef-wind-turbines.shtml`, 2015.

[40] T. Sant. *Improving BEM-based aerodynamic models in wind turbine design codes*. TU Delft, Delft University of Technology, 2007.

[41] V. Smil. *Energy at the crossroads: global perspectives and uncertainties*. MIT press, 2005.

[42] N. Stern. The economics of climate change. *The American Economic Review*, pages 1–37, 2008.

[43] R. W. Thresher, L. P. Mirandy, T. G. Carne, D. W. Lobitz, and G. H. James. Structural dynamic behavior of wind turbines. In *Wind Turbine Technology: Fundamental Concepts in Wind Turbine Engineering, Second Edition*. ASME Press, 2009.

[44] T. Van Engelen. Design model and load reduction assessment for multi-rotational mode individual pitch control (higher harmonics control). In *European Wind Energy Conference*, pages 27–2, 2006.

[45] J. R. P. Vaz, J. T. Pinho, and A. L. A. Mesquita. An extension of bem method applied to horizontal-axis wind turbine design. *Renewable Energy*, 36(6):1734–1740, 2011.

[46] N. Veritas. *Guidelines for design of wind turbines*. Det Norske Veritas: Wind Energy Department, Ris National Laboratory, 2002.

[47] B. Wind. Top wind myths. `http://www.british-wind.co.uk/wind_myths.htmll`.

[48] A. Wright and L. Fingersh. Advanced control design for wind turbines. *Part I: Control Design, Implementation, and Initial Tests, National Renewable Energy Lab., USA*, 2008.

APPENDIX A

DATA FOR S4WT WIND TURBINE

Table A.1: Wind Turbine Properties

Wind turbine type	HAWT
Blade number	3
Blade length	38.75 m
Hub diameter	2.5 m
Rotor axis tilt angle	0 deg
Precone angle	0 deg

Table A.2: Blade Properties

Blade Section	Distance from root (m)	Chord (m)	Twist (rad)	Airfoil
1	0	2.067	0.227	democyl
2	1.148	2.067	0.227	democyl
3	3.444	2.756	0.227	democyl
4	5.740	3.444	0.227	LS1m21
5	9.185	3.444	0.192	LS1m21
6	10.074	2.756	0.136	LS1m21
7	26.407	1.837	0.056	LS1m17
8	35.233	1.148	0.005	LS1m13
9	38.233	0.689	0.048	LS1m13
10	38.75	0.029	0.07	LS1m13

Table A.3: Load Case Properties

	Wind Speed (m/s)	Rotor Speed (rpm)	Blade Pitch
Below-Rated Load Case	8	13	0
Rated Load Case	12	15	0
Above-Rated Load Case	18	15	10

Table A.4: Wind Turbine Material Properties

Young Modulus	100 GPa
Poisson Ratio	0.3
Density	2e3 kg/m^3
Damping	4.54728409e-3 s

Table A.5: Blade Stiffness Properties

Section	Distance (m)	Flap Stiffness (Nm^2)	Edge Stiffness (Nm^2)	Torsional Rigidity (Nm^2)
1	0	50e9	50e9	20e9
2	1.148	30e9	30e9	10e9
3	3.444	20e9	40e9	4e9
4	5.740	5e9	20e9	700e6
5	9.185	1e9	5e9	100e6
6	10.074	500e6	3e9	50e6
7	26.407	200e6	1e9	20e6
8	35.233	70e6	700e6	7e6
9	38.233	30e6	300e6	3e6
10	38.75	10e6	100e6	1e6

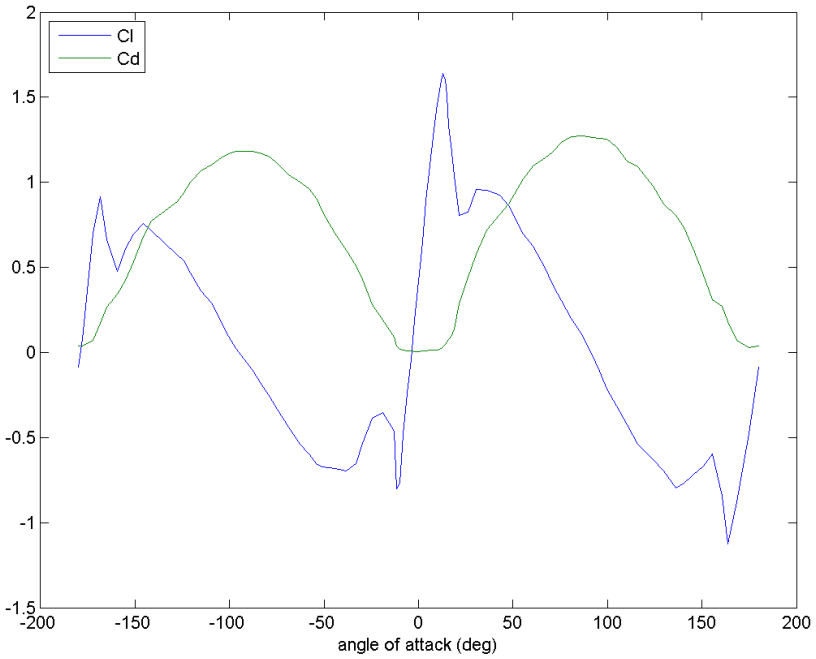

Figure A.1: Lift and Drag Coefficient vs Angle of Attack for Airfoil LS1m13

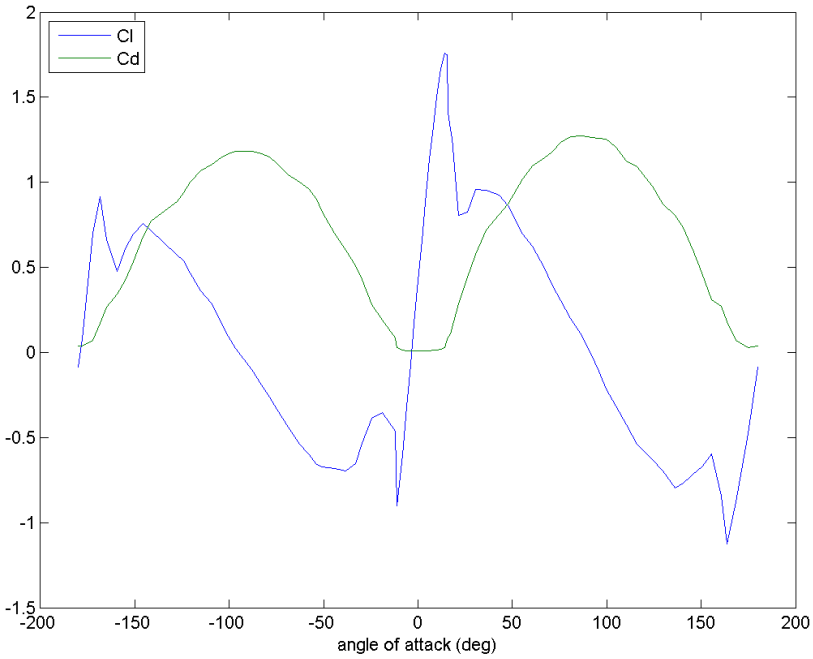

Figure A.2: Lift and Drag Coefficient vs Angle of Attack for Airfoil LS1m17

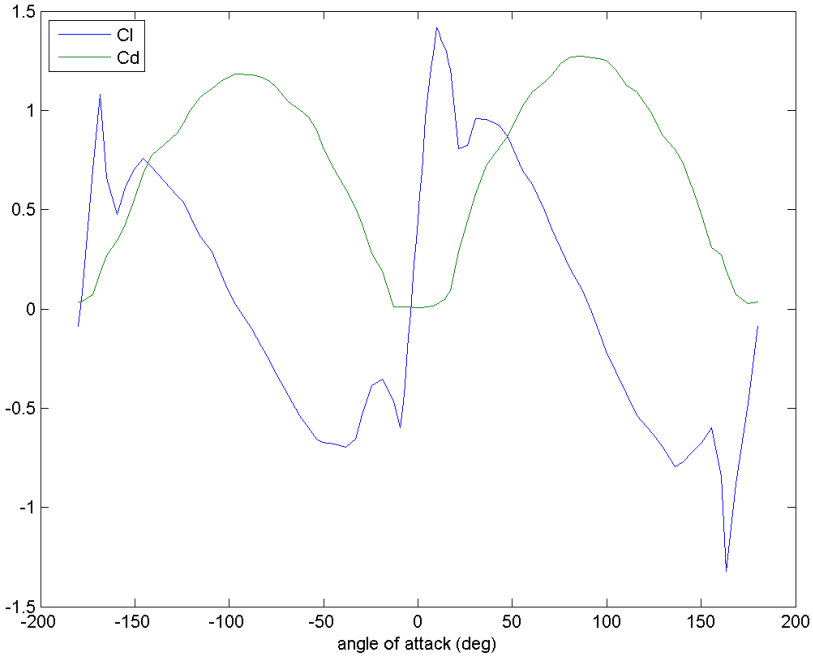

Figure A.3: Lift and Drag Coefficient vs Angle of Attack for Airfoil LS1m21

APPENDIX B

DATA FOR NREL 5MW REFERENCE WIND TURBINE

Table B.1: Blade Properties

Blade Section	dm (kg/m)	dr (m)	Chord (m)	Twist (deg)	Airfoil
1	691	2.73	3.542	13.308	cylinder1
2	424.989	2.73	3.854	13.308	cylinder1
3	406.214	2.73	4.167	13.308	cylinder2
4	372.476	4.1	4.557	13.308	DU40
5	338.625	4.1	4.652	11.48	DU35
6	317.905	4.1	4.458	10.162	DU35
7	290.927	4.1	4.249	9.011	DU30
8	258.275	4.1	4.007	7.795	DU25
9	231.152	4.1	3.478	6.544	DU25
10	189.848	4.1	3.502	5.361	DU21
11	159.752	4.1	3.256	4.188	DU21
12	134.245	4.1	3.010	3.125	NACA64
13	103.020	4.1	2.764	2.319	NACA64
14	86.624	4.1	2.518	1.526	NACA64
15	69.314	2.73	2.313	0.863	NACA64
16	52.534	2.73	2.086	0.370	NACA64
17	20.147	2.73	1.419	0.106	NACA64

Table B.2: Wind Turbine Properties

Wind turbine type	HAWT
Rotor orientation	Upwind
Blade number	3
Blade length	61.5 m
Hub diameter	1.5 m
Rotor axis tilt angle	5 deg
Precone angle	2.5 deg
Cut-in wind speed	3 m/s
Cut-out wind speed	25 m/s
Cut-in rotor speed	6.9 rpm
Rated wind speed	11.4 m/s
Rated rotor speed	12.1 rpm
Gearbox ratio	97:1
Electrical generator efficiency	94.4 percent
Hub inertia about low-speed shaft	115926 kg m^2
Generator inertia about high-speed shaft	534.116 kg m^2

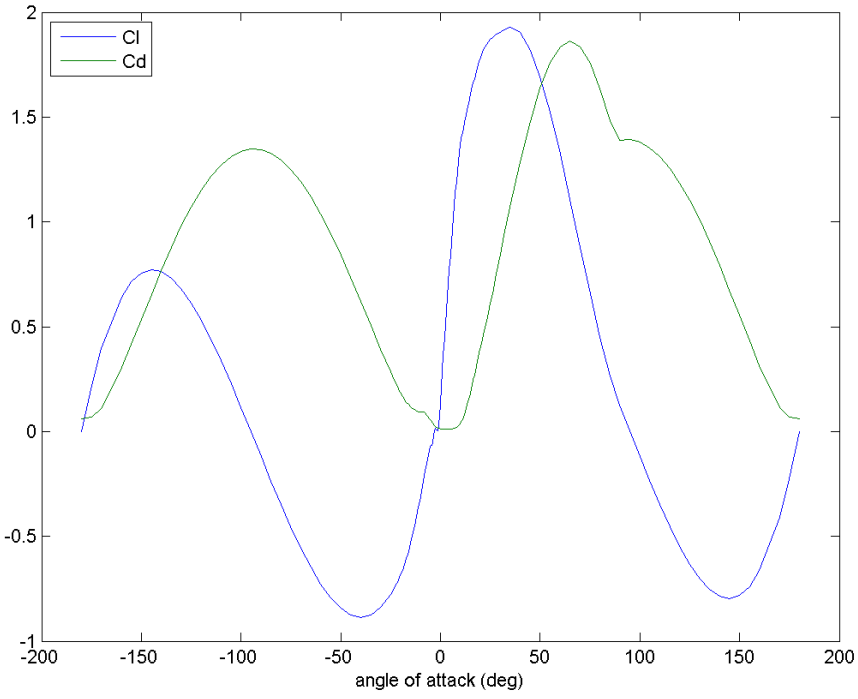

Figure B.1: Lift and Drag Coefficient vs Angle of Attack for Airfoil DU40

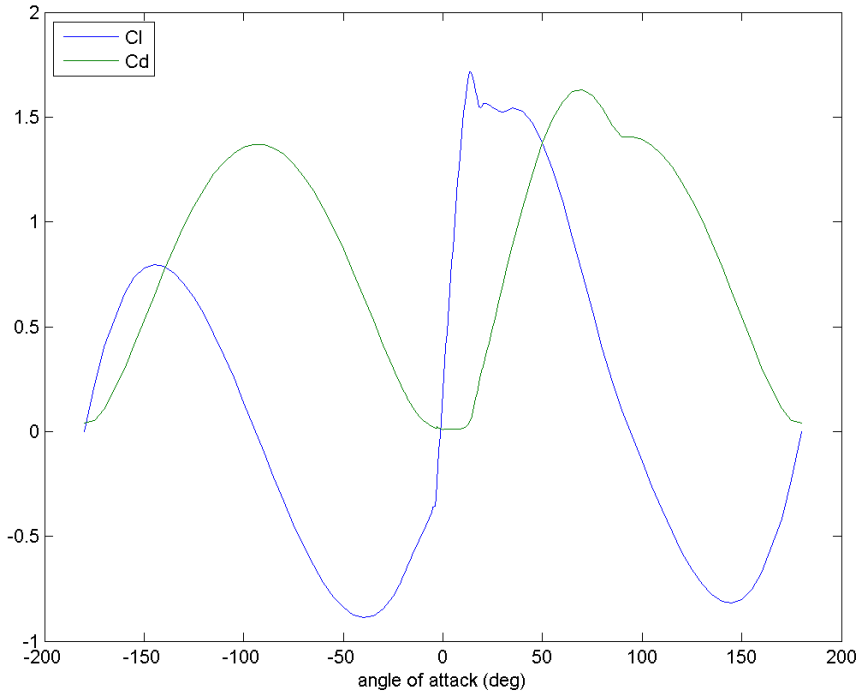

Figure B.2: Lift and Drag Coefficient vs Angle of Attack for Airfoil DU35

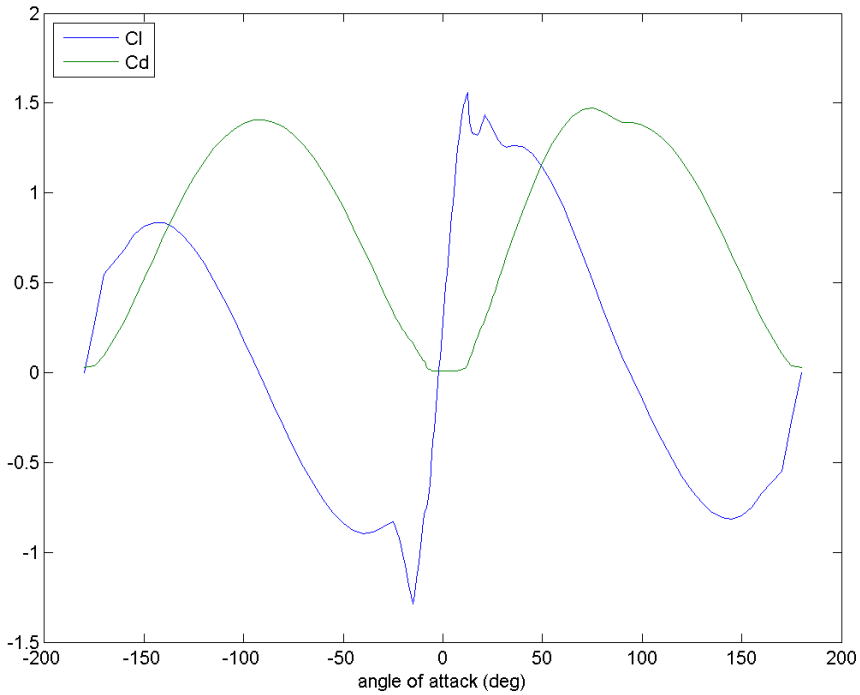

Figure B.3: Lift and Drag Coefficient vs Angle of Attack for Airfoil DU30

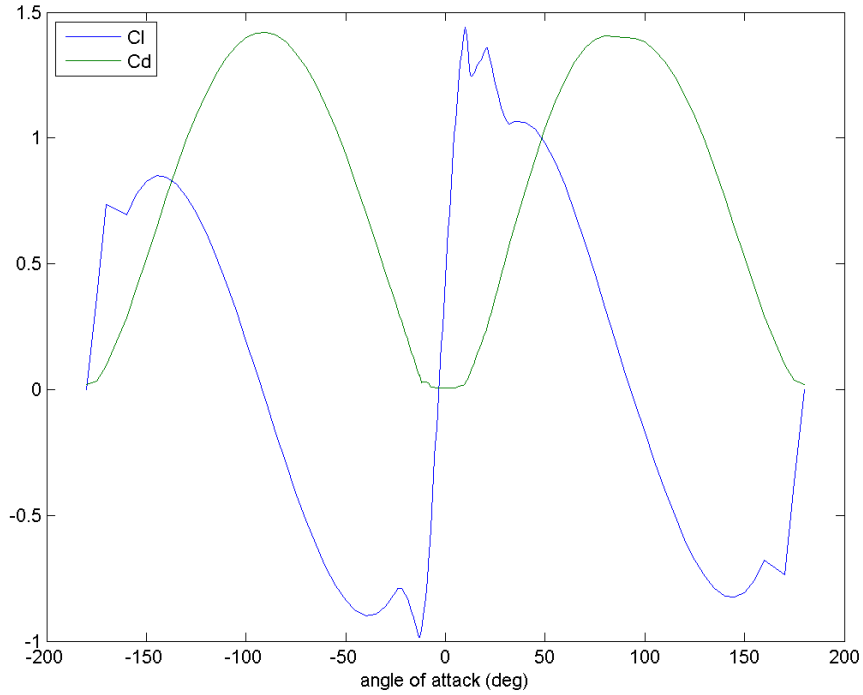

Figure B.4: Lift and Drag Coefficient vs Angle of Attack for Airfoil DU25

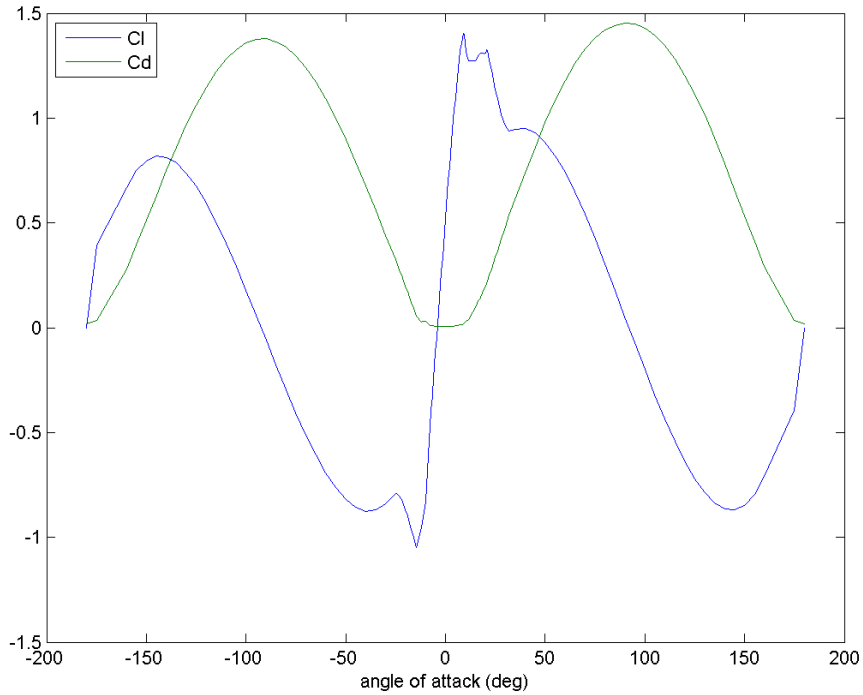

Figure B.5: Lift and Drag Coefficient vs Angle of Attack for Airfoil DU21

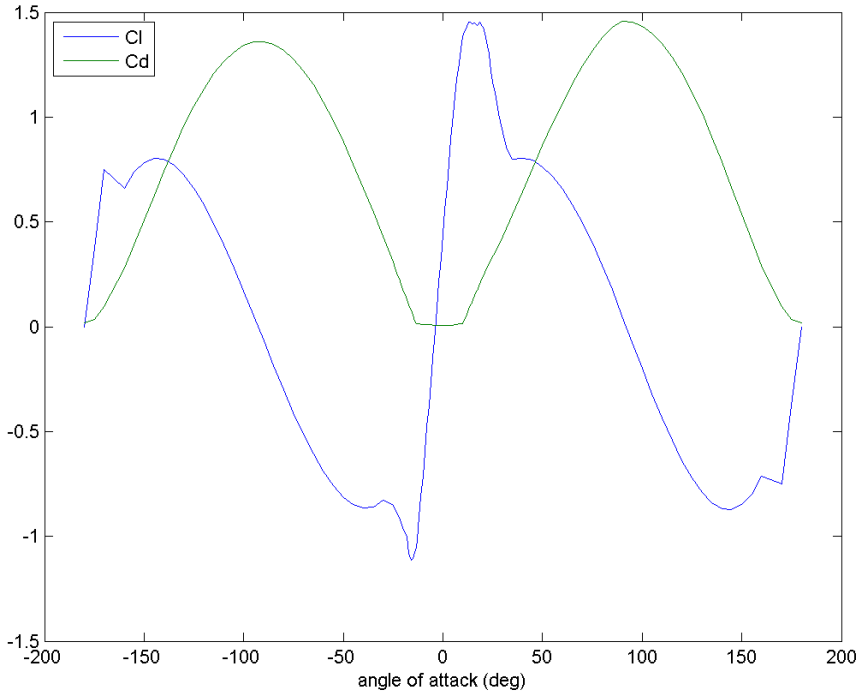

Figure B.6: Lift and Drag Coefficient vs Angle of Attack for Airfoil NACA64